Colloidal transport over complex energy landscapes: From passive particles and self-propelled colloids to transmembrane proteins

Penger Tong

Department of Physics
Hong Kong University of Science and Technology, Hong Kong

The 9th Soft Matter Summer School: Active Soft Matter

UNIST, August 1 - 5, 2022

OUTLINE:

1. Introduction
2. Experimental methods to generate free-energy landscapes
3. Applications of complex free-energy landscapes
4. New challenges for active and living systems
5. Recent studies in three non-equilibrium systems
6. Summary

Collaborators:

Yan Wen, Yusheng Shen, Yun Su, Xiao-Guang Ma, Wei He, Chengjie Lou, Zhihao Li (GTIIT) and Haiqin Wang (GTIIT)

Pik-Yin Lai and Hsuan-Yi Chen (National Central U, Taiwan), Bruce Ackerson (Oklahoma State U, USA), Xinpeng Xu (Guangdong Technion-Israel Institute of Tech.), Pingbo Huang and Yilong Han (HKUST)

Work supported by Hong Kong Research Grants Council

Recent publications:

"Colloidal transport and diffusion over a tilted periodic potential: dynamics of individual particles," X.-G. Ma, P.-Y. Lai, B. J. Ackerson, and P. Tong, Soft Matter, **11**, 1182 (2015).

"Colloidal diffusion over a quasicrystalline-patterned surface," Y. Su, P.-Y. Lai, B. J. Ackerson, X. Cao, Y.-L. Han, and P. Tong, J. Chem. Phys. **146**, 214903 (2017) [Editors' Pick].

"Colloidal diffusion over a quenched two-dimensional random potential," Y. Su, X.-G. Ma, P.-Y. Lai and P. Tong, Soft Matter **13**, 4773 (2017).

"Directed motion of membrane proteins under an entropy-driven potential field generated by anchored proteins," Y.-S. Shen, C.-J. Luo, Y. Wen, W. He, P.-B. Huang, H.-Y Chen, P.-Y. Lai, and P. Tong, Phys. Rev. Research. **3**, 043195 (2021).

"Activity-assisted barrier-crossing of self-propelled colloids over parallel microgrooves," Y. Wen, Z.-H. Li, H.-Q. Wang, J. Zheng, J.-Y. Tang, P.-Y. Lai, X.-P. Xu, and P. Tong (submitted).

1. Introduction

Free-energy landscape is an important concept for the study of diffusion and transport of molecules and (colloidal) particles and has been widely used in many areas of physics, chemistry, biology and materials science.

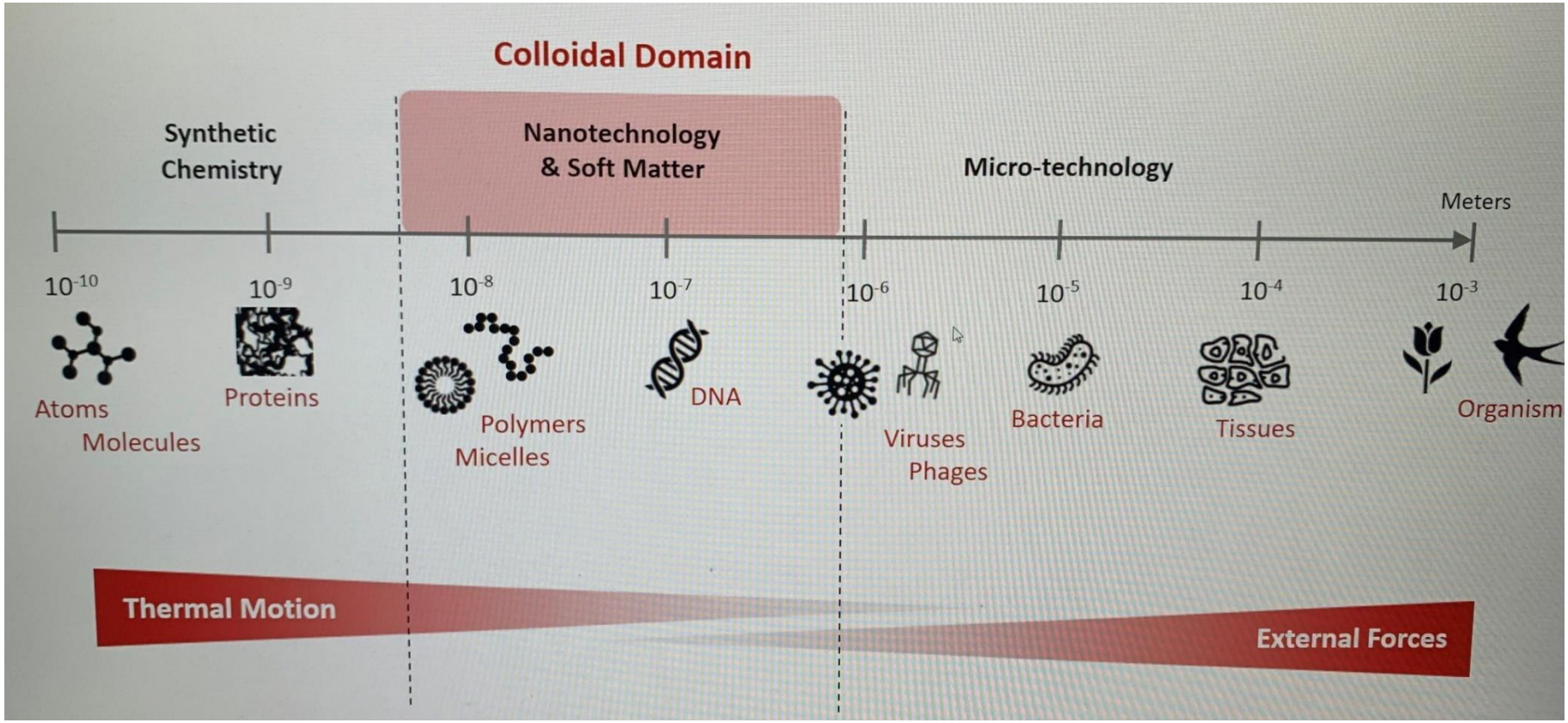

Chem. Soc. Rev. (2013) **42**, 2100 and Bas van Ravensteijn

- Brownian motion, discovered by Scottish botanist Robert Brown in 1827, is one of the most studied subjects in statistical physics.
- Small (colloidal) particles (e.g., pollen grains) immersed in an *infinite* fluid move around randomly, which can be described by the displacement vector,

$$\Delta\mathbf{x}(\tau) = \mathbf{x}(t+\tau) - \mathbf{x}(t)$$

$$\langle \Delta\mathbf{x}^2(\tau) \rangle = 2dD_0\tau; \quad d = 1, 2, 3$$

$$D_0 = \frac{k_B T}{\xi}; \quad \xi = 6\pi\eta a; \quad \mu = \frac{1}{\xi}$$

$$P(\Delta x) = \frac{1}{(4\pi D_0 \tau)^{1/2}} e^{-\Delta x^2/(4D_0\tau)}$$

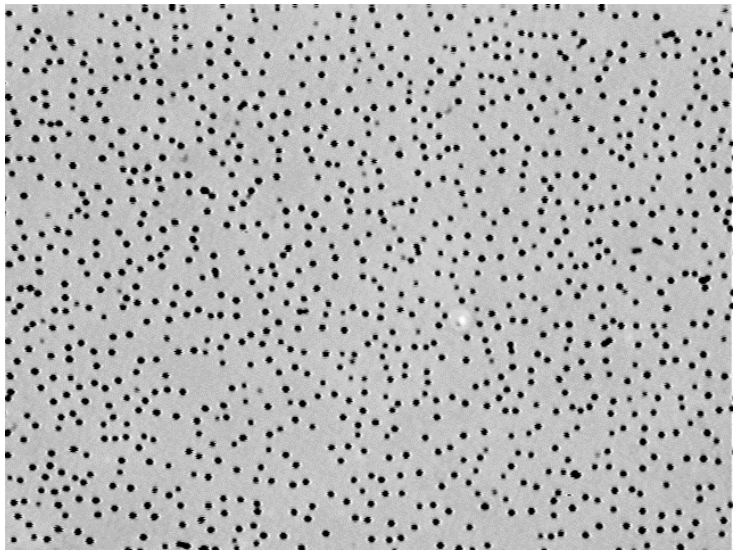

Generalization and applications

- Effects of (frozen) spatial confinement: near a wall, at a liquid-air interface, between two walls, in a narrow channel, on a fractal, and in porous media ...

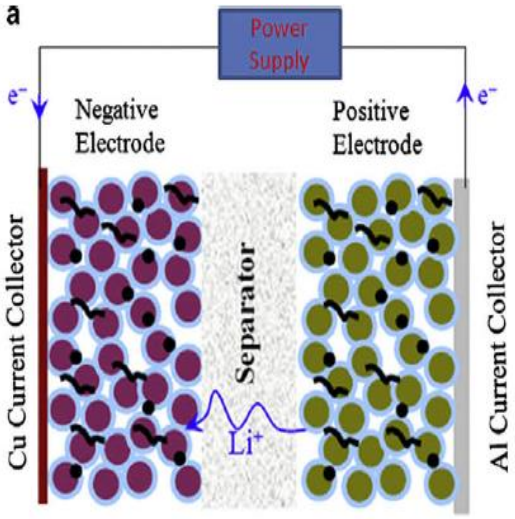

Diffusion of Li^+ within electrodes of a battery

"colloidal glass" made of particles with two different sizes

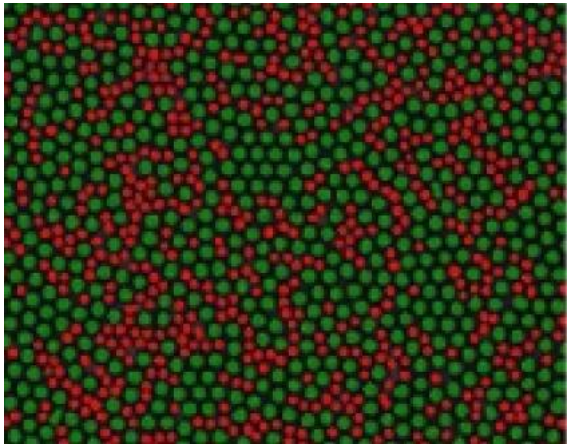

S. J. Harris, Chem. Phys. Lett. 485, 265 (2010)

- Effects of (fluctuating) neighboring particles: particle concentration and finite size effects, an effective mean field?

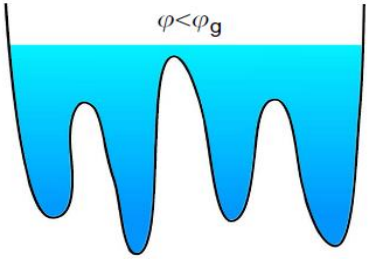

liquid

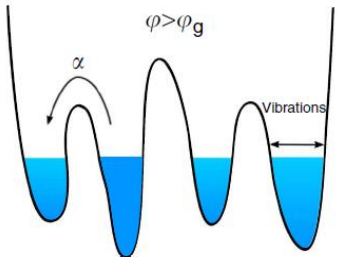

glass

- The external potential fields (or free-energy landscapes) are often disordered, and disorder has many different forms.
- There are few experimental systems in which one can actually visualize the energy landscape, and thus much of the work done so far is through computer simulations.

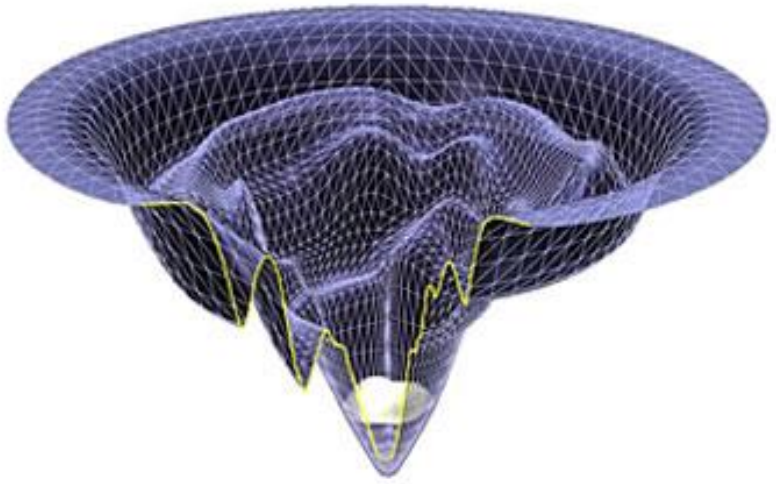

- A physical model system in which one can directly measure the potential landscape and track individual particle trajectories is, therefore, extremely valuable for testing different theoretical ideas.

Recent development of optical microscopy and particle tracking

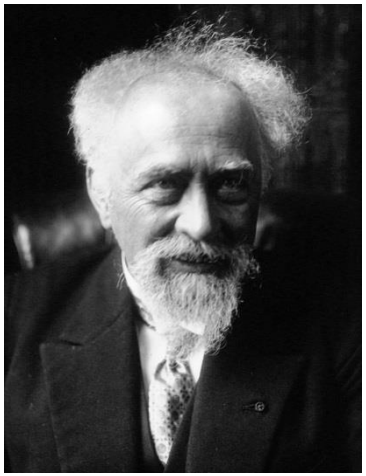

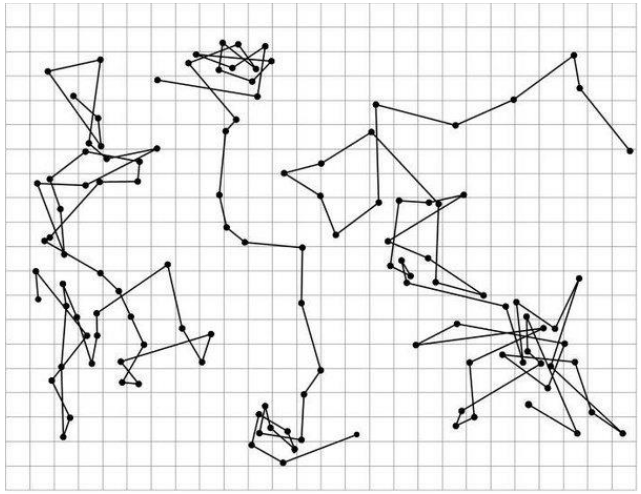

- spatial resolution: ~1 μm
- time resolution: 30 s
- single particle tracking
- manually carried out for a short period of time
- particles: pollen grains, resin

In 1908, Jean Perrin tested Einstein's prediction with manual tracking

- spatial resolution: ~10 nm
- time resolution: 1 μs (high-speed camera)
- simultaneous tracking of ~100 particles
- computer controlled over a long period of time
- Specially synthesized uniform spheres, quantum dots, and fluorescently labeled molecules

2. Experimental methods to generate free-energy landscapes

Colloidal particles (0.5-5 μm in size) suspended in a solution as "big atoms"

They are small enough to have Brownian motion, big enough to be visible under an optical microscope, and also slow enough so that their motion can be recorded by a camera; they are available for different materials, shapes, and sizes.

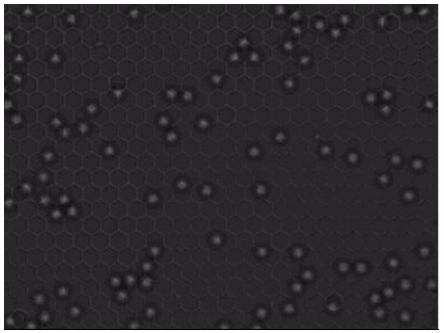

Periodic potential

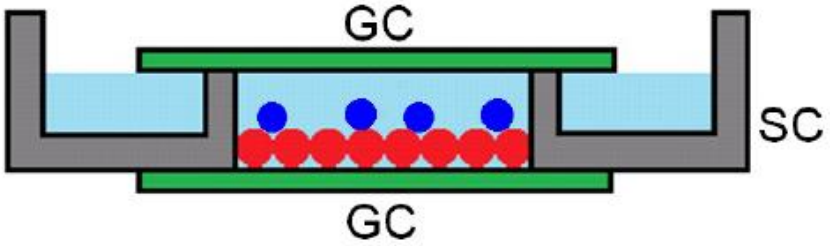

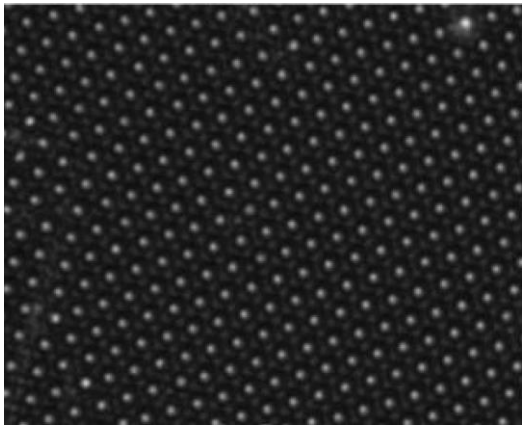

Close packed monolayer of uniform silica spheres on the substrate forms a 2D colloidal crystal. Its corrugated surface provides a periodic gravitational potential $U(x,y)$ for the top diffusing particles.

We add 5×10^4 images together, each containing ~150 particles, and compute the number of particles in each pixel area, from which we obtain the population probability histogram $P_s(x,y)$. It relates to the underlying potential landscape $U(x,y)$ via the Boltzmann distribution:
$P_s(x,y) \approx \exp[-U(x,y)/k_BT]$.

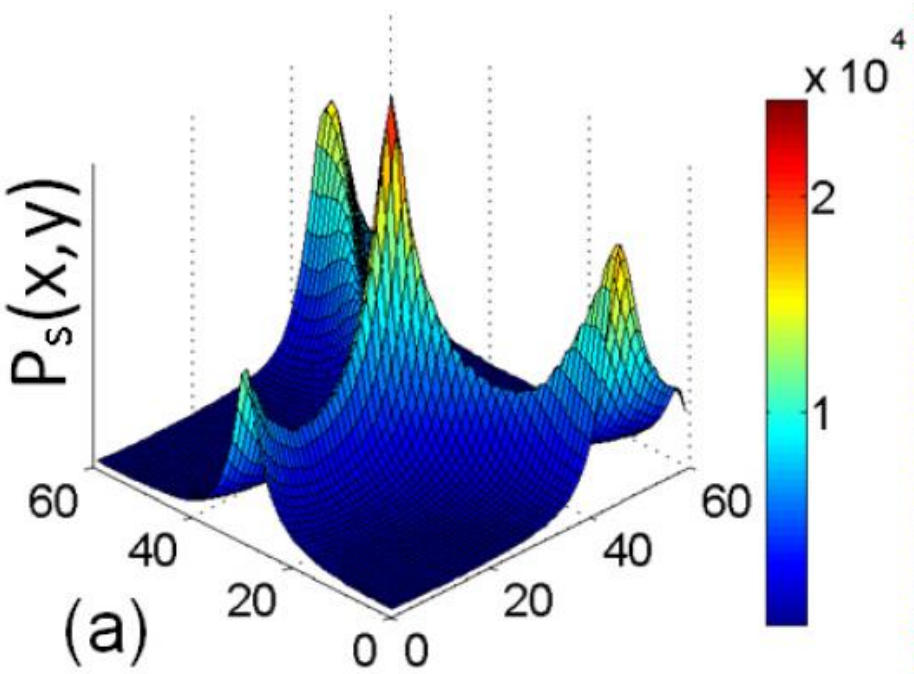

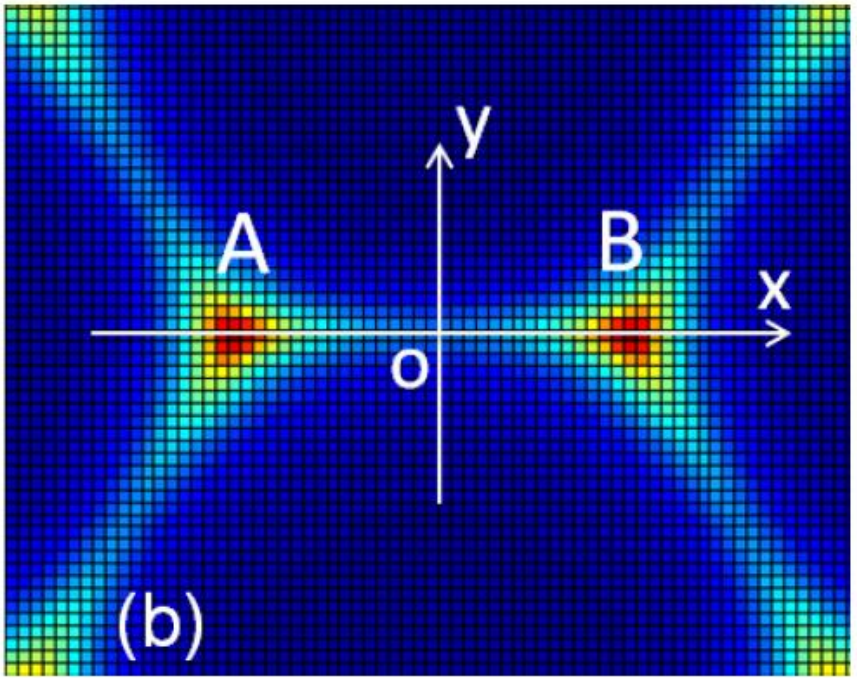

3D plot of the population probability histogram $P_s(x,y)$ averaged over more than 100 periodic areas

Top view of the measured $P_s(x,y)$ for the 2.1/2.9 sample.

Gravitational potential landscape of the rugged surface

$$\frac{U(x,y)}{k_B T} = -\ln[P_s(x,y)]$$

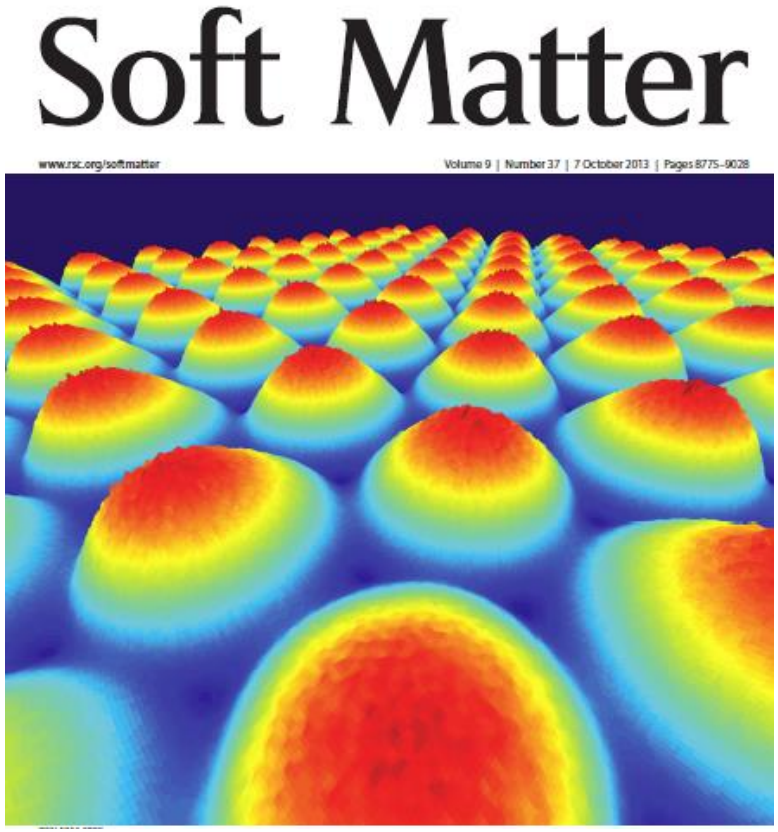

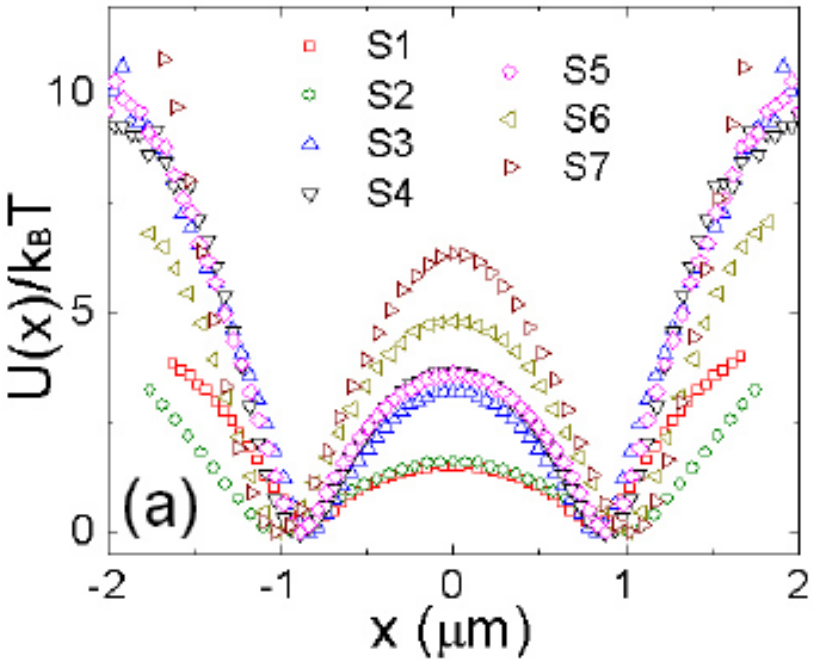

Measured potential landscape $U(x)/k_BT$ as a function of x for seven different samples

Ma *et al.*, Soft Matter **9**, 8775 (2013)

Random potential with a precise control

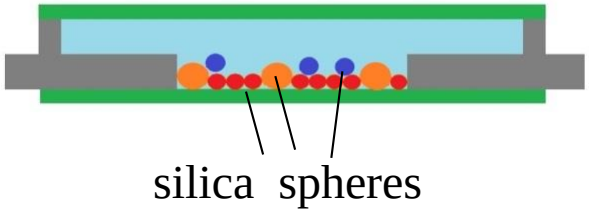

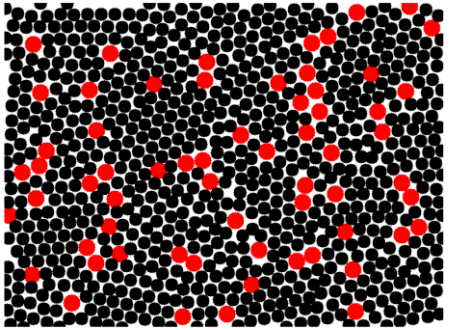

A mixture of bidisperse silica spheres form different patterns of 2D random close packing. A fixed configuration is used to provide a quenched 2D random potential $U(x,y)$ for the top diffusing particles. d_S = 2.47 μm, d_L = 2.94 μm, $n_L/n_S = 0.16$.

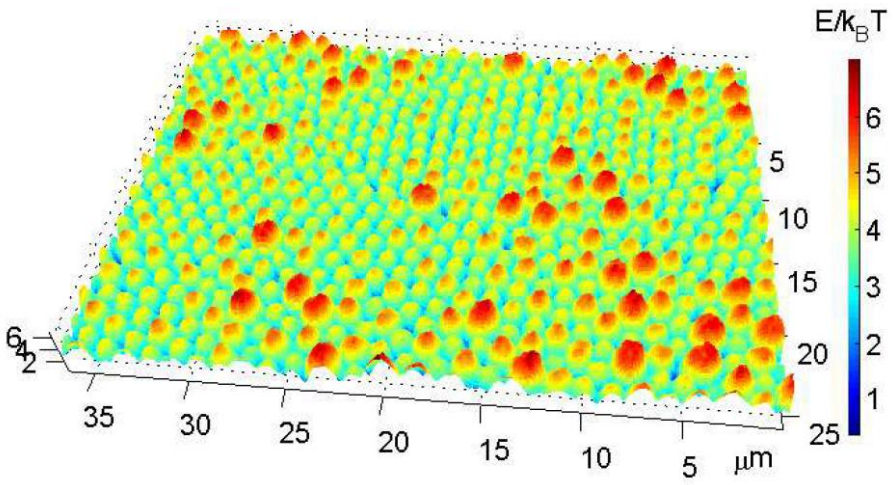

Measured random potential

Su, *et al.*, Soft Matter **13**, 4773 (2017)

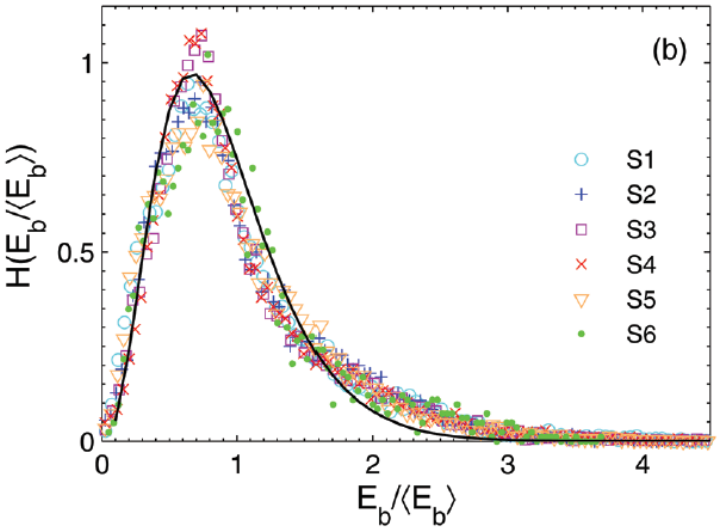

Distribution of energy barrier height for different diffusing particles

Quasi-crystalline-patterned surface

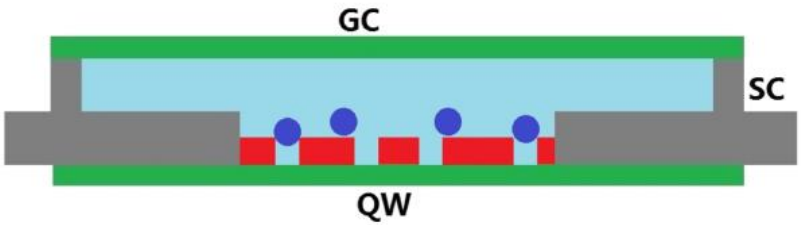

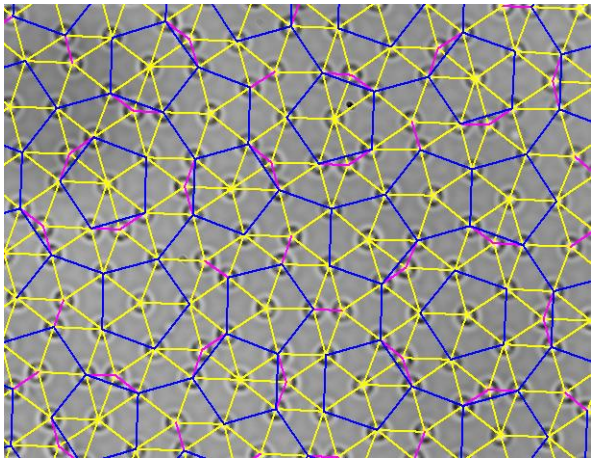

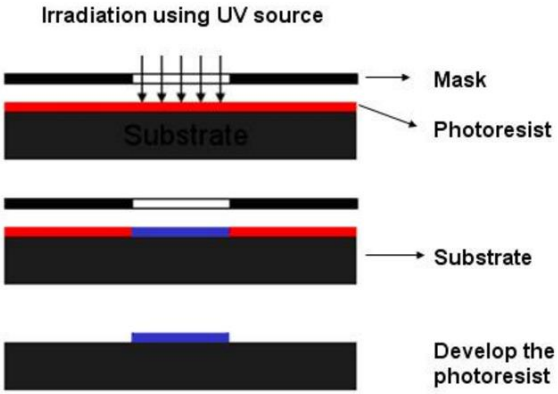

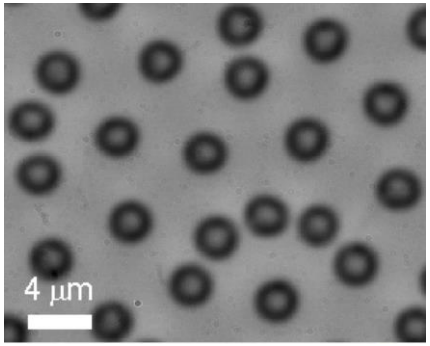

A variety of patterned substrates can be made by photolithography.

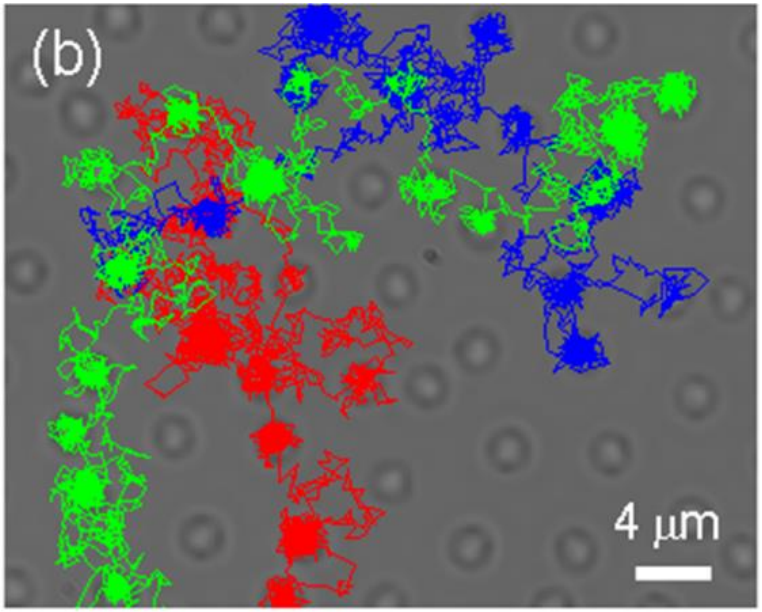

Particle trajectories reveal a trap-and-go motion.

Su, *et al*., J. Chem. Phys. **146**, 214903 (2017)

3. Applications of complex free-energy landscapes

Studies of equilibrium barrier crossing dynamics

(i) Diffusion over the periodic potential

$$\Delta\mathbf{r}(\tau) = \mathbf{r}(t+\tau) - \mathbf{r}(t)$$

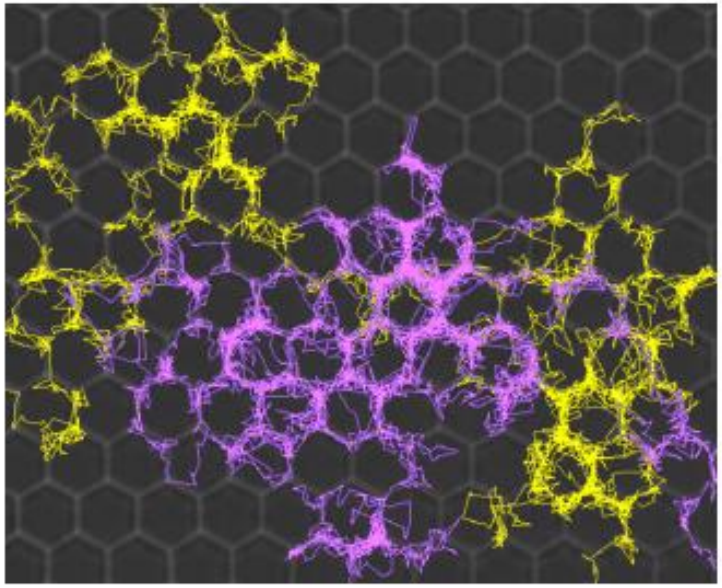

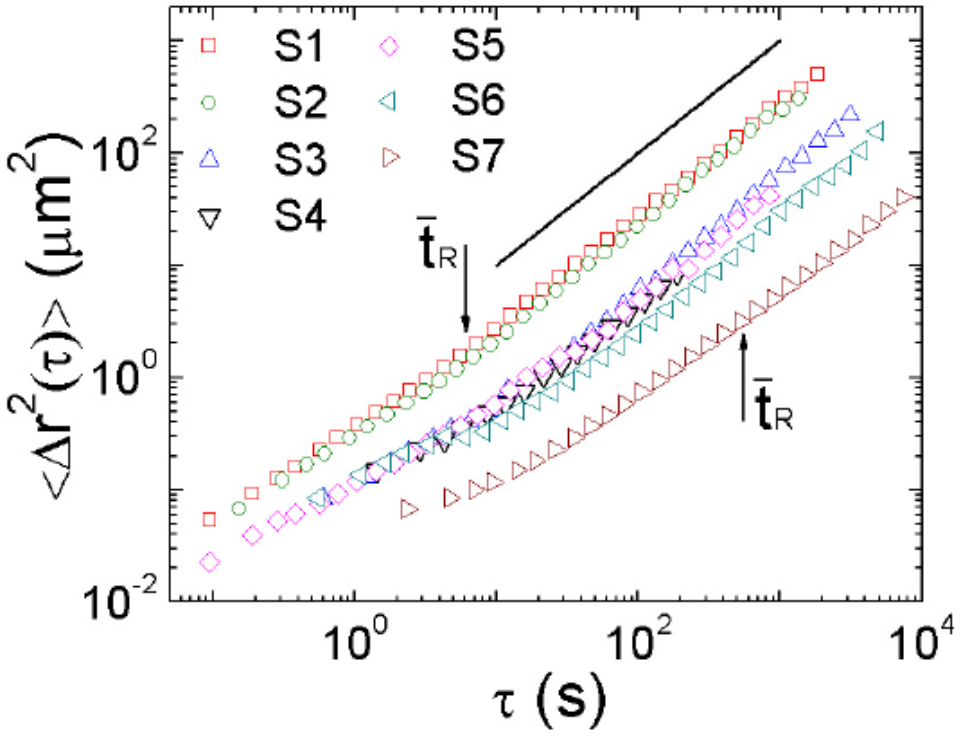

Two 1-h-long trajectories (yello and pink) of the diffusing particles over the bottom colloidal crystal for the 2.1/2.9 sample

Ma *et al.*, Soft Matter **9**, 8775 (2013)

Log-log plot of the measured MSD as a function of delay time for seven different samples

Comparison with the exact theoretical results (Lifson and Jackson, 1962):

$$\frac{D_0}{D_L} = \frac{4}{3}\langle e^{U(x)/k_BT}\rangle_\lambda \langle e^{-U(x)/k_BT}\rangle_\lambda$$

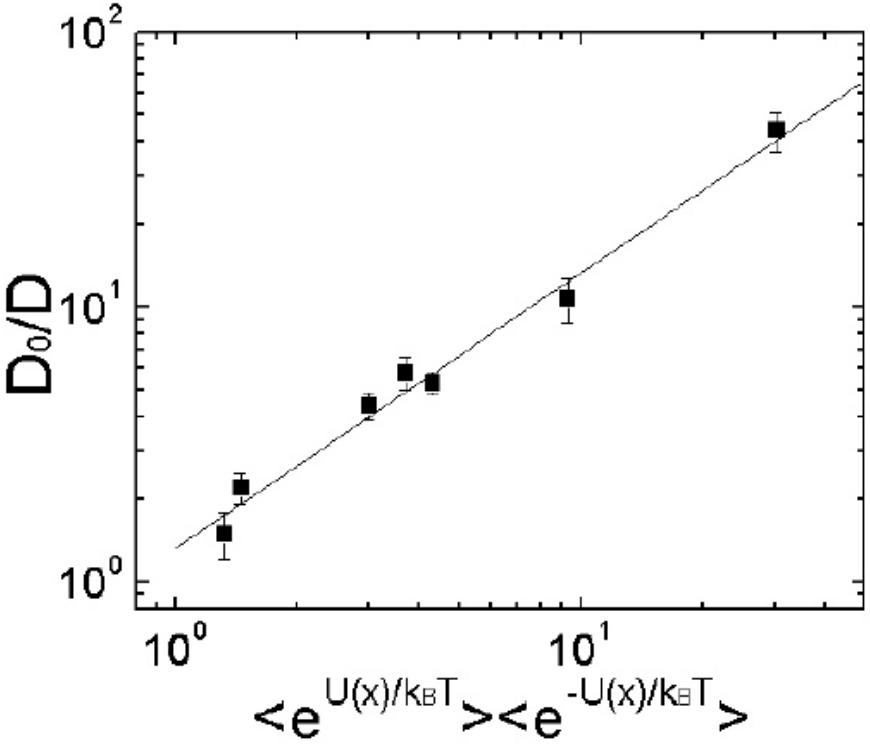

Comparison between the measured D_0/D_L at low surface coverage and the theoretical prediction for seven samples

$$\frac{\overline{t_R}}{t_0} = \frac{1}{3}\langle e^{U(x)/k_BT}\rangle_\lambda \langle e^{-U(x)/k_BT}\rangle_\lambda$$

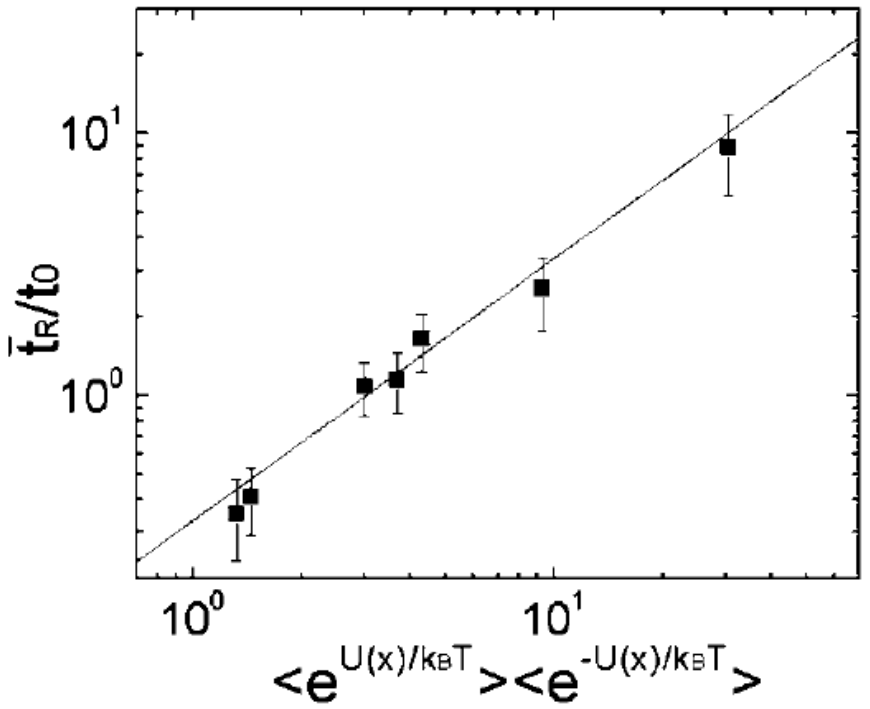

Normalized mean-first-passage-time t_R/t_0 for seven colloidal samples

Comparison with the Arrhenius-Kramers equation:

$$\frac{D_0}{D} \approx \frac{4}{3}\frac{2\pi k_B T}{(U_0^{"}|U_b^{"}|)^{1/2}\lambda^2} e^{E_b/k_B T} = \frac{4}{3}\nu e^{E_b/k_B T}$$

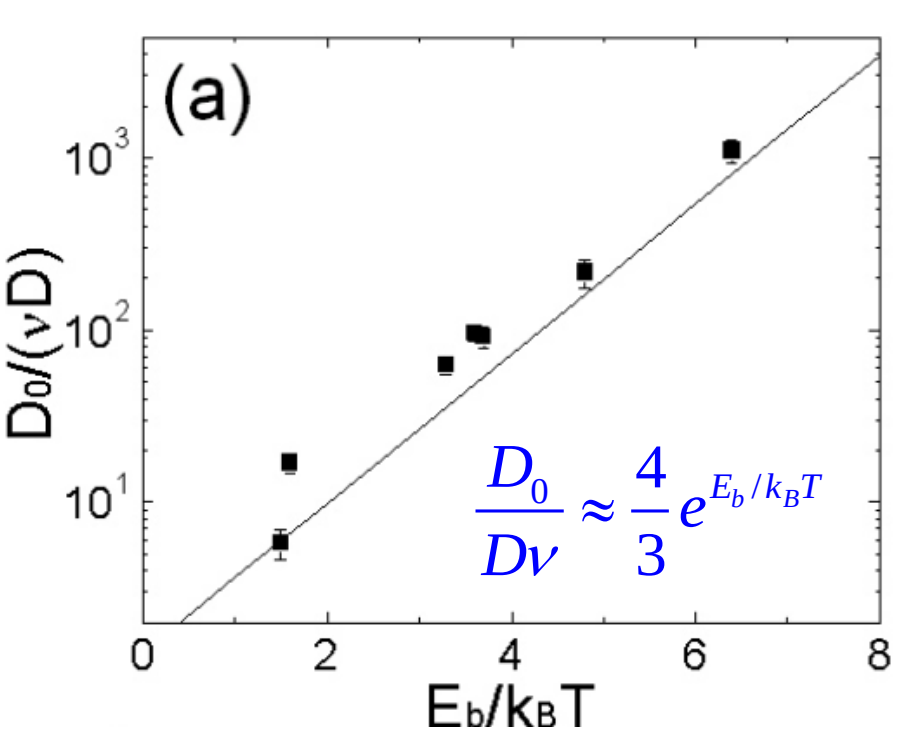

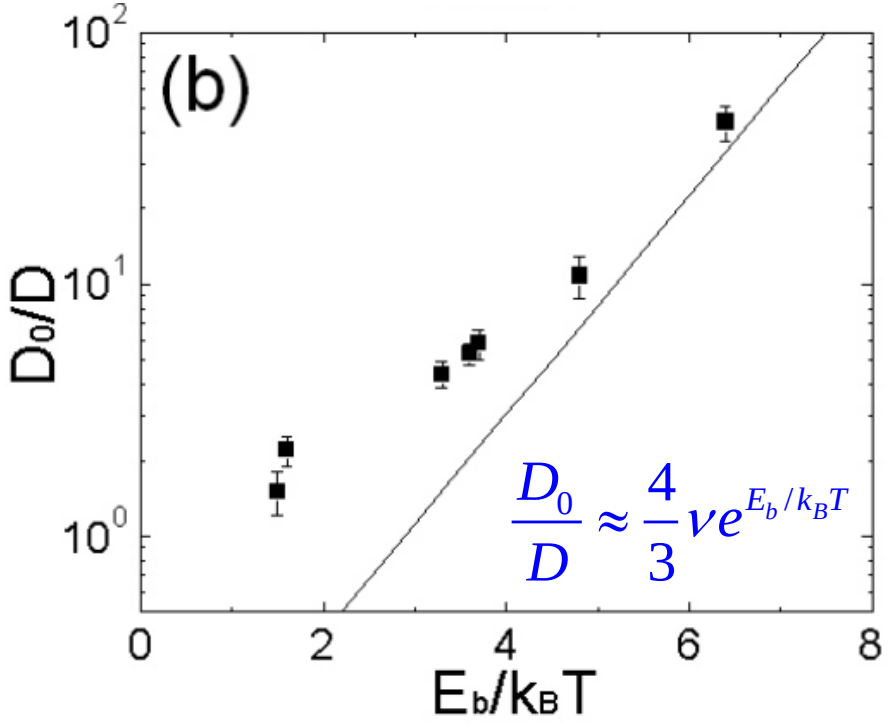

Measured $D_0/(\nu D)$ as a function of the energy barrier height E_b/k_BT

Measured D_0/D as a function of the energy barrier height E_b/k_BT

Ma *et al.*, Soft Matter **9**, 8775 (2013)

(ii) Diffusion over a random potential

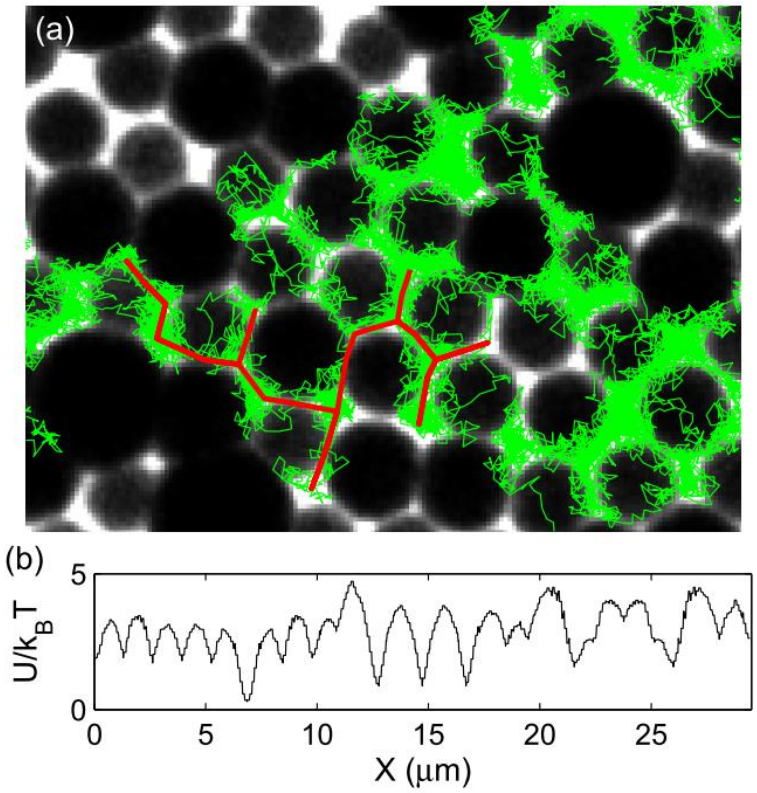

20 min-long single-particle trajectory showing that the particle moves along a quasi-1D 'path area' connecting the traps most of the time.

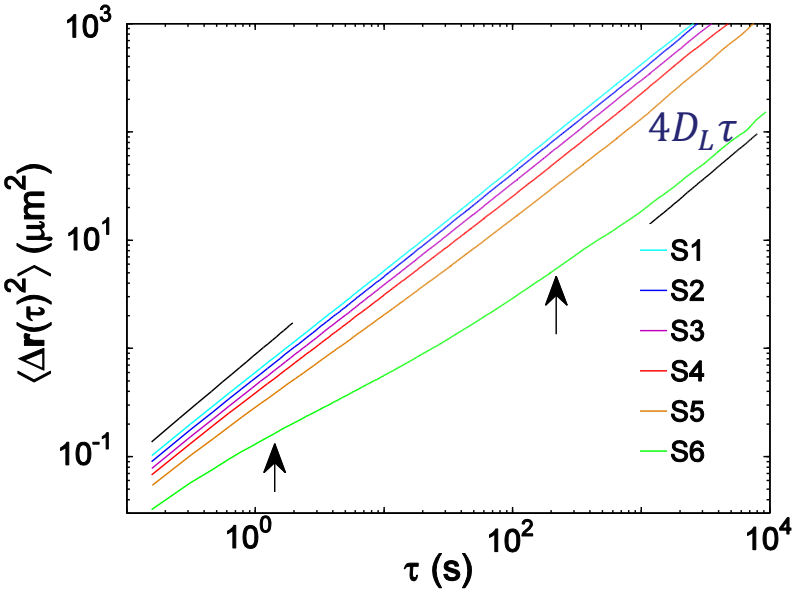

Measured MSD exhibits a dual crossover behavior: short-time diffusion → subdiffusion in a wide range of τ → long-time diffusion.

Long-time diffusion coefficient D_L

Comparison between the measured D_L and theoretical predictions

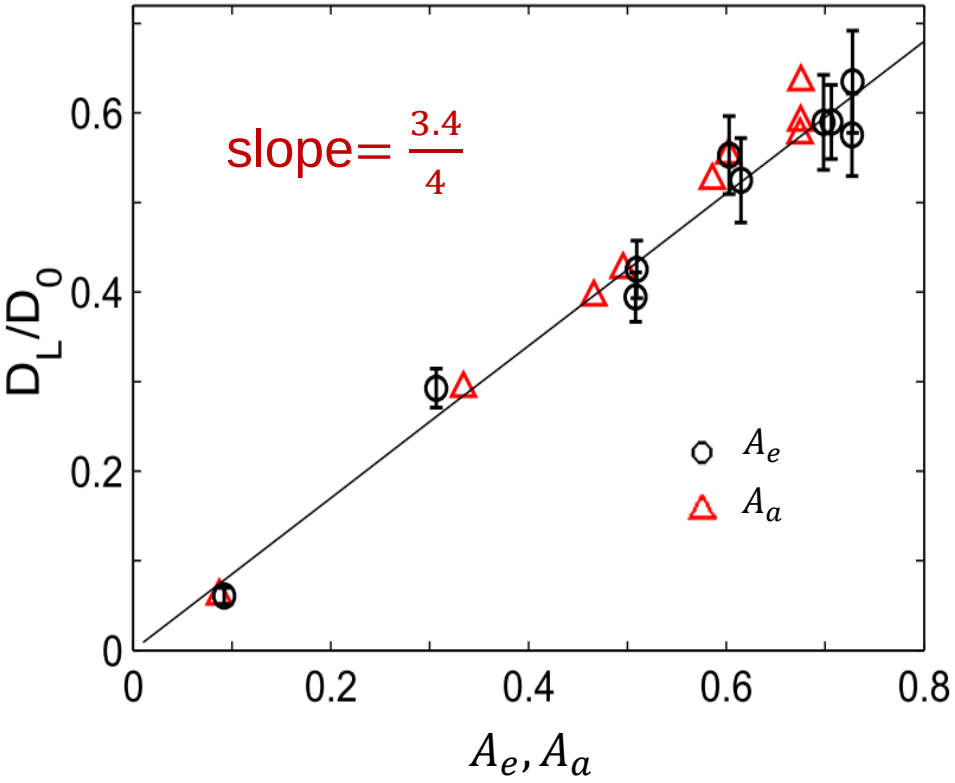

Exact result

$$\frac{D_L}{D_0} = \frac{n}{4}\frac{1}{\left\langle \exp\left(\frac{U}{k_B T}\right)\right\rangle_{path}\left\langle \exp\left(\frac{-U}{k_B T}\right)\right\rangle_{path}} = \frac{n}{4}A_e$$

Zwanzig, PNAS, 1988

Approximate result

$$\frac{D_L}{D_0} \approx \frac{n}{4}\frac{1}{\left\langle \frac{\exp(E_b/k_B T)}{E_b/k_B T+1}\right\rangle_{E_B}} = \frac{n}{4}A_a$$

$$\left\langle \frac{e^{E_b/k_B T}}{\nu_2(E_b)}\right\rangle_{E_b} = \int \frac{e^{E_b/k_B T}}{\nu_2(E_b)} H(E_b)\,dE_b$$

Su, *et al.*, Soft Matter **13**, 4773 (2017)

(iii) Diffusion over a quasicrystal lattice

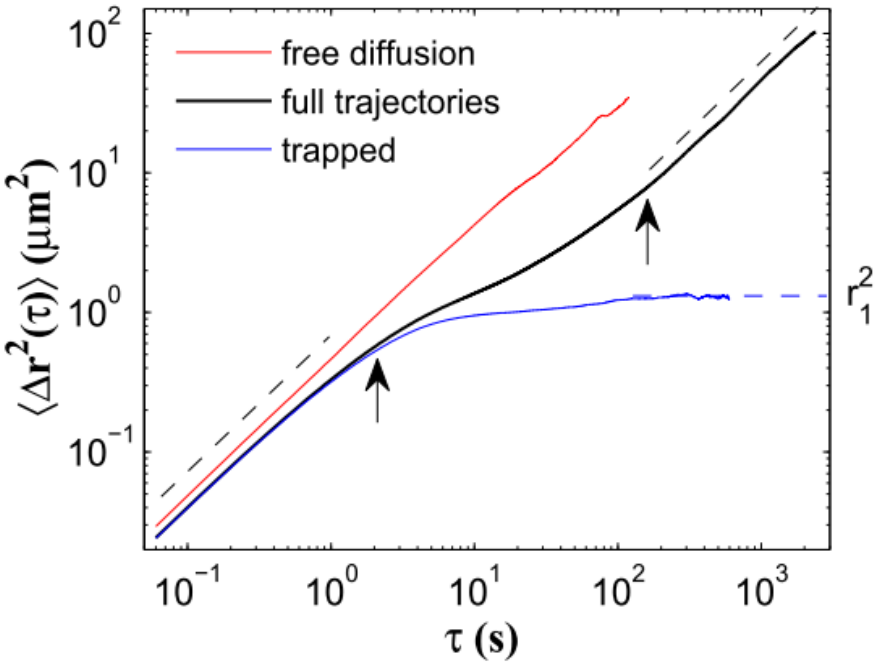

MSD of full trajectories exhibits a dual-crossover behavior owing to the transient confinement by the traps.

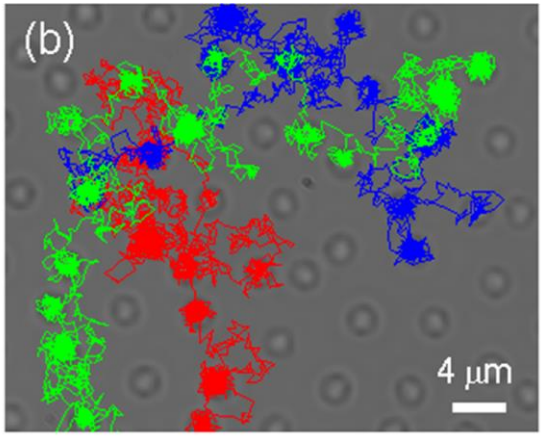

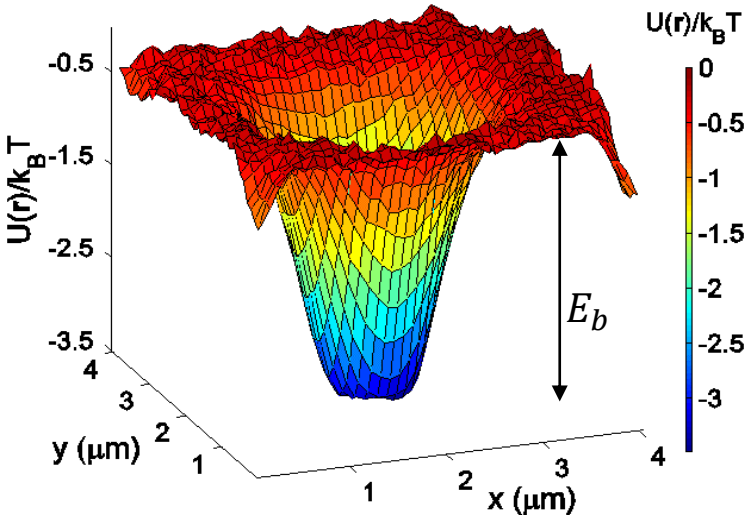

Trapping potential $U(x, y)$ obtained from the population probability distribution $P(x, y)$

Su, *et al.*, J. Chem. Phys. **146**, 214903 (2017)

MSD of full trajectories with increasing E_b

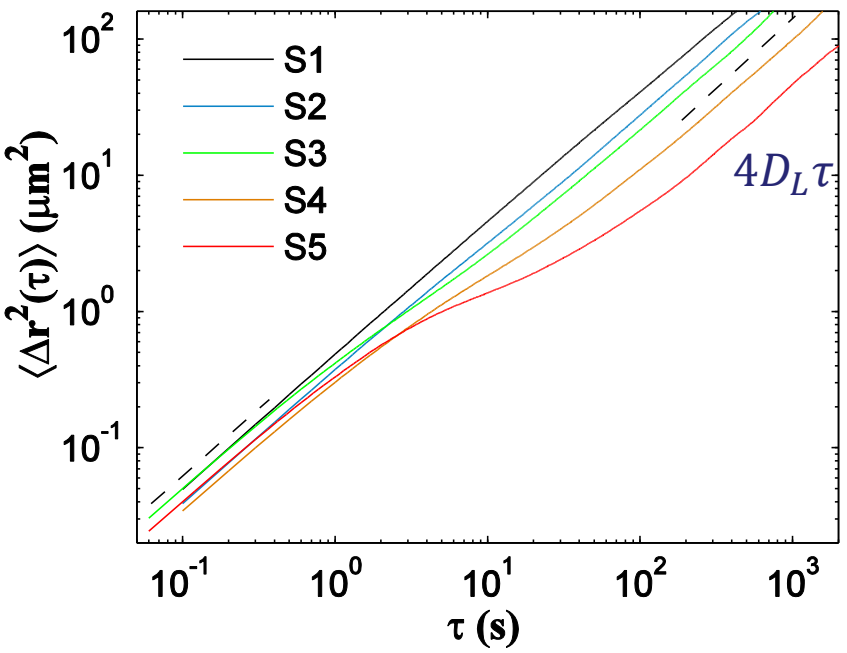

Comparison with the two-state model

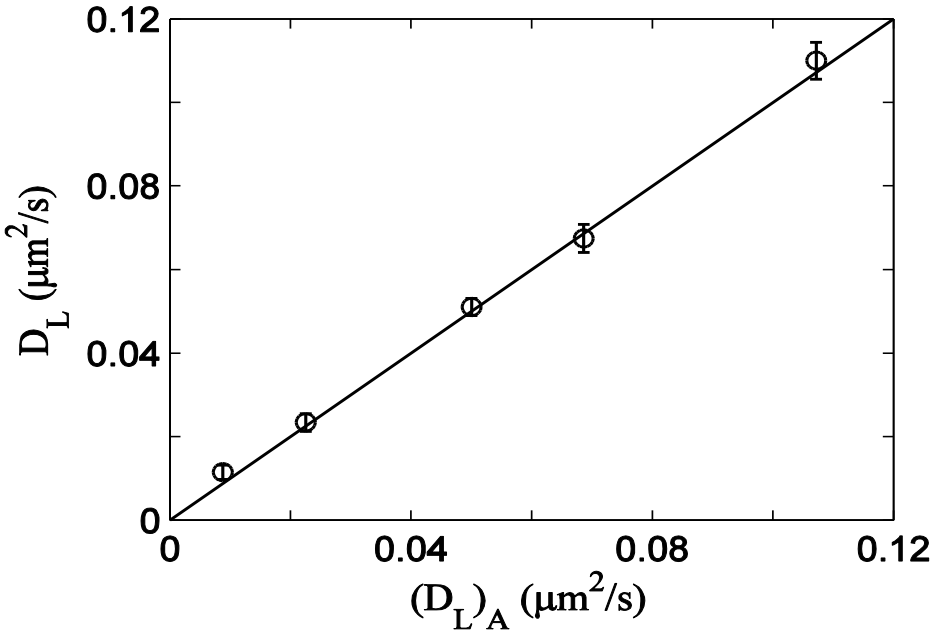

Larger E_b results in smaller D_L and longer subdiffusion region.

$$(D_L)_A = c_0 D_0 + c_1 D_1$$

$$= \frac{1}{1 + c_1/c_0} \left(D_0 + \frac{c_1}{c_0} \frac{r_1^2}{4\bar{t}_1}\right)$$

Su, *et al.*, J. Chem. Phys. **146**, 214903 (2017)

- The two-layer colloidal system is a useful platform for the study of colloidal transport and diffusion over different potential landscapes.
- Use of electric field, light intensity gradient, or lithographic template to generate interesting potentials.

Electrostatic ion traps for single-molecule electrometry

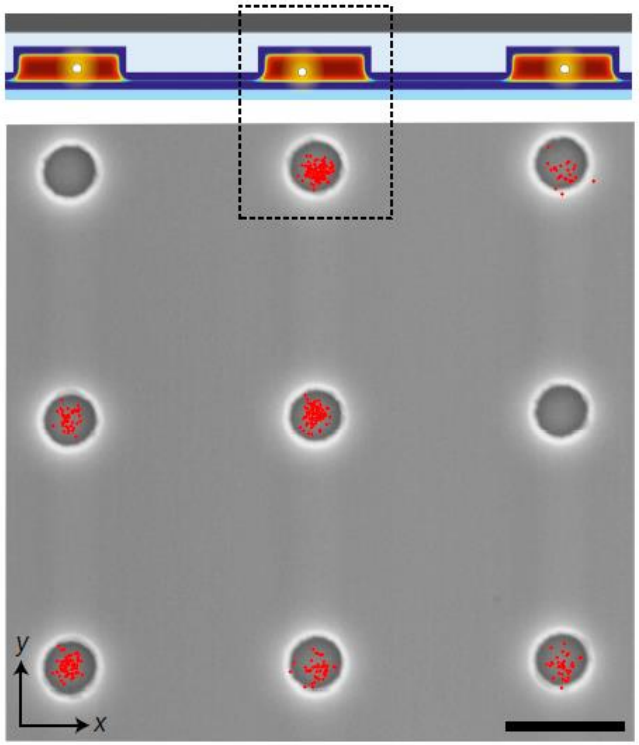

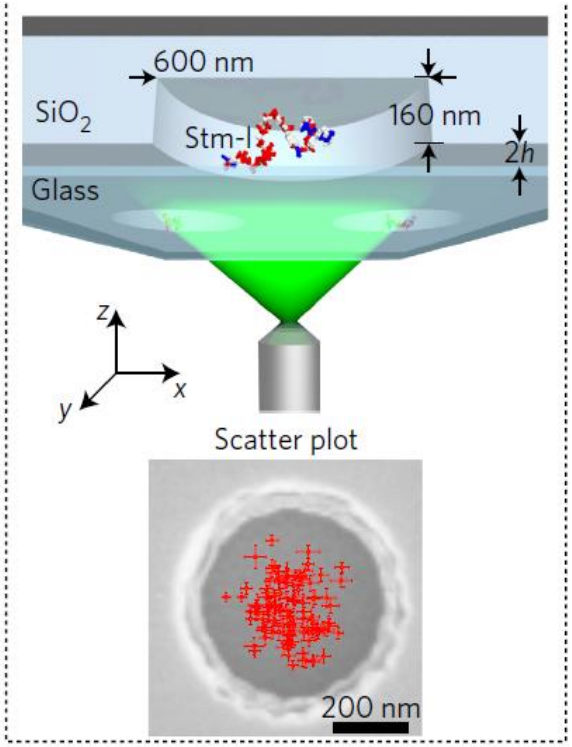

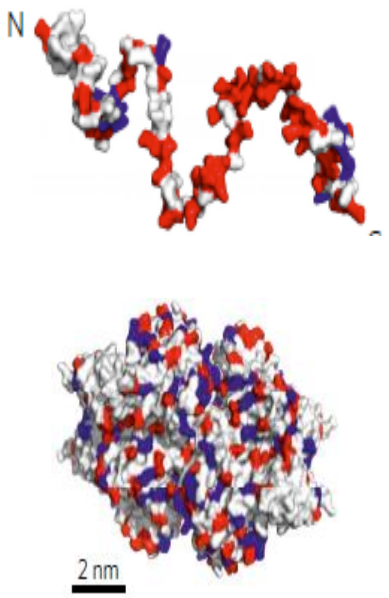

Krishnan et al., Nature Nanotechnology, 2017

4. New challenges for non-equilibrium (active and living) systems

- Most theoretical models for equilibrium systems are 1D, whereas the real environments of practical interest are often 2D and 3D.
- Disorder has many different forms, and the idealized theoretical models, such as the random barrier, random trap and continuous random walk models, may not apply to real experimental systems.
- Study of interesting non-equilibrium systems, in which detailed balance (DB) and Boltzmann statistics do not apply in general.

(i) Active colloids over complex potential landscapes

- Active colloids (self-propelled particles (SPPs) or Janus particles) can move autonomously through a viscous fluid by taking up energy from the surrounding environment and converting it into directed motion (micro/nano swimmers/robots).

- Active colloids exhibit a rich array of emergent behaviors that can be understood only within the framework of non-equilibrium physics.
- Applications of active colloids require physical understanding of their response to complex environments.
- Many theoretical models have been developed to describe the motion of SPPs in a trapping potential,

$$\frac{dx}{dt} = -\mu \nabla U(x) + v_0 \vec{u} + \sqrt{2D_0}\eta$$

The orientation vector $\mathbf{u}(\theta, \varphi)$ follows a stochastic equation that involves the persistence time τ_p of the Janus particles and varies among Run-and-Tumble particles (RTPs), Active Brownian particles (ABPs), and Active Ornstein-Uhlenbeck particles (AOUPs).

- Experiments with well-characterized SPPs are, therefore, very valuable in testing different ideas and providing new insights into the non-equilibrium statistical properties of active colloids.

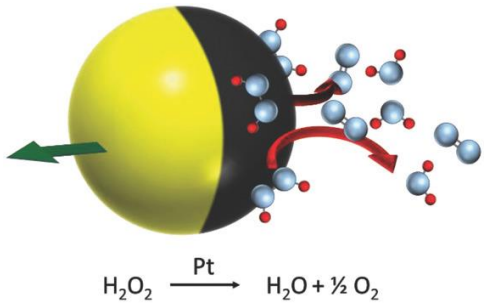

One candidate model system consists of silica or polystyrene micro-spheres half-coated with platinum (Pt) and suspended in hydrogen peroxide (H_2O_2).

Advanced Science, **5** (2), 2017, DOI: (10.1002/advs.201700528)

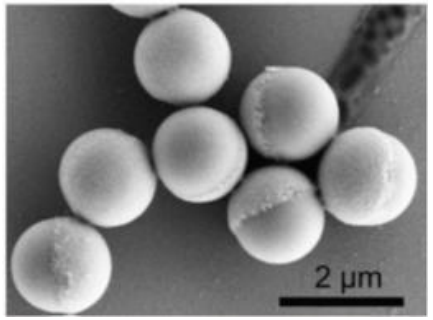

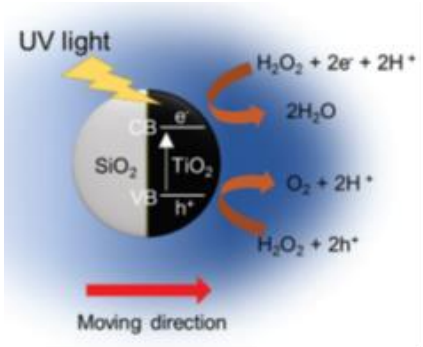

light-activated, self-propelled Janus spheres with a half cap of anatase TiO_2 coated on a silica (SiO_2). When dispersed in an aqueous solution of H_2O_2 (1.5%, pH ≈ 7), they exhibit self-propulsion under UV illumination ($\lambda \approx 365$ nm).

Singh, D. P., Choudhury, U., Fischer, P. & Mark, A. G. Adv. Mater. **29**, 1701328 (2017)
Mou, F., Li, Y., Chen, C., Li, W., Yin, Y., Ma, H. & Guan, J. Small **11**, 2564 (2015)

(ii) Protein diffusion on live cell membrane

Fluid mosaic model of Singer and Nicholson (1972)

Hydrodynamic model of Saffman and Delbrück (PNAS 1975)

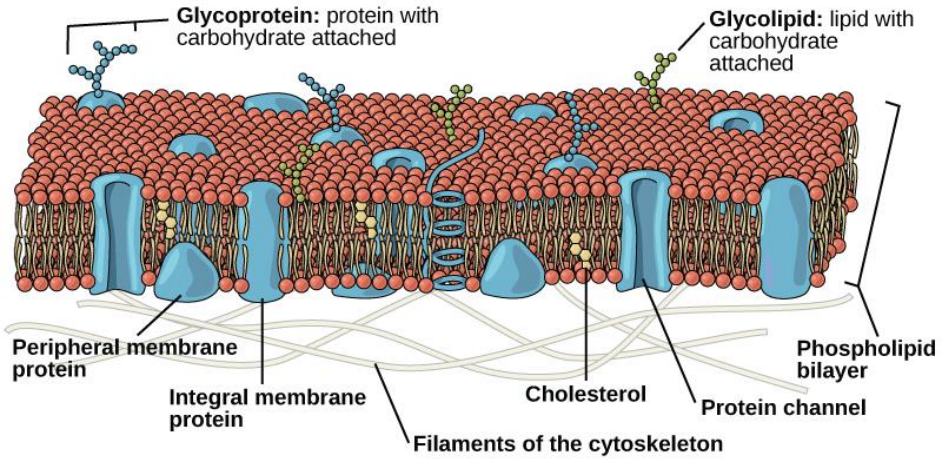

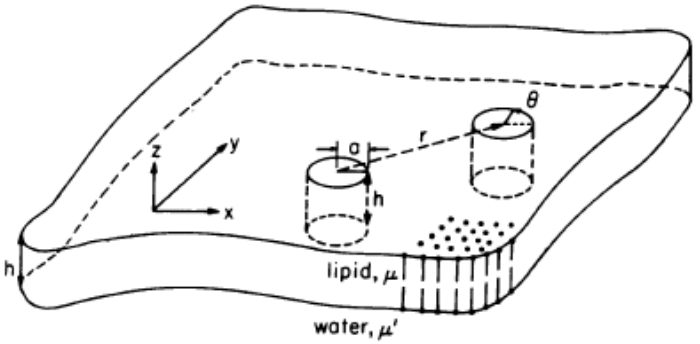

Protein motion in a viscous layer bounded by aqueous phases on both sides

$$D = \frac{k_B T}{4\pi\mu h}\left(\ln\frac{\mu h}{\mu' a} - 0.5772\right)$$

- Actual cell membranes are more mosaic than fluid. They display an intriguing array of structural and dynamic complexities of lipids/ cholesterols and various proteins.

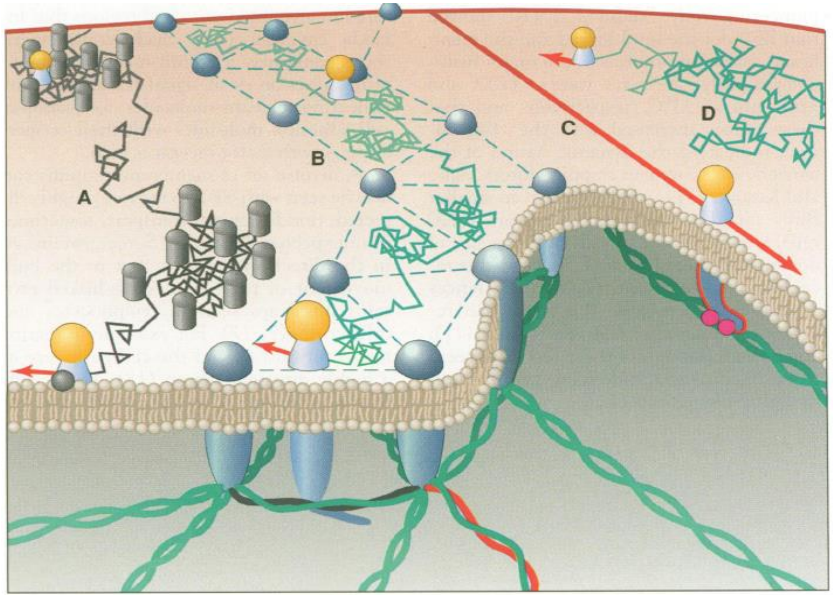

A: hindering by obstacle clusters
B: confinement by cytoskeleton traps (fences, 0.3-1 μm)
C: directed motion along microtubeles (motor driven)
D: free diffusion

Revision on Fluid Mosaic Model (Jacobson *et al.*, *Science*, 1995)

- Nature uses Brownian motion as a basic molecular process in many biochemical reactions and cellular signaling that sustain life. How does the Brownian motion function in this crowded and heterogeneous environment? Can we obtain structural information from single molecule dynamics?

5. Recent studies in three non-equilibrium systems

(1) Colloidal transport over a tilted periodic potential

Diffusive barrier crossing will become very rare if $E_b >> k_BT$. The energy barrier is lowered when an external force is applied to the particle. Force-assisted barrier crossing has been widely used in physics, chemistry and biology, such as single molecule force microscopy.

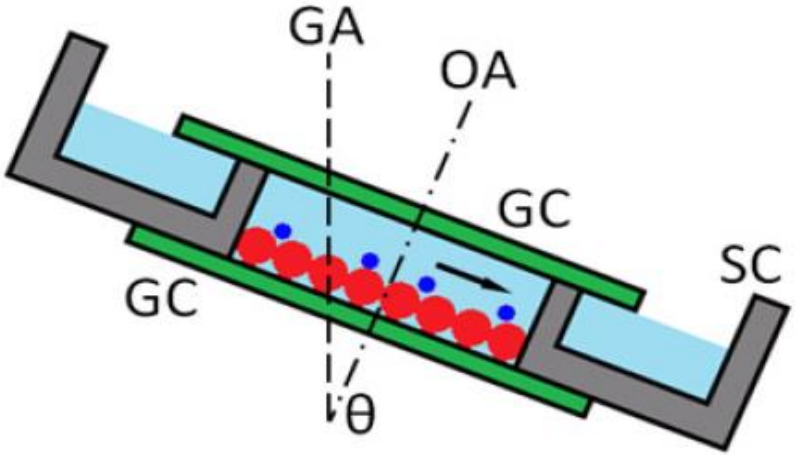

Experimental setup

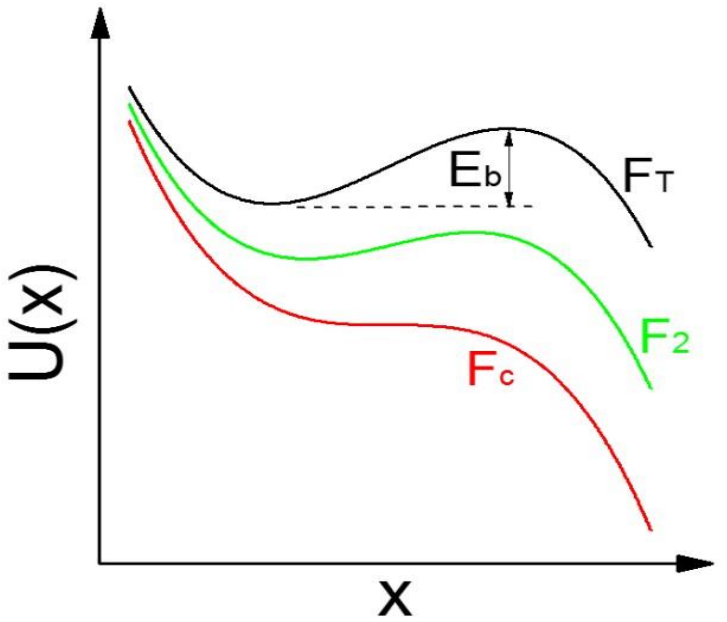

Gravitational force on the top layer particle, $F(\theta) = \Delta m\, g \sin\theta$

$$U(x) = U_0(x) - Fx$$

Single-molecule force microscopy widely used in biology

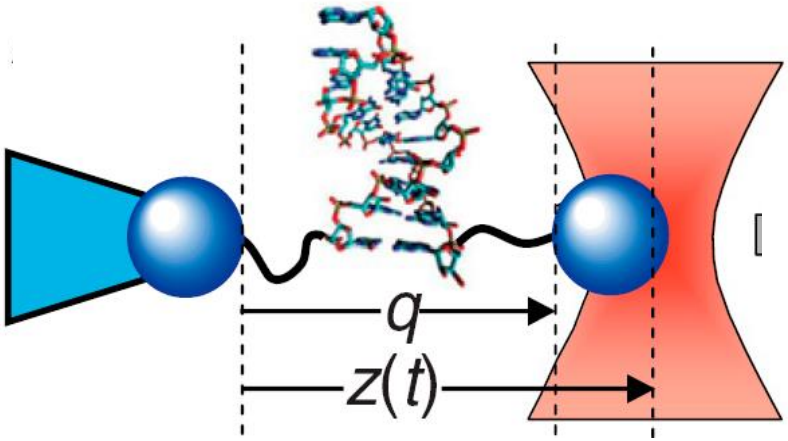

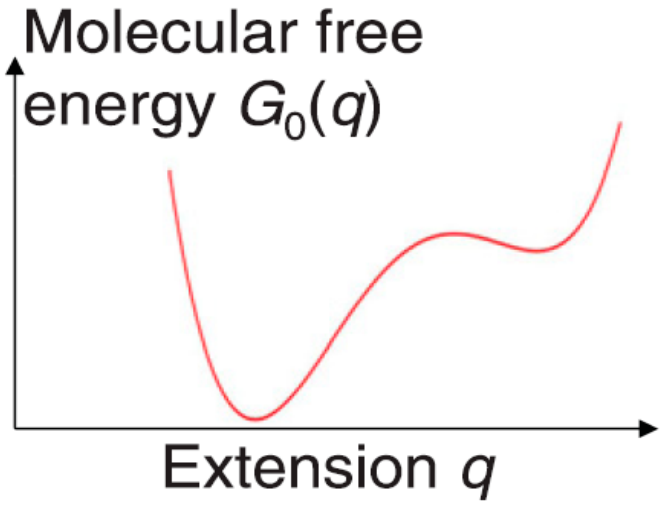

Hummer et al., PNAS (2010)

How to find the (unknown) free-energy landscape from a single-molecule pulling experiment?

Measurements of the trajectory, velocity, and diffusion coefficient of the top diffusing particles

$$G(\Delta x,\tau) \sim \exp[-\frac{1}{2}\frac{(\Delta x - v\tau)^2}{2D_S\tau}]$$

F in the [1,1] direction

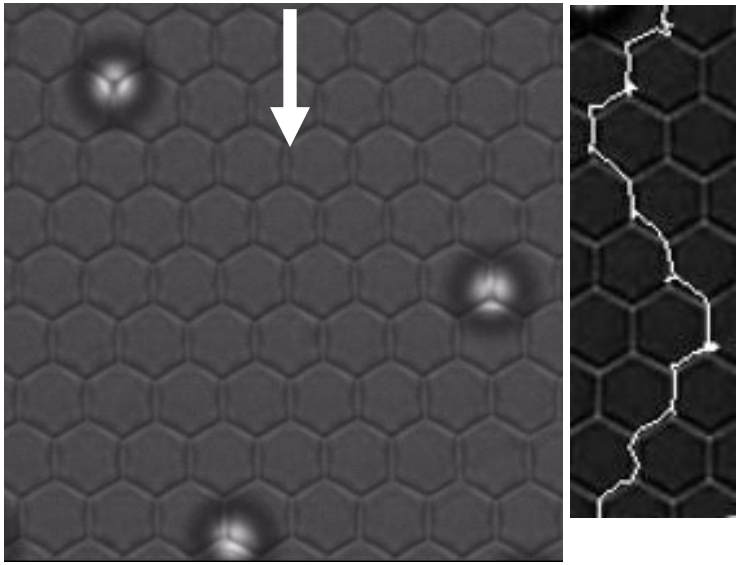

Measured particle trajectories for sample S2 with $E_b/k_BT \approx 6.7$

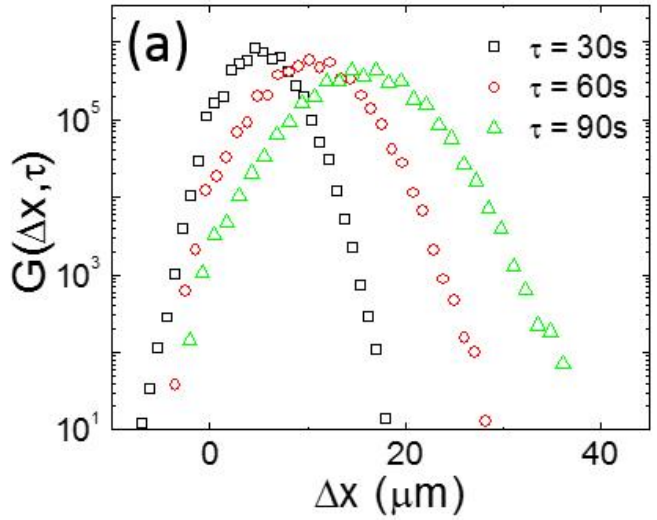

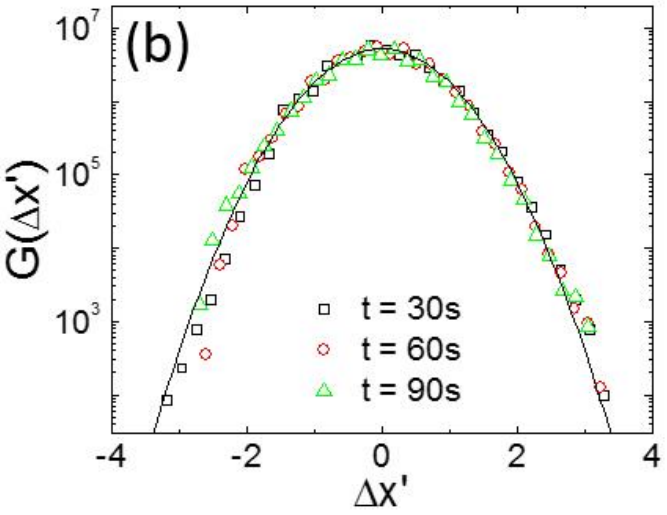

$$\Delta x(\tau) = x(t+\tau) - x(t)$$

$$v = \frac{\langle \Delta x(\tau)\rangle}{\tau};\quad \langle \Delta x^2(\tau)\rangle = 2D_S\tau$$

Measured mean drift velocity v/v_t as a function of the applied force F/F_t, where $v_t = D_0/\lambda$ is a velocity unit with D_0 being the free diffusion with no tilt ($\theta = 0$) and $F_t = k_B T/\lambda$ is a force unit (thermal force).

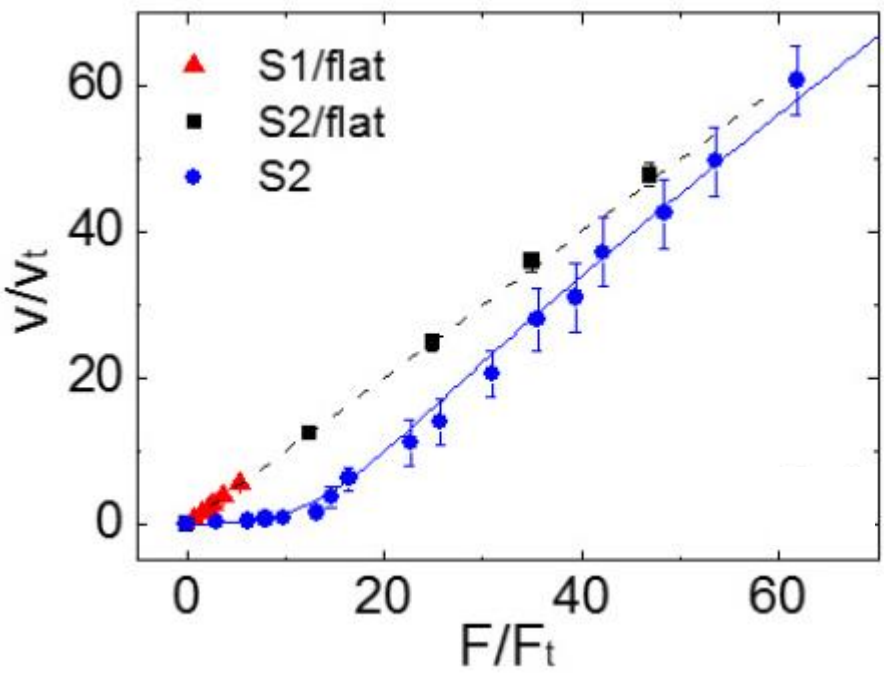

$$v = \frac{D_0}{\lambda}\frac{1-e^{F/F_\lambda}}{\frac{1}{\lambda}\int_0^\lambda dx I_+(x)}$$

$$I_+(x) = \frac{1}{\lambda}\int_0^\lambda dy e^{[U(x)-U(x-y)]/k_B T}$$

Stratonovich, Radiotekh. Elecktron. (1958)

- Because of constant forcing, the mean velocity v (or particle flux) $\neq 0$ (which breaks the detailed balance)
- Measured v/v_t is significantly hindered by the underlying energy landscape $U_0(x)$.

(i) When F is mall, one can expand v in powers of F/F_t:

$$\mathrm{v} = \frac{F}{\xi_0 \langle e^{U(x)/k_BT} \rangle_\lambda \langle e^{-U(x)/k_BT} \rangle_\lambda} \simeq \frac{F}{(\xi_0 / \nu) e^{E_b/k_BT}}$$

Solution of washboard potential with $\xi_{eff} \approx (\xi_0 / \nu) e^{E_b/k_BT}$

(ii) In the intermediate force range, $F_t < F < F_c$, we find v (and D) are of Arrhenius-Kramers form,

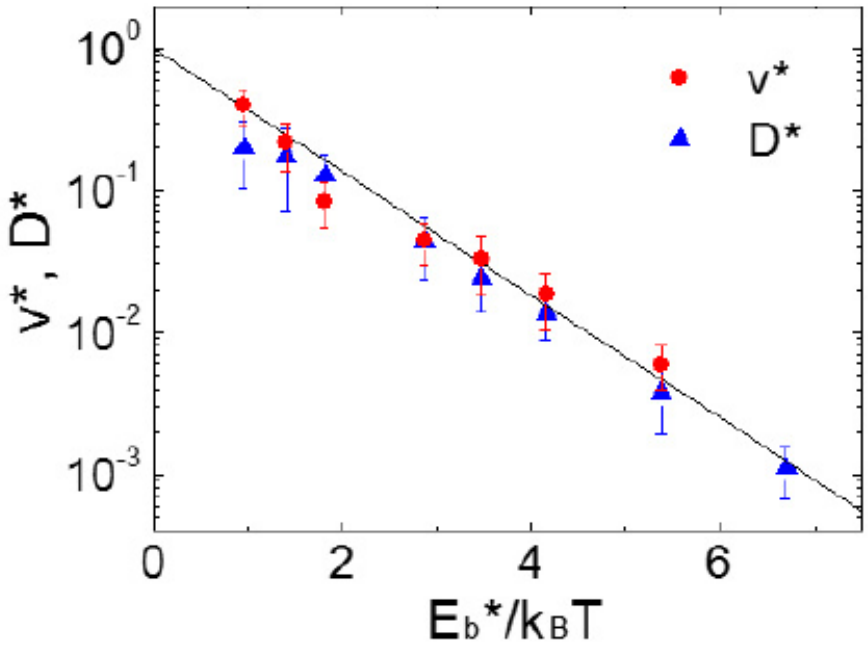

$$\mathrm{v} = \frac{F_c}{\xi} \nu'(F) \, \mathrm{e}^{-E_b^*(F)/k_BT}$$

$$\nu'(F) \approx \left[1 - \left(\frac{F}{F_c} \right)^2 \right]^{1/2}$$

$$E_b^*(F) \approx E_b \left(1 - \frac{F}{F_c} \right)^{3/2}$$

Normalized plot with $v^* = v/[v_c \nu'(F)]$ Ma *et al.*, Soft Matter, **11**, 1182 (2015)

(iii) "Phase diagram" of force-assisted particle flux

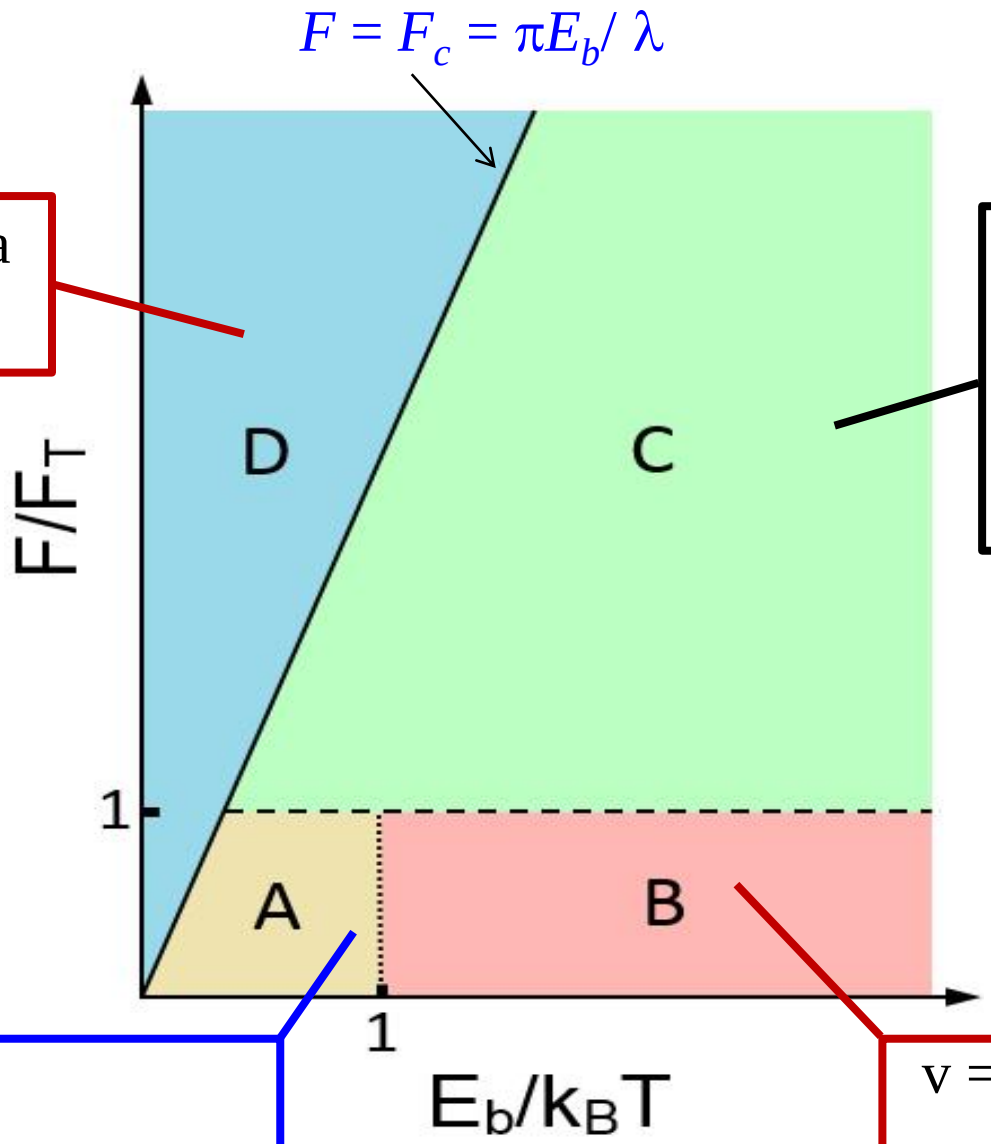

v = F/ξ_0 for a flat incline

v = $(F_c/\xi_0)\nu'(F)$ exp[$-E_b^*(F)/k_BT$]

modified Arrhenius-Kramers form

v = $F/(\xi_0 R)$

$R = \langle e^{-U(x)/k_BT} \rangle \langle e^{U(x)/k_BT} \rangle$

v = $(F/\xi_0)\nu$ exp[$-E_b/k_BT$]

Arrhenius-Kramers form

(iv) Equilibrium and non-equilibrium population PDFs, $P_{ls}(x)$ and $P_{ss}(x)$

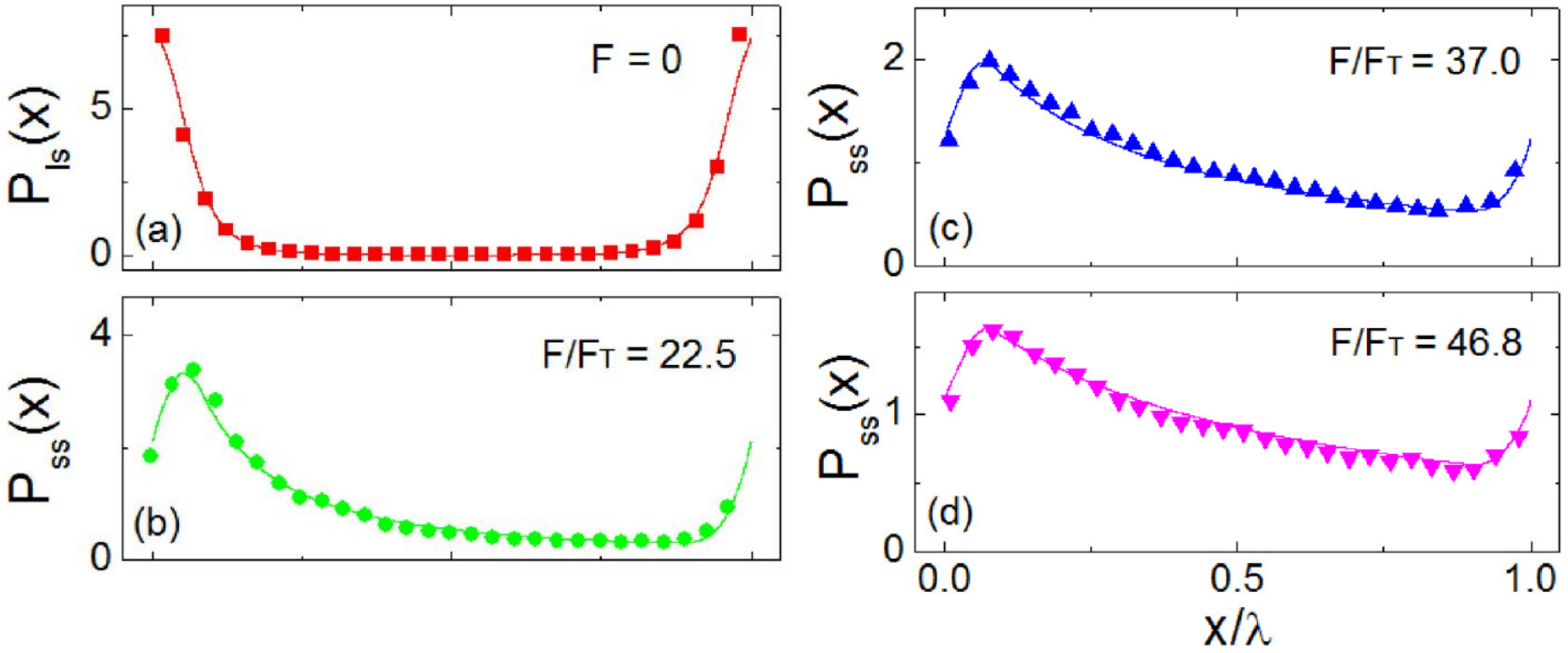

Measured $P_{ss}(x)$ becomes more asymmetric and shows more deviations from the Boltzmann distribution with increasing F.

Ma *et al.*, Phys. Rev. E **91**, 042306 (2015)

(v) Reconstructed equilibrium potential $U_0(X)$ (or Boltzmann distribution $P_B(X)$) from the steady-state PDF $P_{ss}(X)$ and flux J_{ss}

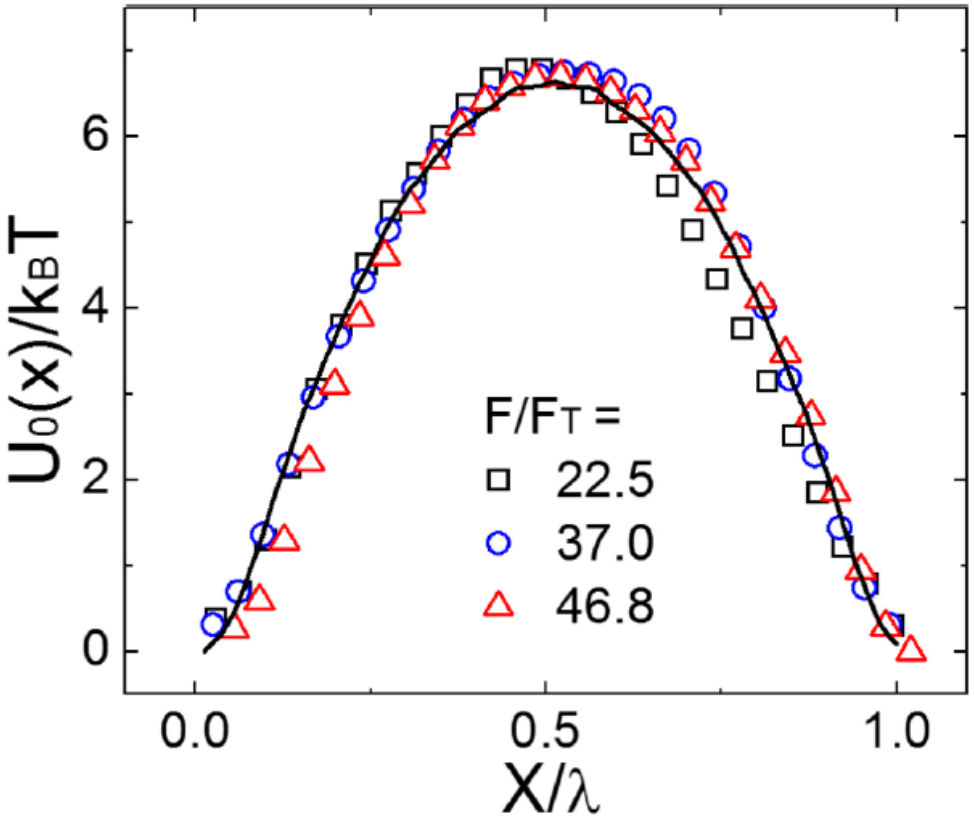

$$\frac{U(x)-U(0)}{k_BT} = -\ln\frac{P_{ss}(x)}{P_{ss}(0)} - \frac{J_{ss}}{\lambda}\int_0^x \frac{dy}{P_{ss}(y)}$$

with $U(x) = U_0(x) - Fx$

Ma *et al.*, Phys. Rev. E **91**, 042306 (2015)

(vi) Comparison between the measured and calculated barrier heights $E_b^*(F)$ as a function of F/F_c

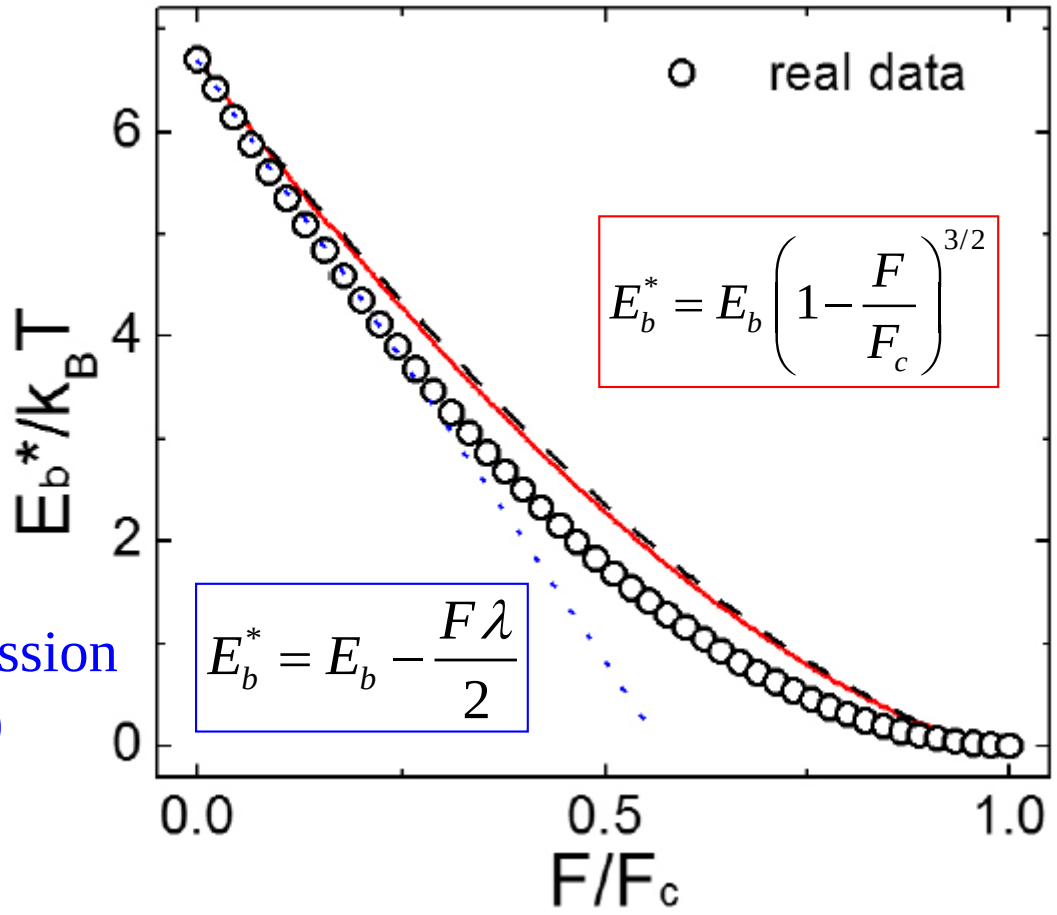

Garg's expression (dashed line)

Bell's expression (dotted line)

Experimentally obtained E_b^* using the measured $U(x) = U_0(x) - Fx$

What we learned from this work

The two-layer colloidal system is a useful platform for the study of colloidal transport and diffusion over different potential landscapes. It opens the door to studying a wide range of interesting problems associated with the non-equilibrium population PDF and escape dynamics of both passive and active colloids in complex environments.

- Use of electric field, light intensity gradient, or lithographic template to generate interesting potentials, such as those with hierarchical structures.
- Use of the obtained particle trajectories to study interesting properties of non-equilibrium dynamics and to test different theoretical predications, such as the fluctuation theorems and hidden Markov models with and without external (dc and ac) forces.
- Study of concentration effects from single particle to many particles and directed self-assembly.
- Study of shape effects of diffusing particles from dimers to polymer chains, such as DNA chains.
- Development of useful protocols for effective sampling of rare events.

- Measurement of forward and backward transition probabilities and entropy production rate in a tilted potential

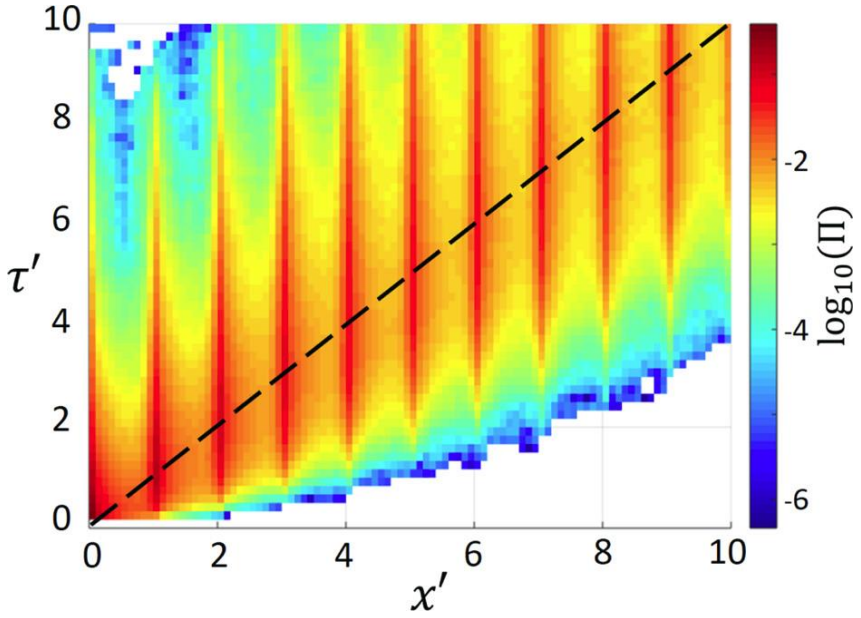

DB-like relation:

$$\frac{\Pi(x_1, x_2, \tau)}{\Pi(x_2, x_1, \tau)} = e^{-[U(x_2)-U(x_1)]/k_B T}$$

with $U(x) = U_0(x) - Fx$

Phys. Rev. E **96**, 012601 (2017)

Measured forward transition probability:

$\Pi(0, x', \tau')$ with x' = x/λ and $\tau' = \tau / (\lambda / v)$

For equilibrium processes, we have $P(x_1)\Pi(x_1, x_2, \tau) = P(x_2)\Pi(x_2, x_1, \tau)$.

$$\frac{\Pi(x_1, x_2, \tau)}{\Pi(x_2, x_1, \tau)} = \frac{P_B(x_2)}{P_B(x_1)} = e^{-[U_0(x_2)-U_0(x_1)]/k_B T}$$

(2) Dynamics of self-propelled colloids over parallel microgrooves

Self-propulsion force: $\boldsymbol{F} = F_0\,\mathbf{u}(\theta, \varphi)$ $= (v_0/\mu)\mathbf{u}$, with a persistence time τ_p

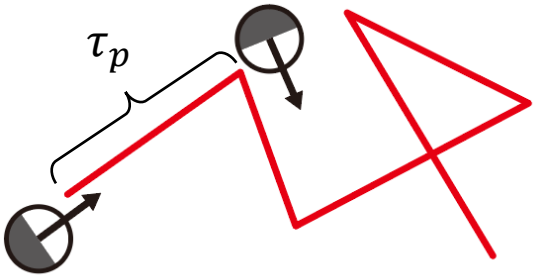

Travelling time τ_0 inside the confining force, $F_e = -dU_0(x)/dx$

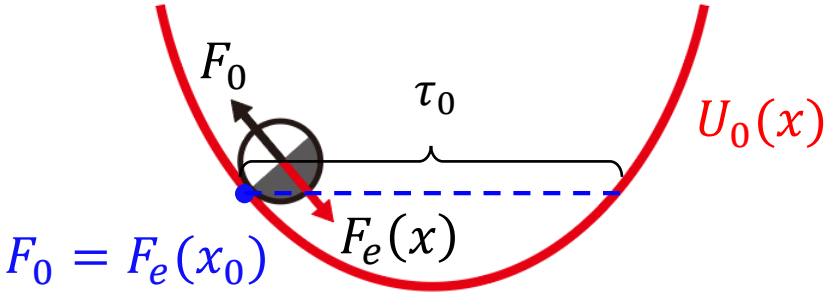

Two dynamically distinct states:

$\tau_p \gg \tau_0$: particle accumulation occurs at the force balance locations

$\tau_p \ll \tau_0$: elevated effective temperature

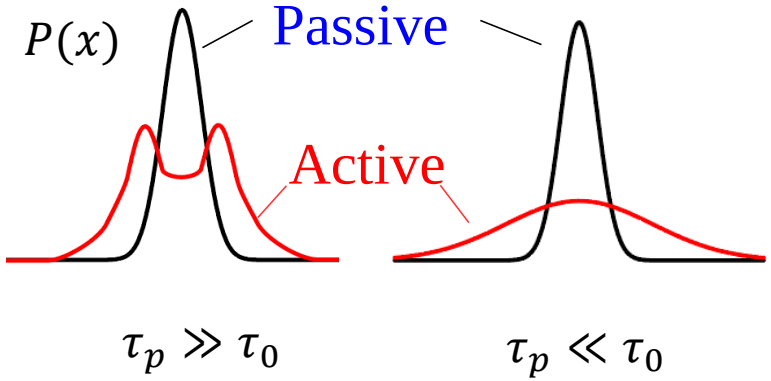

- This is a well-controlled experimental systems with the lateral motion of SPPs across a groove being confined but the longitudinal motion along the groove is unrestricted.

Why do we want to study self-propelled particles (SPPs) in complex environments?

(a) Simplified model systems for the study of physics of living systems:

- bacteria in natural habitats
- motor proteins in a living cell

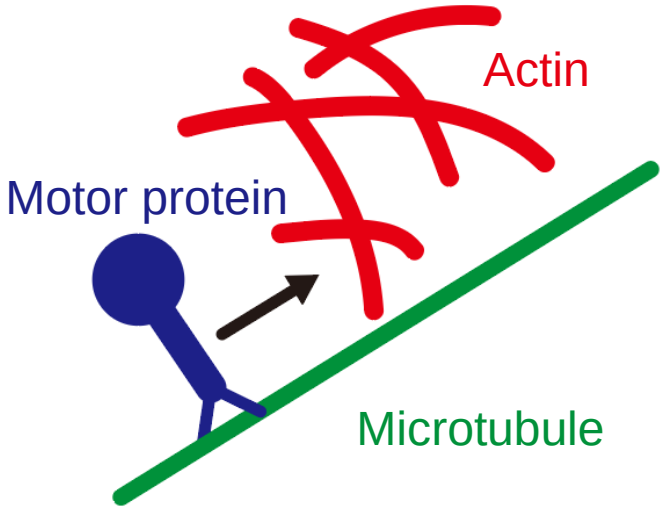

(b) Better understanding for applications of SPPs:

- directed cargo transport
- drug delivery

(c) New insights into non-equilibrium physics

(i) Experiment methods

Generation of a periodic potential for SPPs

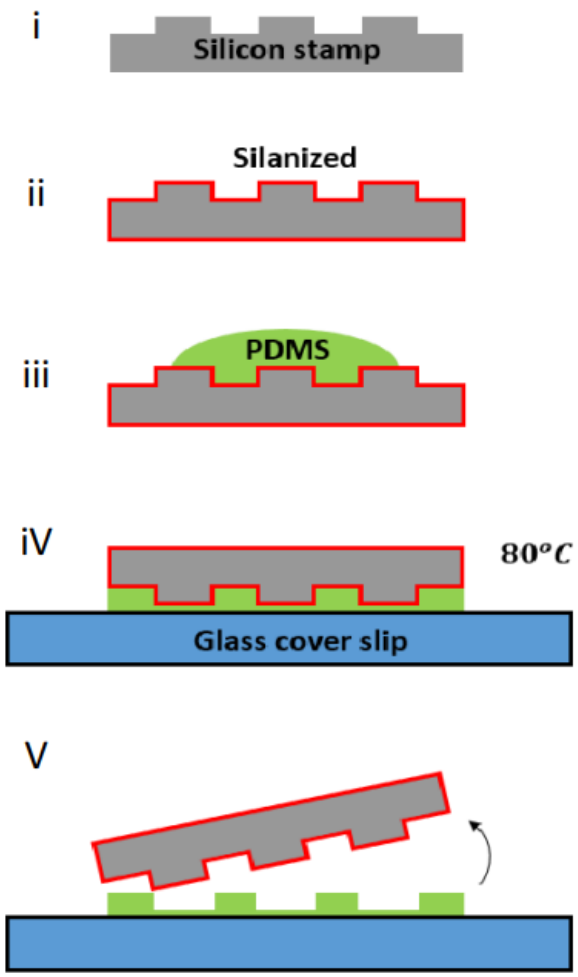

- Photolithography is used to construct a microgroove-patterned polydimethyl-siloxane (PDMS) substrate.
- The rugged surface of the substrate provides a gravitational potential $U_0(x)$ for SPPs.

Side view of the sample cell

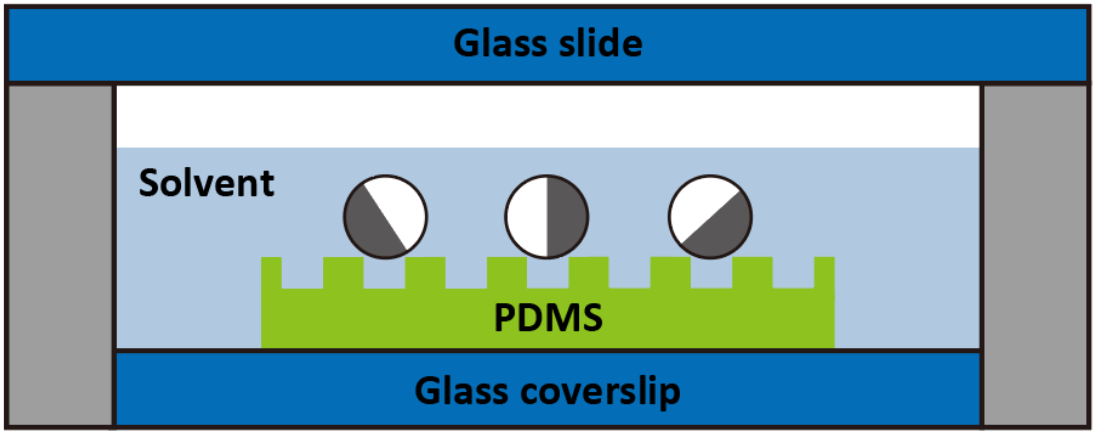

Single-particle tracking under an inverted microscope

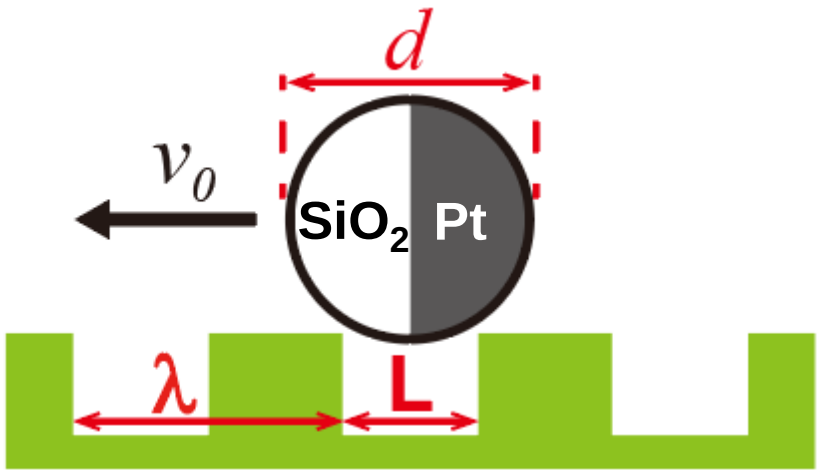

Pt-SiO_2 Janus particles in the H_2O_2 solution are used in the experiment

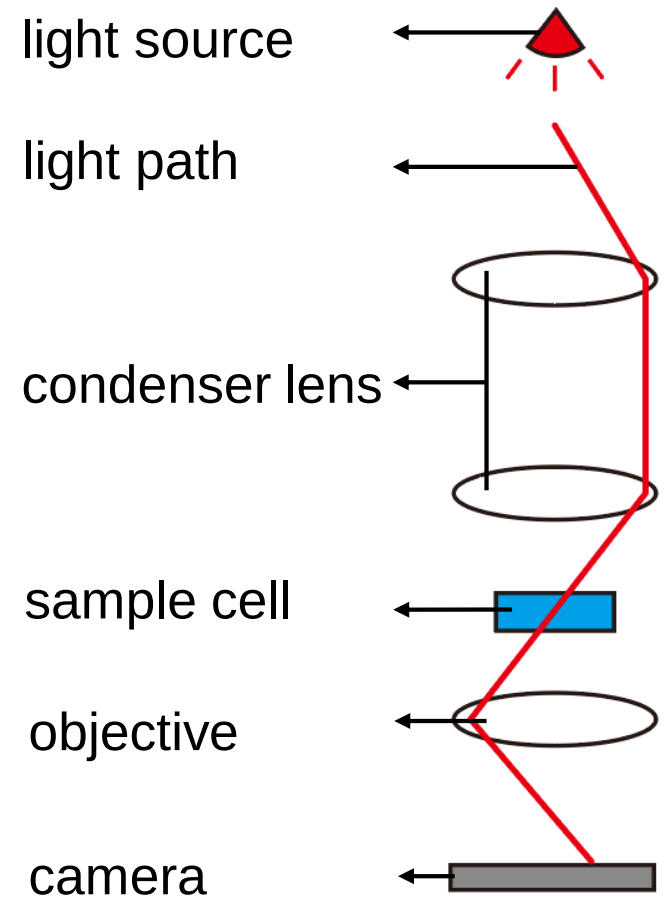

Sample	$d\ (\mu m)$	$L\ (\mu m)$	$\lambda\ (\mu m)$	$\tau_p\ (s)$
S1	2.96	1	2	11
S2	2.4	2	3	6.5

(ii) Experimental results

Active state:

Pt-SiO_2 Janus particles
in 0.2 w/w% H_2O_2 solution

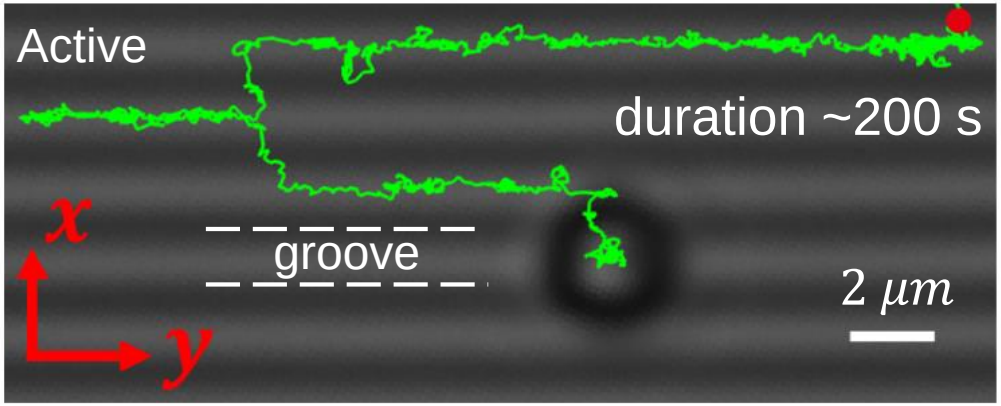

Passive state:

Pt-SiO_2 Janus particles
in water

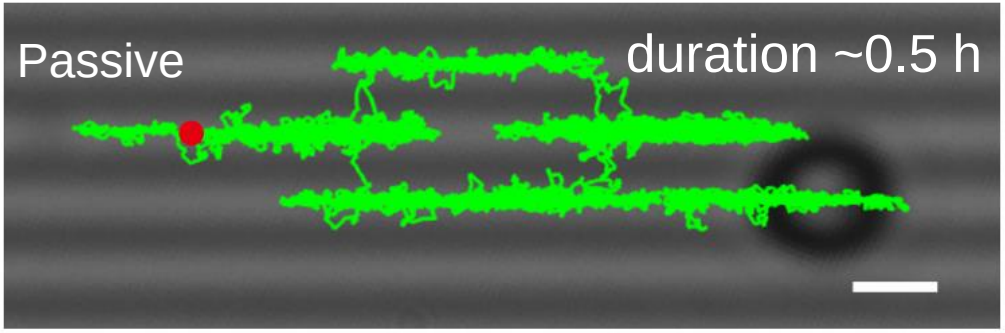

- Because of the spatial confinement imposed by the microgrooves, the lateral motion of the Janus particles in the *x*-direction is confined with occasional hopping.
- Particle's motion along the *y*-axis parallel to the microgroove is unrestricted.

(a) Mean-squared displacement (MSD) along the microgroove

- Trajectory-based velocity v_{0i}: $\frac{d\langle \Delta y^2(\tau)\rangle_i}{d\tau} = 2D_0 + \frac{2}{3}v_{0i}^2\tau$
- Trajectories are divided into different subgroups based on a common set of velocity bins (real-time calibration).
- The ensemble averaged v_0 for each subgroup:

$$\langle \Delta y^2(\tau)\rangle = 2D_0\tau + \frac{2}{3}v_0^2\tau_p[\tau + \tau_p(e^{-\tau/\tau_p} - 1)]$$

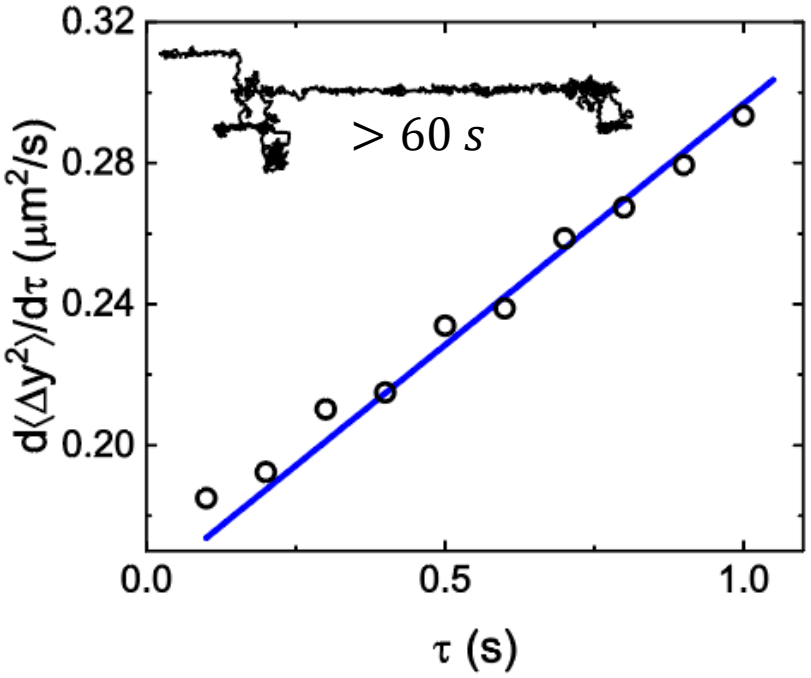

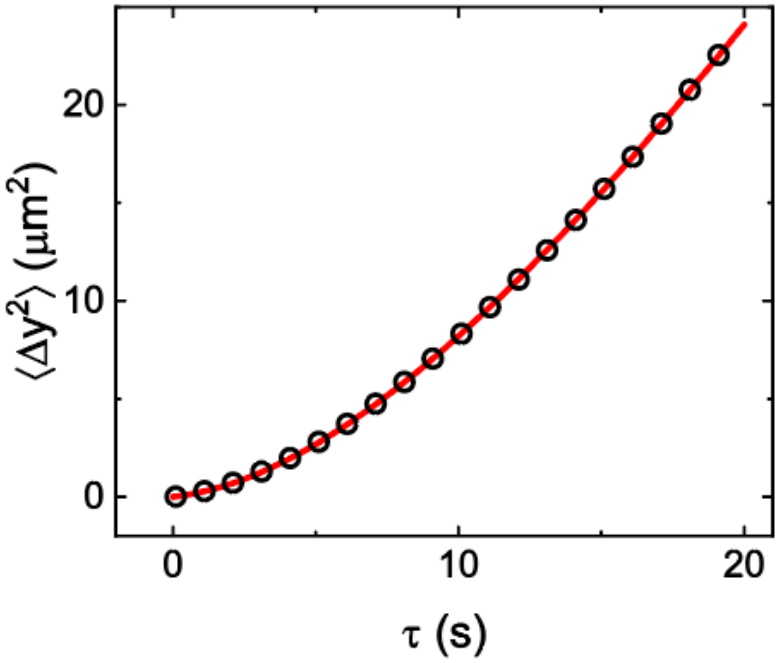

(b) Effective potential in the x-direction normal to microgroove

Probability density function (PDF) $P(x; v_0)$

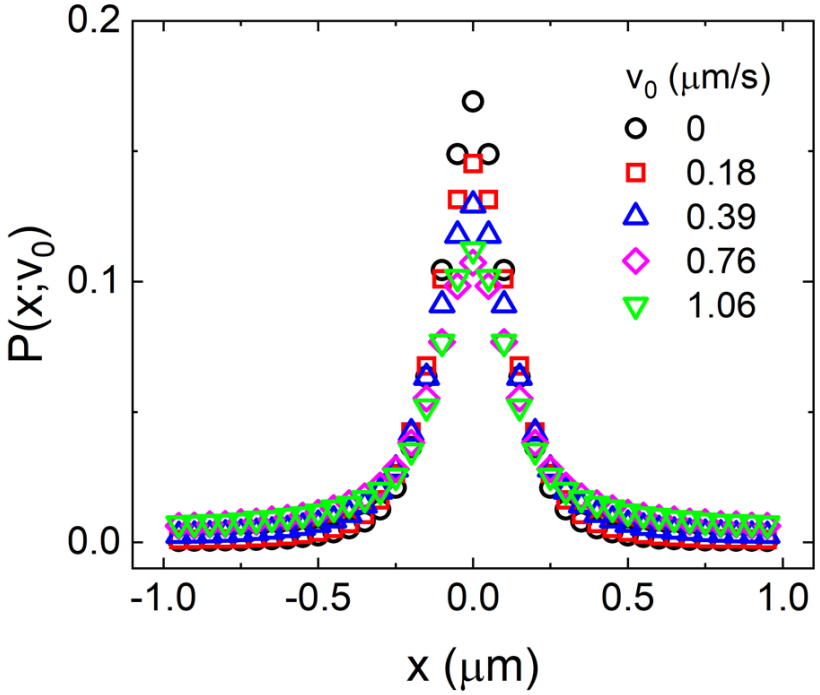

Effective potential $\frac{U_{\text{eff}}(x;v_0)}{k_B T} \equiv -\ln P(x; v_0)$

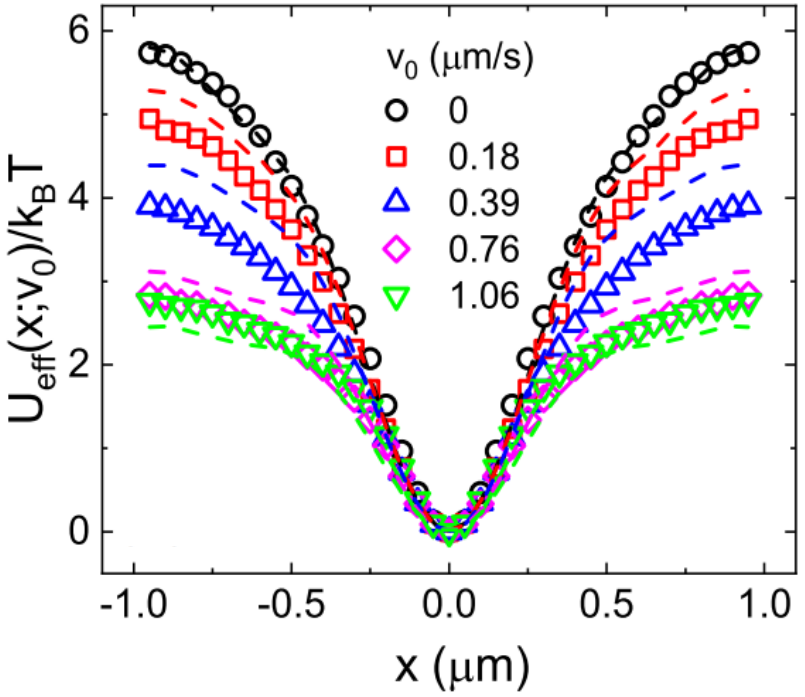

- Barrier height $E_b(v_0) \equiv U_{\text{eff}}(\lambda/2; v_0)$ decreases with v_0 for $v_0 \leq 0.76\ \mu m/s$.
- No particle accumulation is observed.
- Numerical simulations for run-and-tumble particles (dashed lines) agree with the experimental results.

Fixed angle approximation

When the particle's orientation remains unchanged during an escape attempt, i.e., when $\tau_p \gg t_0 \equiv k_B T/(kD_0)$:

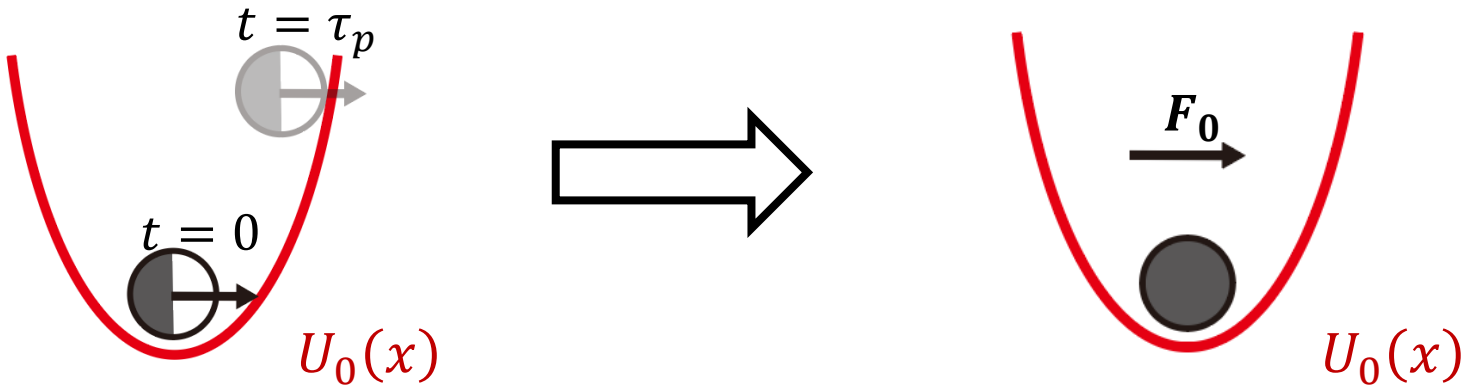

Self-propulsion force $F_0 = v_0/\mu$ can assist the Janus particles to hop over the free-energy barrier imposed by the external potential $U_0(x)$.

Similar to passive particles under an external force F_0, which lowers the energy barrier.

Measured barrier height difference $\Delta E_b(v_0) = U_{\mathrm{b}}(0) - U_{\mathrm{b}}\left(\frac{\lambda}{2}; v_0\right)$

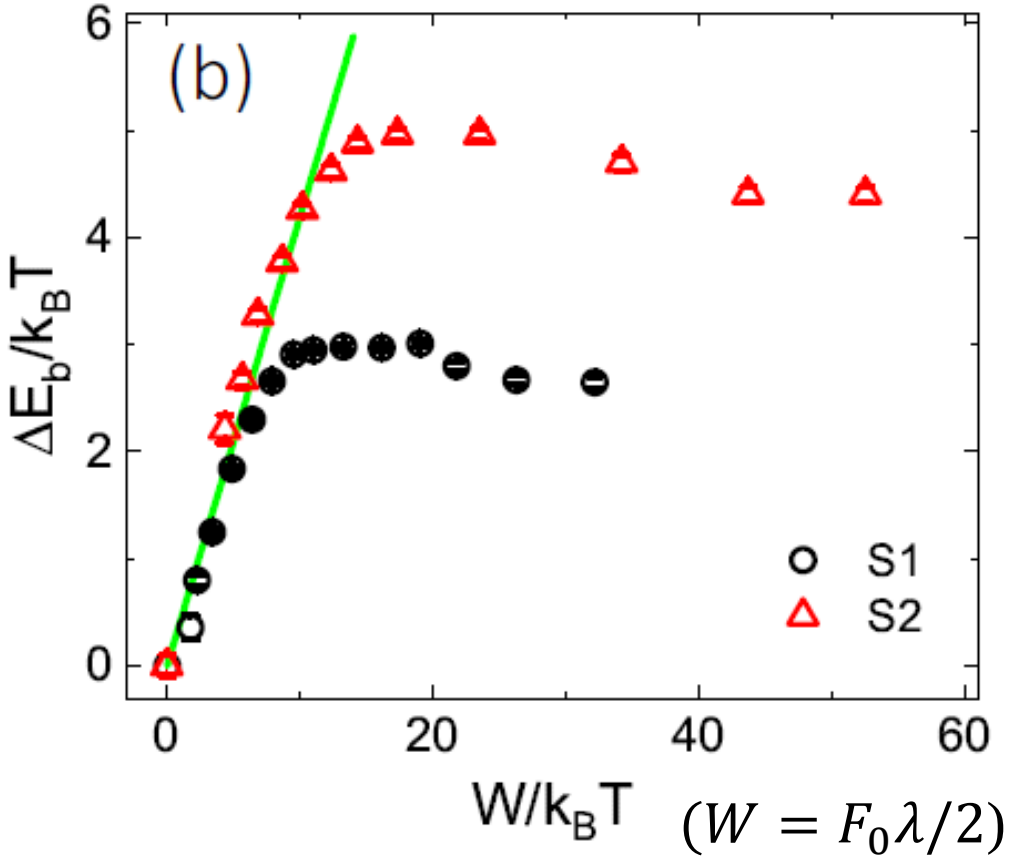

$(W = F_0\lambda/2)$

Measured barrier height difference $\Delta E_b = aW$ with the fitted value $a = 0.42$ very close to the predicted value $a = 0.41$.

Reconstructed potential $U_0(x) = U_{\text{eff}}(x; v_0) + aF_0|x|$

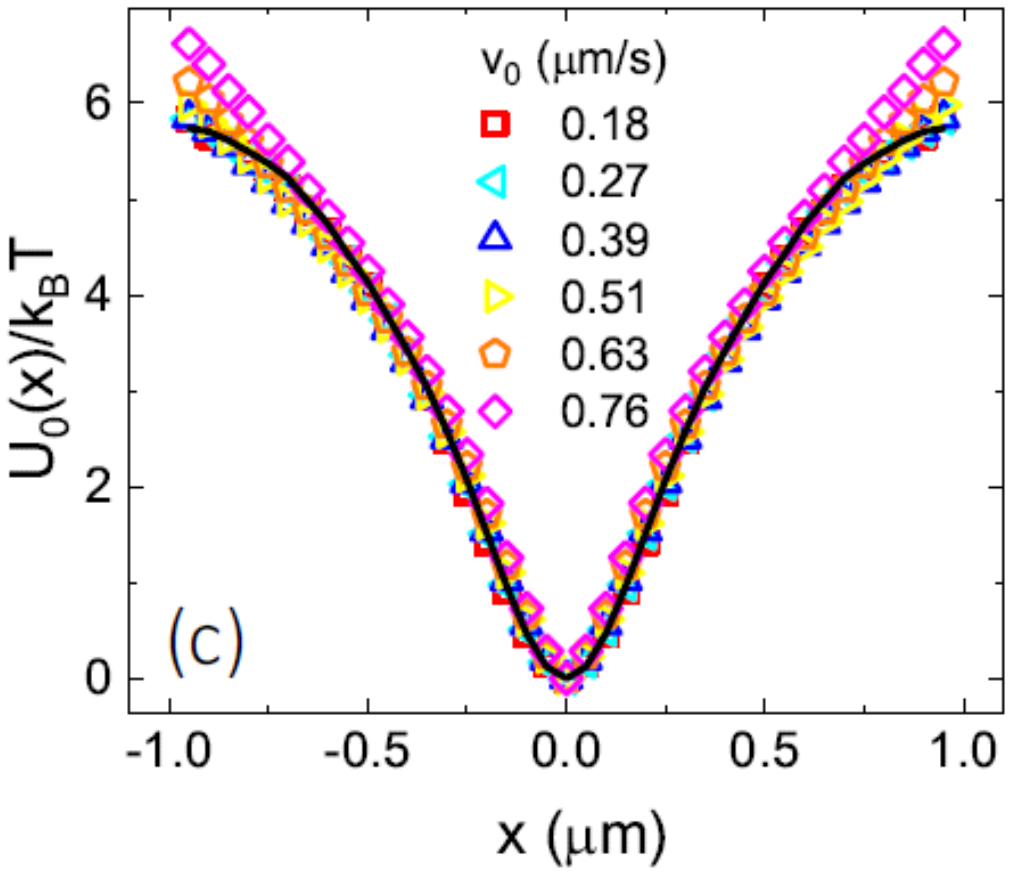

Reconstructed potential $U_0(x)$ has a scaling form independent of v_0 (black solid line), in good agreement with theory.

(c) Dwell time t_d for a SPP to stay in the same groove

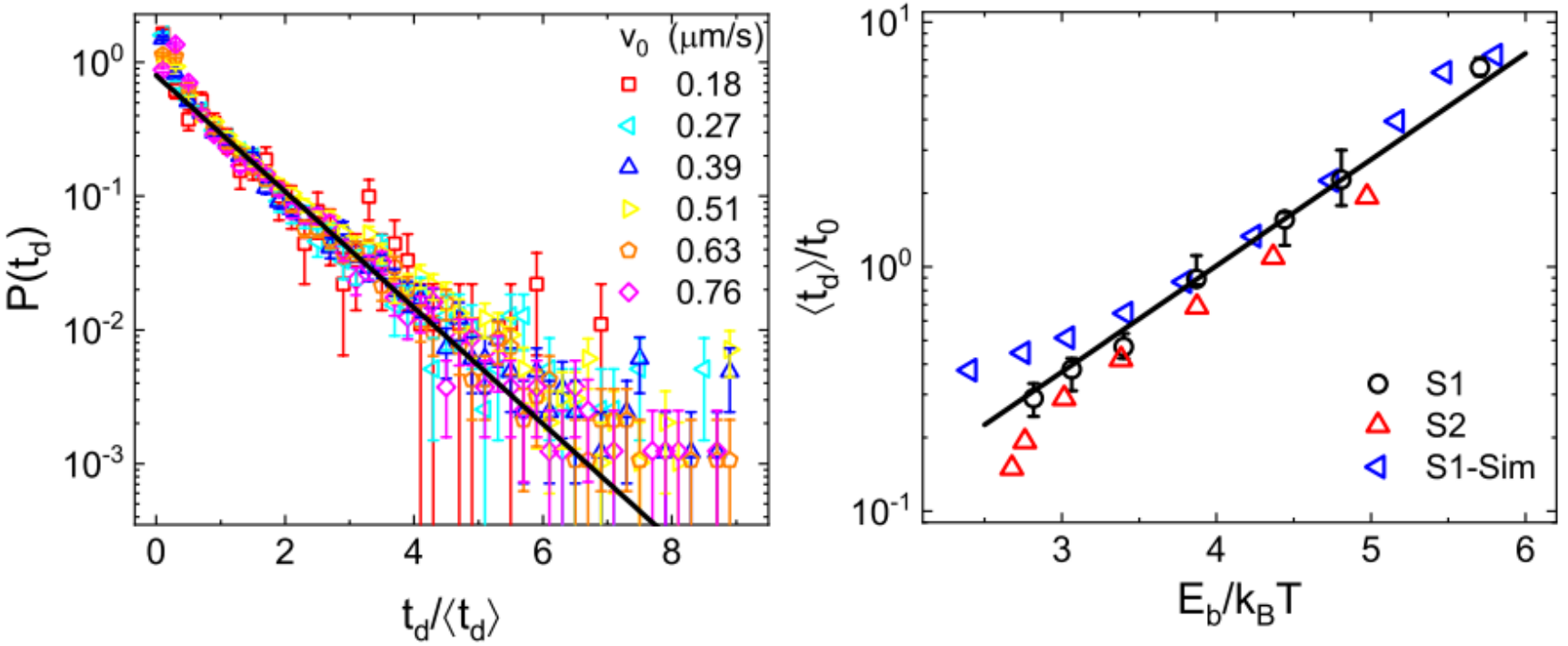

- PDF of the dwell time t_d: $P(t_d) \propto \exp(-t_d/\langle t_d\rangle)$
- The mean dwell time $\langle t_d\rangle/t_0$ with t_0 being the diffusion time follows a Kramers-like relation: $\langle t_d\rangle/t_0 \propto \exp(E_b(v_0)/k_BT)$

(d) Examination of particles accumulation

Langevin equation for the Brownian dynamics simulations of run-and-tumble particles (RTPs):

$$\dot{\boldsymbol{r}} = v_0\hat{\boldsymbol{u}} - \mu_0\nabla U(x) + \sqrt{2\tilde{D}_0}\boldsymbol{\eta}$$

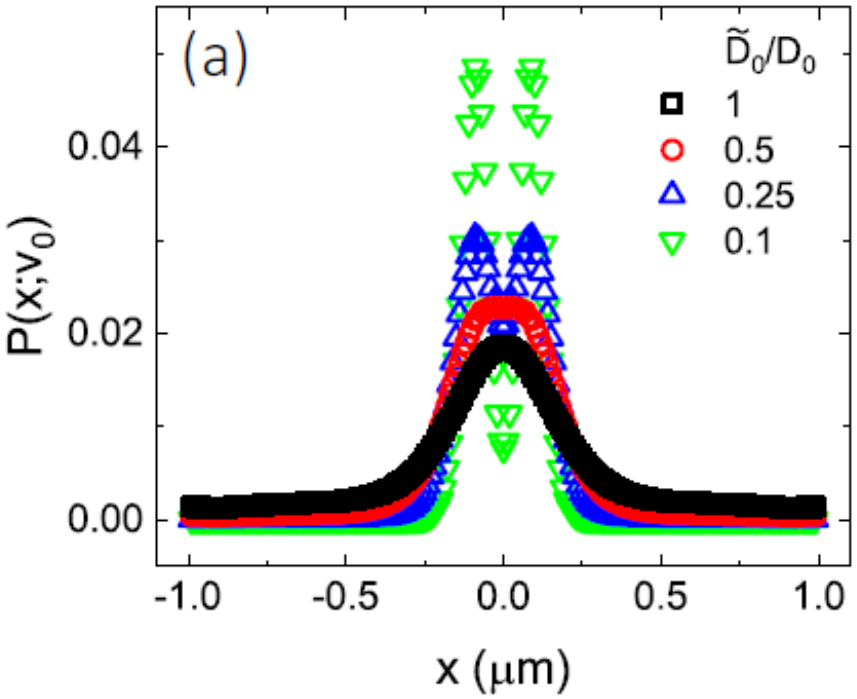

- Brownian broadening: each single peak at the force balance position x_0 is broaden by Brownian translation. Double peaks can not be resolved when the peak width $\sigma \approx (2D_0t_0)^{1/2}$ (≈ 0.17 μm) is large than the peak separation x_0 (≈ 0.09 μm, or $\tilde{D}_0/D_0 > 0.25$).

Langevin equation for the Brownian dynamics simulations of run-and-tumble particles (RTPs):

$$\dot{\boldsymbol{r}} = v_0\hat{\boldsymbol{u}} - \mu_0\boldsymbol{\nabla}U(x) + \sqrt{2\tilde{D}_0}\boldsymbol{\eta}$$

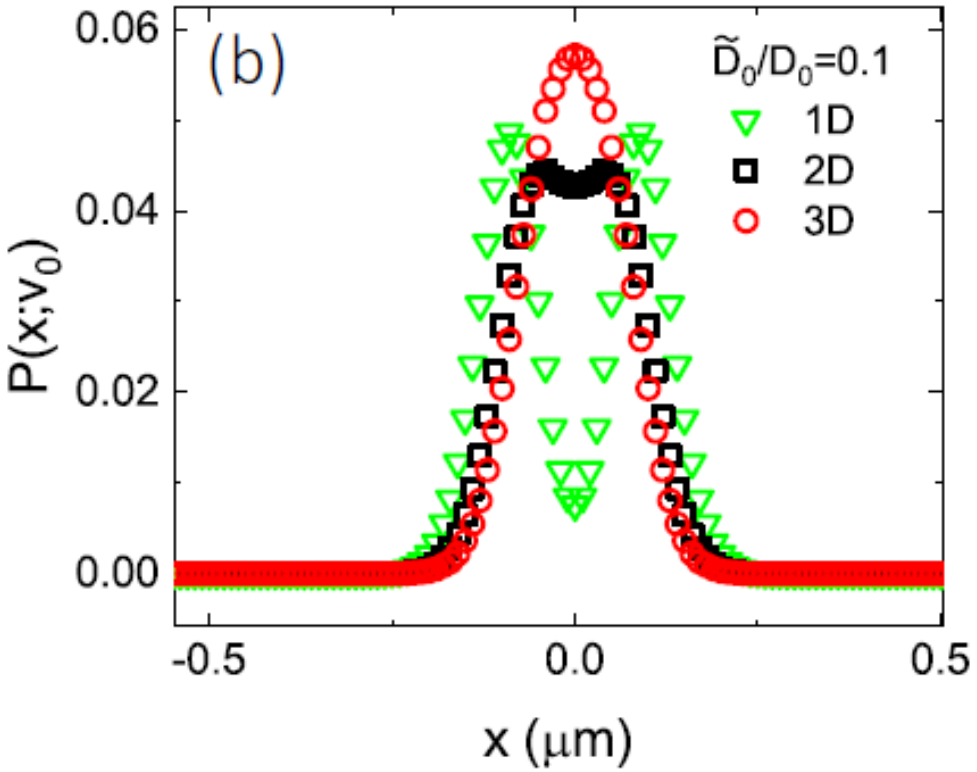

- Dimensional Broadening: the two peaks become closer and finally merge into a single peak for 3D rotation.

What we learned from this work:

- Parallel microgrooves provide a useful experimental platform for the study of the dynamics of SPPs in an external potential $U_0(x)$, which can be designed by using a microgroove-patterned PDMS substrate. The self-propulsion speed v_0 can be accurately measured from $\langle \Delta y^2(\tau) \rangle$.

- The barrier height, $E_b \equiv U_{\text{eff}}(\lambda/2; v_0)$, is found to decrease with v_0. The effective potential can be well described by $U_{\text{eff}}(x; F_0) = U_0(x) - aF_0|x|$ under the fixed angle approximation.

- Because of Brownian broadening and dimensional broadening, no particle accumulation is observed even when $\tau_p \gg \tau_0$.

- The escape events of the SPPs over the effective potential $U_{\text{eff}}(x; F_0)$ are well described by a Poisson process and a Kramers-like relation holds, once the self-propulsion force $F_0$is properly included into the effective potential $U_{\text{eff}}(x; F_0)$.

(3) Protein diffusion on live cell membrane

- Muscle cells cultured from Xenopus (African clawed frog) embryos, a model system to study the neuromuscular junction.
- Acetylcholine receptor (AChR) is a transmembrane protein (a ligand-gated ion channel) and its lateral movement on membrane is important for synapse formation.

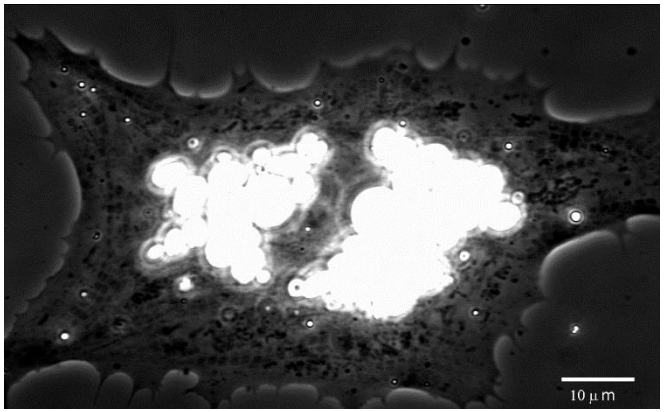

bright field image of a muscle cell (stage 22) with yolk in the center

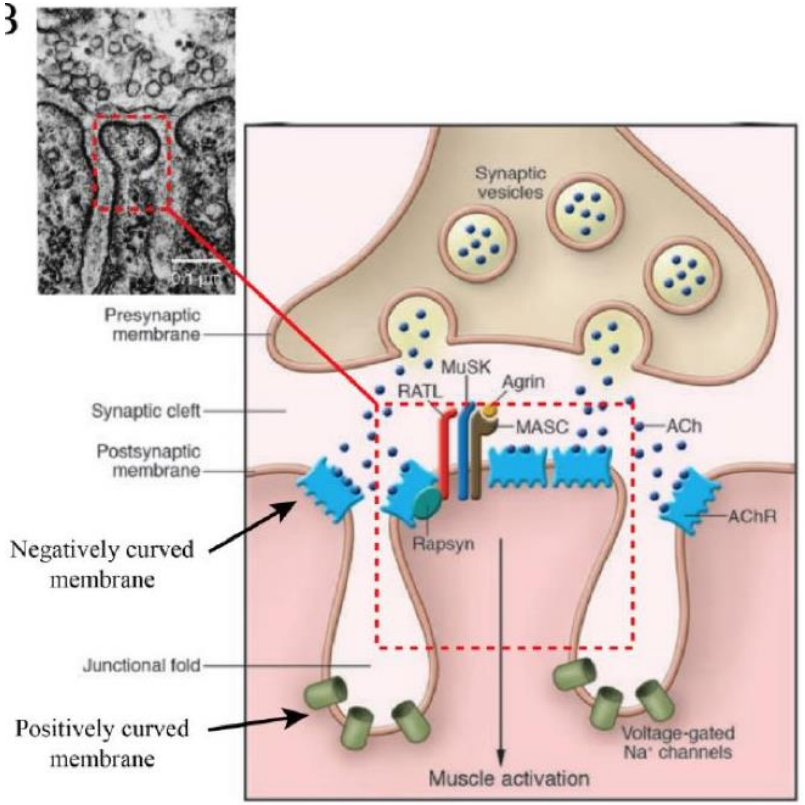

Structure of the nicotinic acetylcholine receptors (AChR)

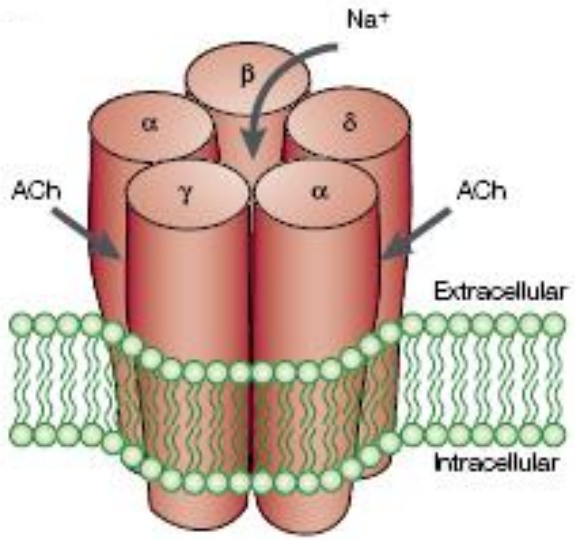

height: 20 nm
diameter: 7 nm

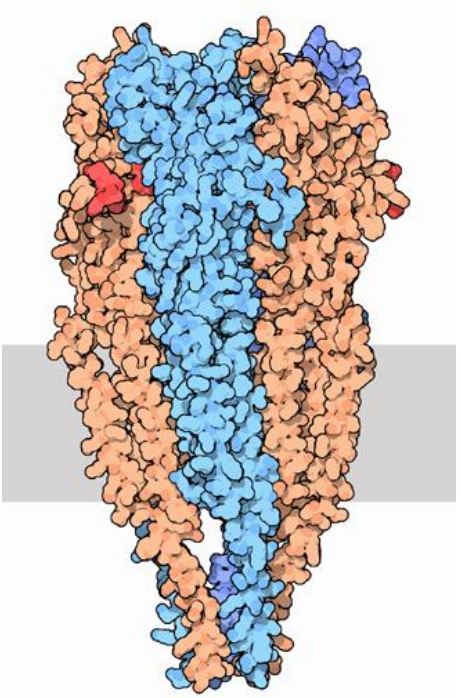

A cation selective, ligand-gated ion channel

Biolinkers: biotinylated α-bungarotoxin

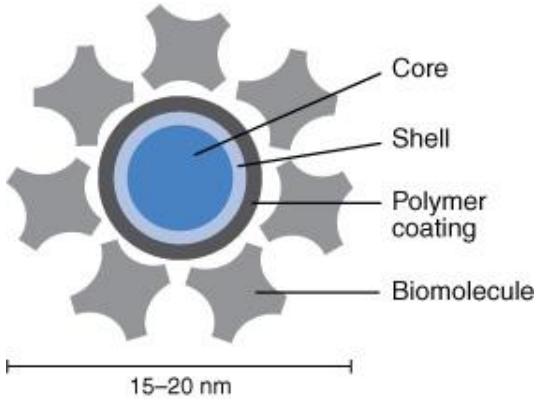

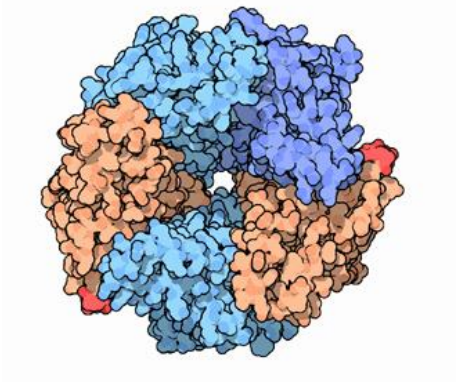

Labeled by quantum dots (QDs)

Fluorescent imaging of QD labeled AChRs

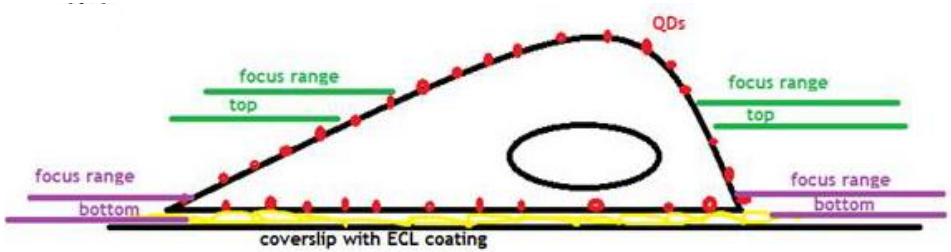

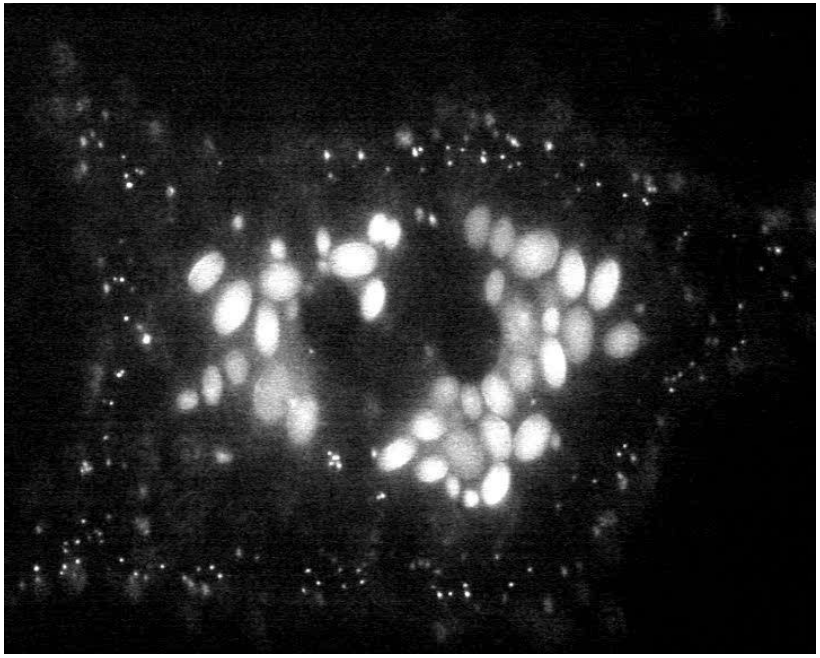

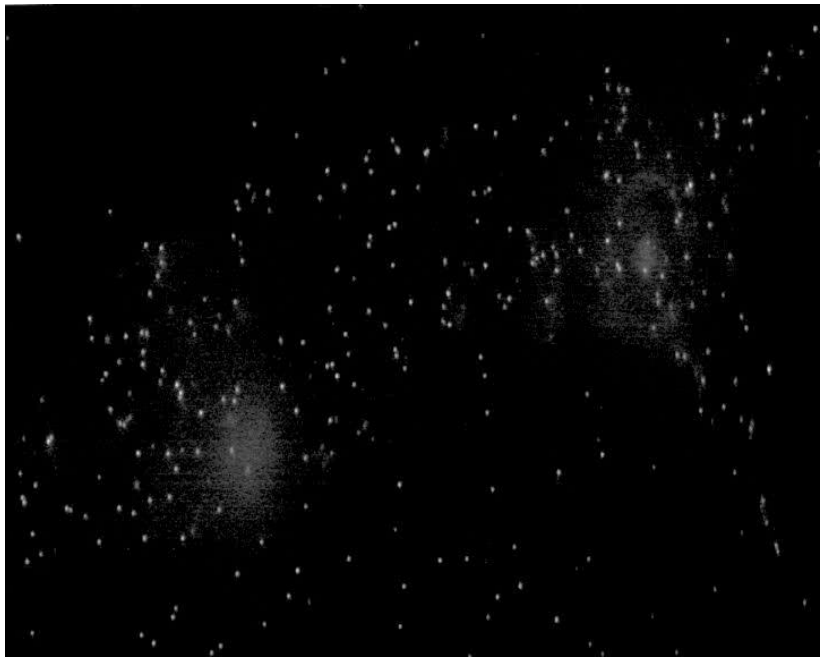

Focused on the middle plane of the cell

Focused on the bottom plane facing the substrate

（i） Dynamic heterogeneity of mobile AChRs

The structurally identical AChRs reveal a huge amount of dynamic heterogeneities; some move fast and some move slow, and some do not move at all (immobile).

AChR trajectories

Trajectories of Brownian particles

Single AChR trajectory

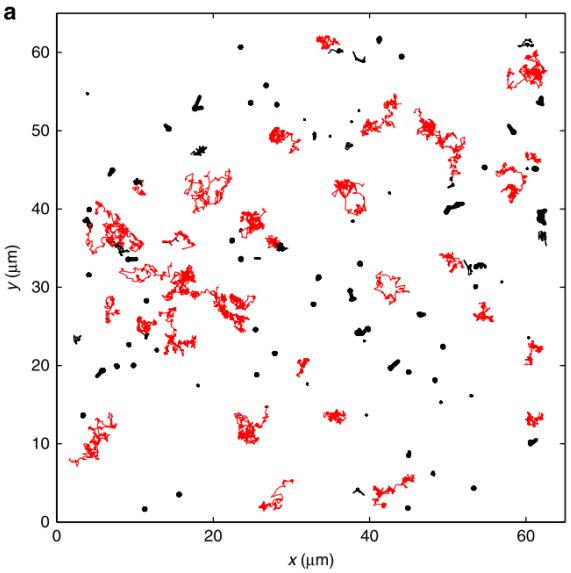

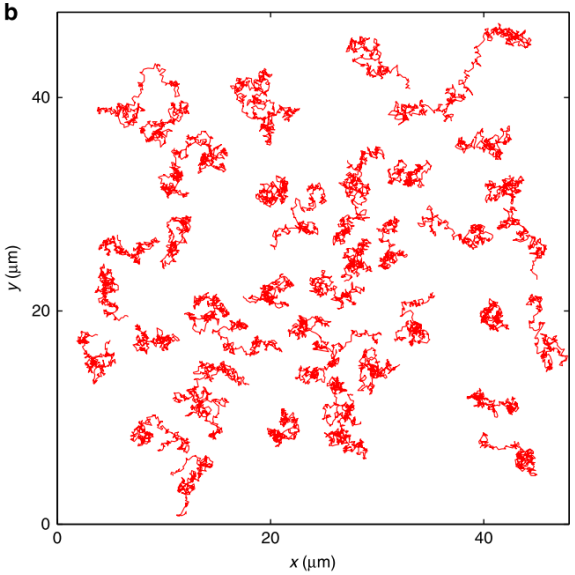

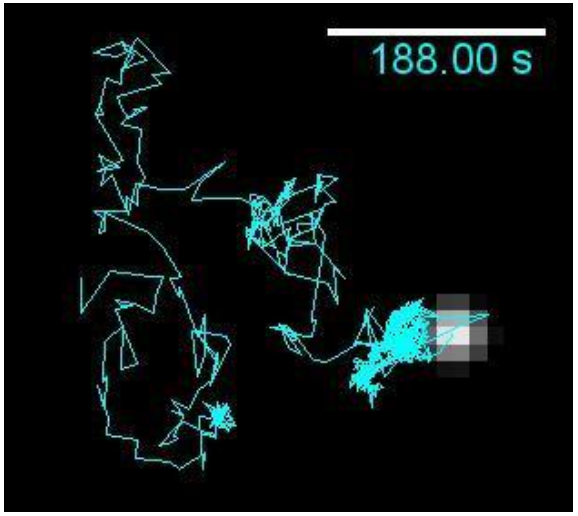

This suggests that AChRs move in a very complex landscape having both “lateral” interactions with other proteins/lipids on the membrane and “vertical” interactions with the underneath cytoskeletal cortex.

What are the trapping potential and interaction landscape of live cell membrane?

The radius of gyration R_g quantifies the size of the area occupied by a trajectory. Normalized R_g'= $Rg/\langle Rg\rangle$ with $\langle Rg\rangle = [(2/3)D_L\tau]^{1/2}$

$$R_g^2 = \frac{1}{N}\sum_{i=1}^{N}\left[(x_i-\bar{x})^2+(y_i-\bar{y})^2\right]$$

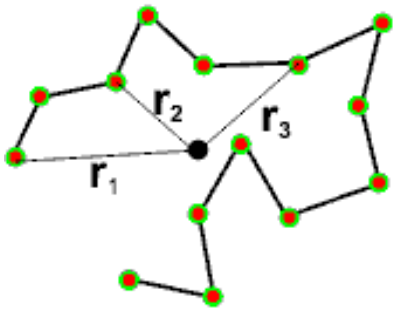

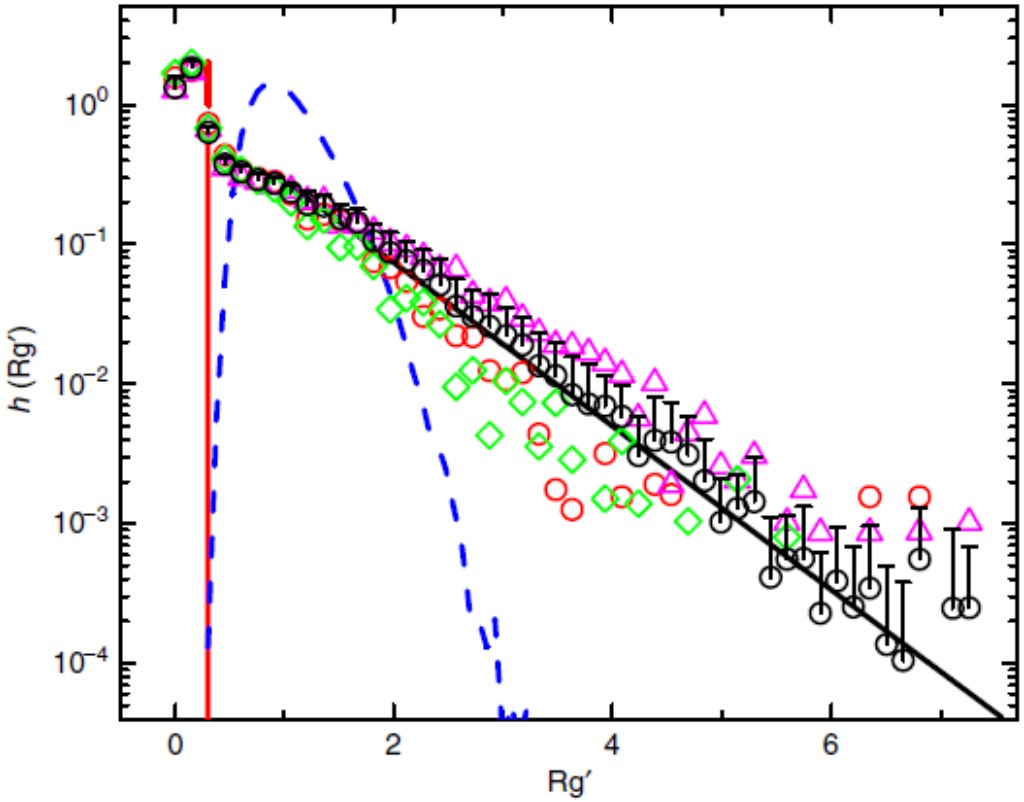

PDFs of R_g' for AChRs from different frogs and embryos and from cells cultured at different days and at different delay times τ all have a long exponential tail (dynamic heterogeneity).

W. He *et al*., Nature Communications **7**:11701 (2016)

Protein mobility is characterized by the mean square displacement (MSD)

$$\langle \Delta \mathbf{r}^2(\tau) \rangle = 4D_L\tau \text{ with } \Delta \mathbf{r}(\tau) = \mathbf{r}(t+\tau) - \mathbf{r}(t)$$

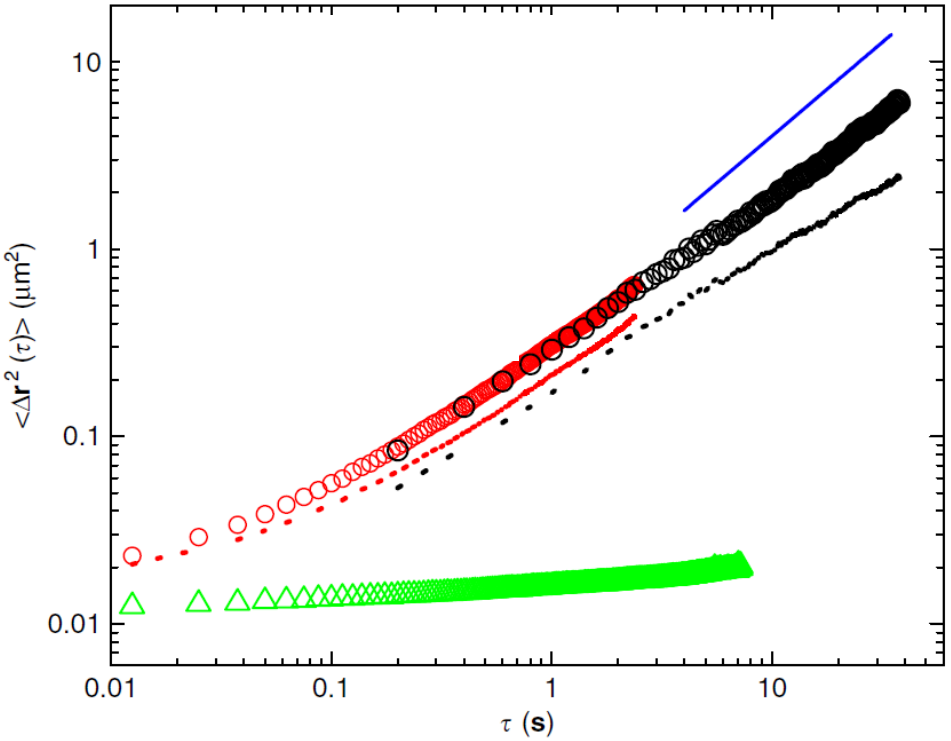

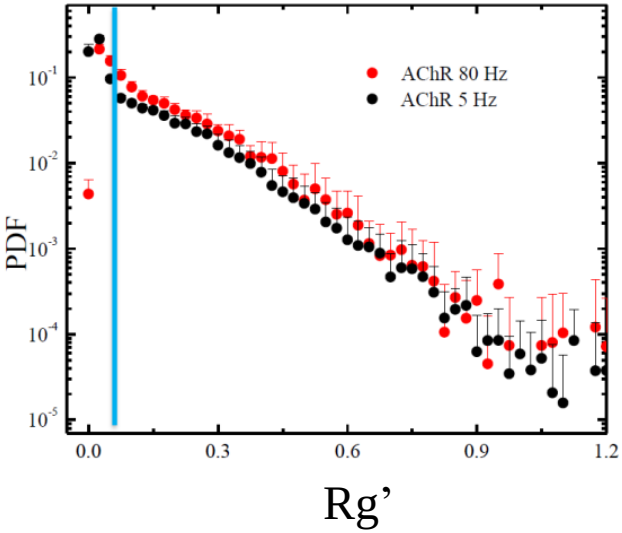

- Immobile AChRs cause the "non-ergodicity" of MSD. "Ergodicity" recovers when the immobile AChRs are removed from the statistics.
- Subdiffusive behavior, $\langle \Delta \boldsymbol{r}^2(\tau) \rangle \sim \boldsymbol{\tau}^{\alpha}$ with $0.4 < \alpha < 0.9$, at intermediate τ.
- At long time limit ($\tau > 4$s), MSD becomes diffusive with $\alpha \approx 1$.

- MSD values of AChR are a linear function of τ even for very large values of τ, suggesting that the cell membrane is really fluidic for transmembrane proteins (no permanent fence is found).

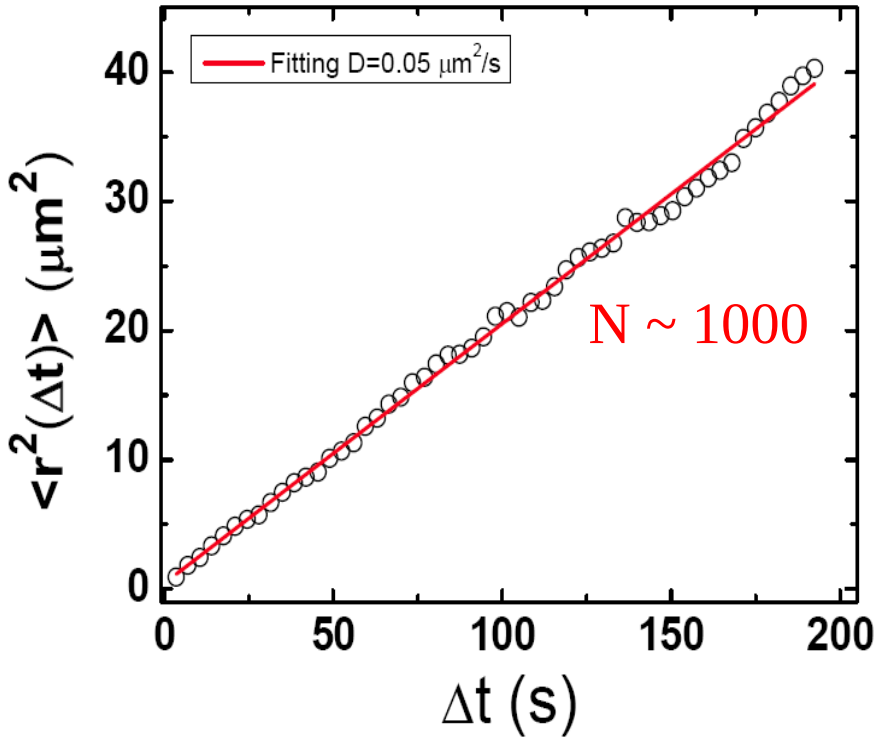

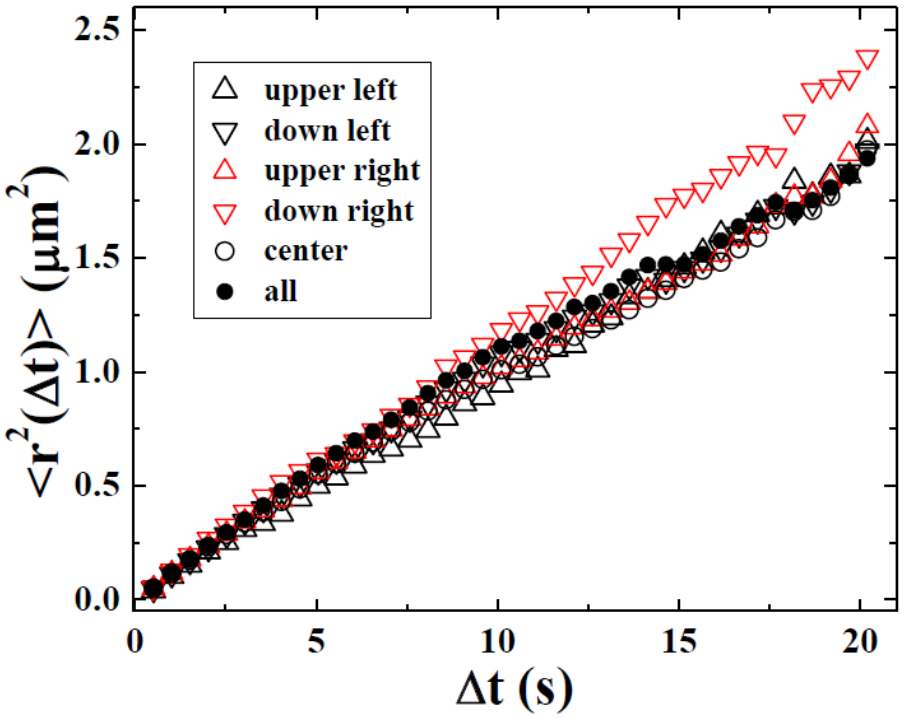

- MSD values of AChR in different regions of the same cell remain approximately the same.

$\langle D_L \rangle = 0.041 \pm 0.015\ \mu m^2/s$ $\langle \gamma \rangle = 0.64 \pm 0.17$

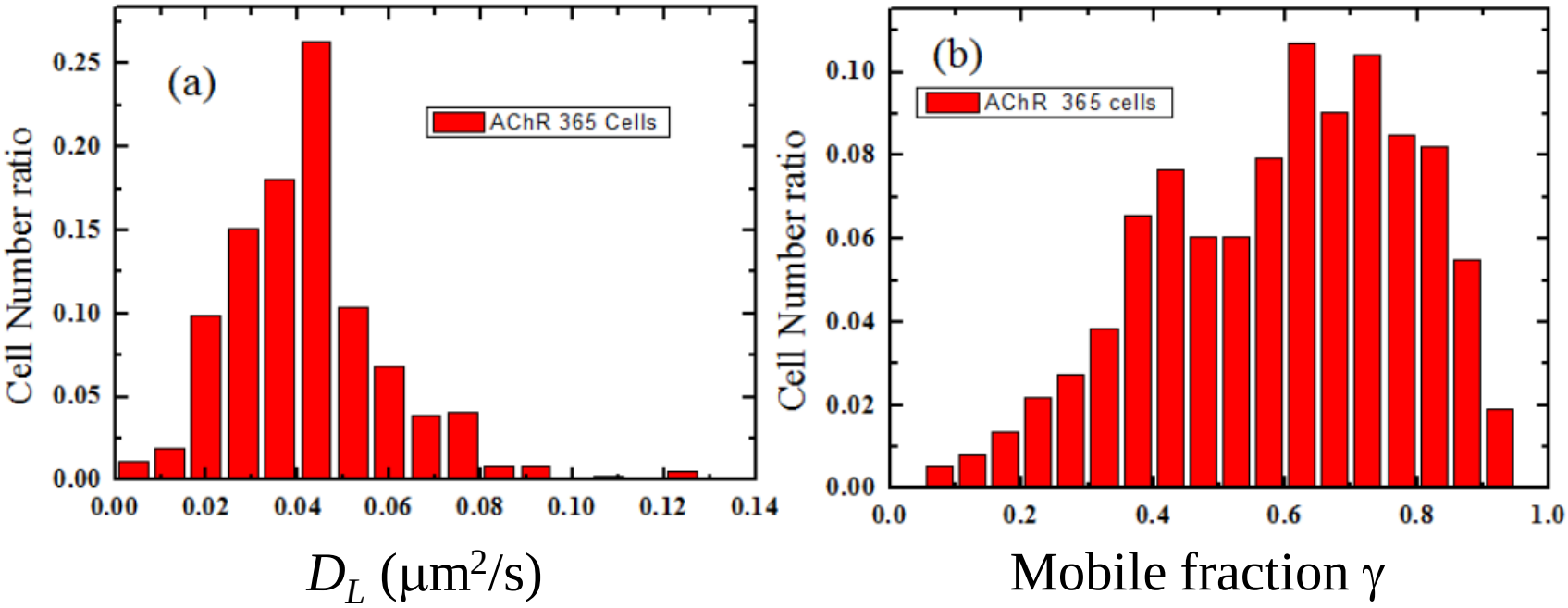

- Diffusion coefficient D_L and mobile fraction γ vary among cells from different frogs and embryos and cultured at different days.
- The mean values of D_L and γ for the same batch of cells can be used as indexes to characterize the mobility and interaction of membrane proteins in live cells.

W. He *et al*., Nature Communications **7**:11701 (2016)

Probability density function (PDF) of the normalized displacements, $\Delta x' = \Delta x/(2D_L\tau)^{1/2}$ and $\Delta y' = \Delta y/(2D_L\tau)^{1/2}$

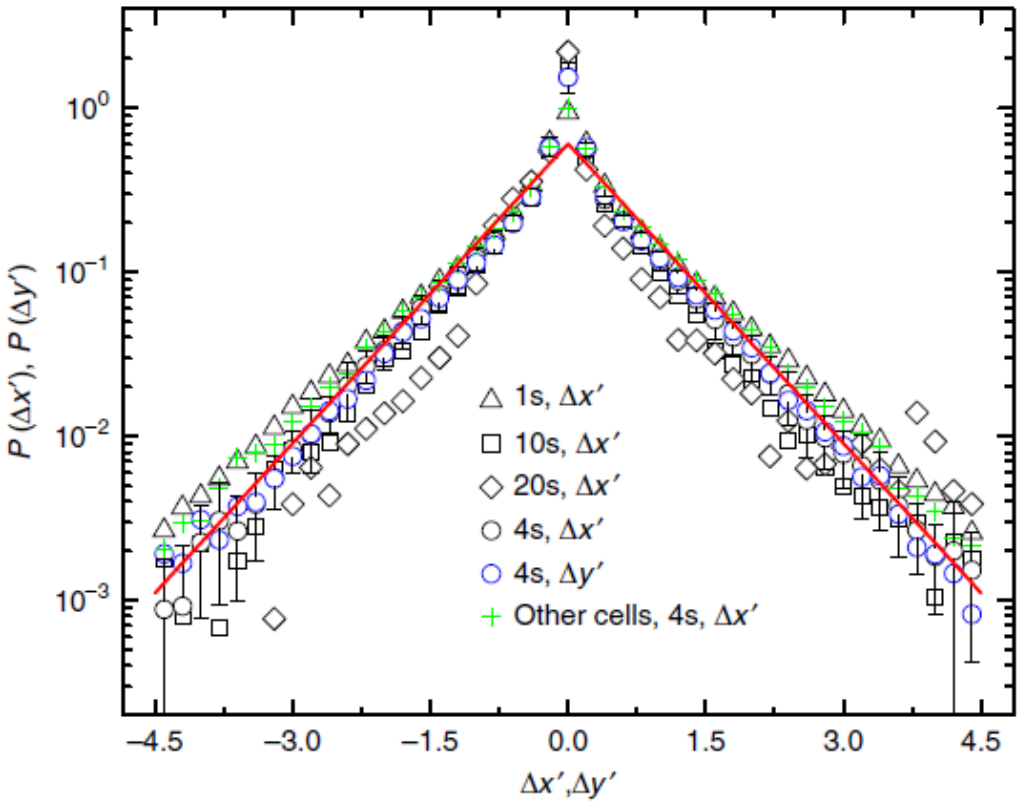

PDFs for AChRs from different mother frogs, embryos, cells and at different delay times τ.

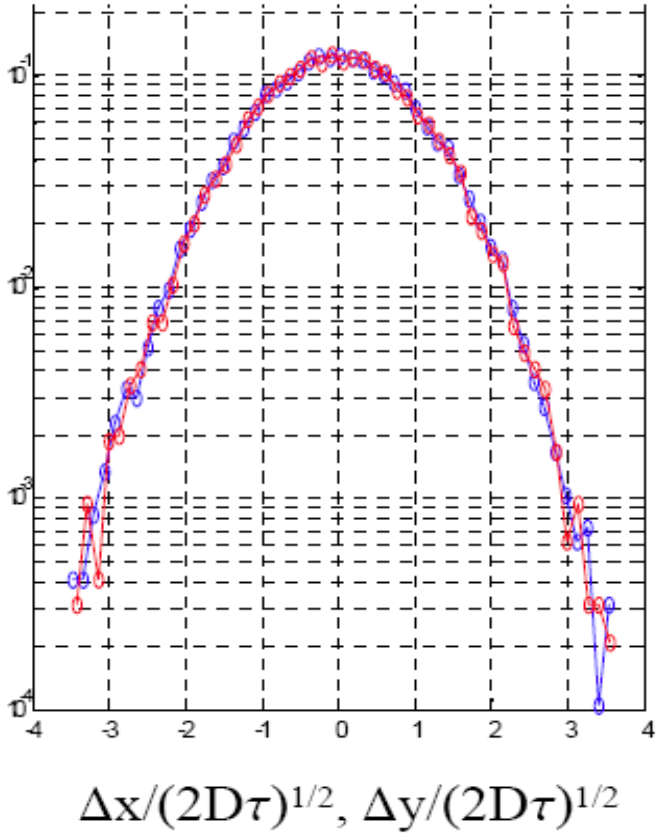

PDFs obtained from a monolayer of silica spheres (d = 1.1 μm) near a glass substrate.

Because of the dynamic heterogeneity of individual AChR trajectories, non-Gaussian fluctuations can be generated by a convolution of a set of independent subgroups, each obeys the Gaussian statistics with its own diffusion coefficient δ:

$$g(\Delta x;\delta) = \frac{1}{(4\pi\delta\tau)^{1/2}} e^{-\Delta x^2/4\delta\tau}$$

$$P(\Delta x') = \int_0^\infty g(\Delta x;\delta)\, f(\delta) d\delta$$

If the diffusion coefficient δ has an exponential-like distribution:

$$f(\delta) = \frac{1}{D_L} e^{-\delta/D_L}$$

The PDF of the normalized $\Delta x' = \Delta x/(2D_L\tau)^{1/2}$ then takes the form:

$$P(\Delta x') = \int_0^\infty g(\Delta x;\delta)\, f(\delta) = \frac{1}{\sqrt{4D_L\tau}} e^{-\sqrt{2}|\Delta x'|}$$

This model thus provides a physical explanation of the observed exponential $P(\Delta x')$ and the predicted decay rate $\beta = \sqrt{2}$ agrees with the measured $\beta = 1.4$.

PDF of "instantaneous" diffusion coefficient $\delta = \langle \Delta \mathbf{r}^2(\tau) \rangle_t / (4\tau)$ with τ = 1s and t = 4s.

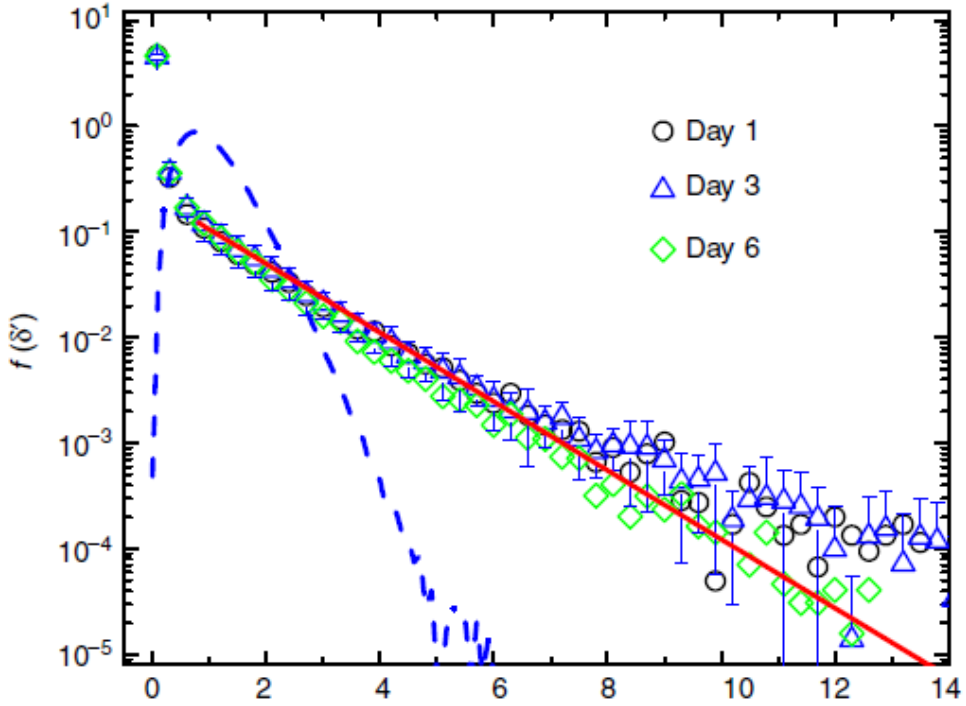

$\delta' = \delta / D_L$

PDFs of the normalized δ' have a long exponential tail (dynamic heterogeneity), and they are universal independent of the cell origin and time lapse.

What is the biological significance of the observed dynamic heterogeneity and non-Gaussian statistics?

Dynamic picket-fence model:

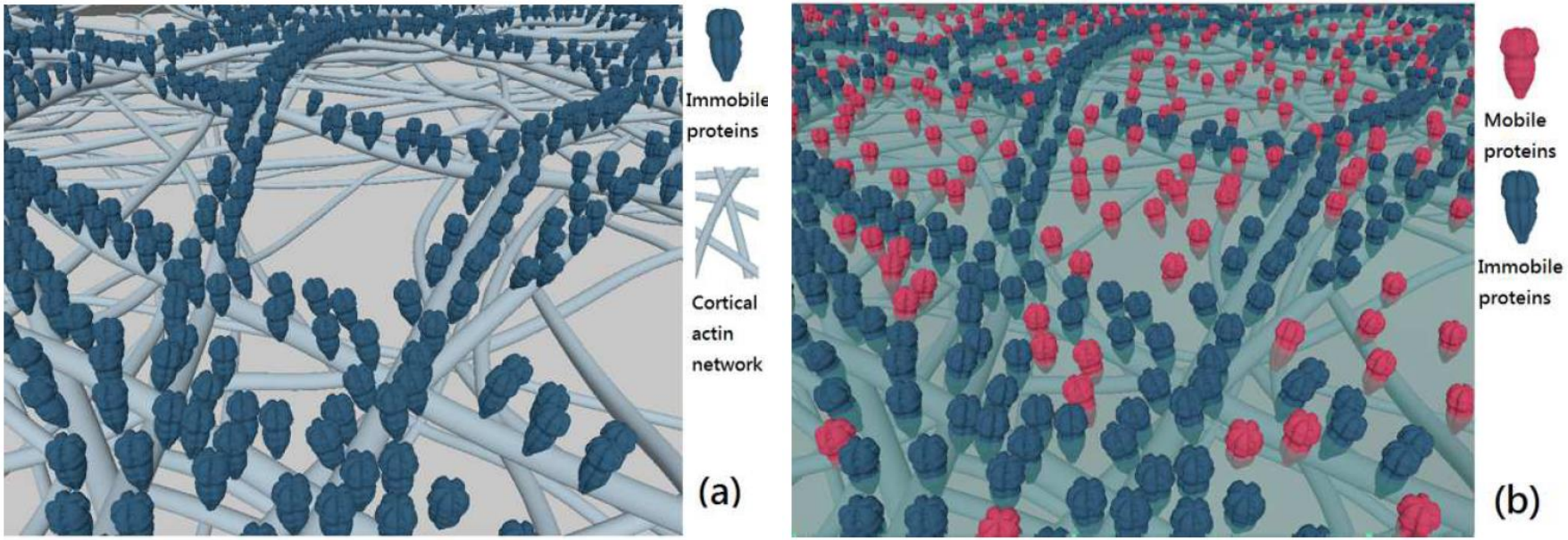

- Anchored proteins form a continuous random network, partitioning the membrane into domains (corrals) of various sizes.
- The motion of membrane molecules within each corral is hindered by the rigid boundary of the corrals, giving rise to size-dependent δ.
- The slow-active remodelling of the cortical actin network changes the spatial distribution of the corrals, giving rise to non-Gaussian statistics.

(ii) Directed motion of membrane proteins under an entropy-driven potential field generated by anchored proteins

How a protein molecule wades through and functions in the tightly packed crowd either inside the cell or on the cell membrane?

- At large distances up to the size of a cell, the cell utilizes motor proteins to drive directed transport of cargos along the cytoskeletal filamentous tracks.

- At small distances, the cell utilizes diffusion for molecular transport. An example is the release and diffusion of small neurotransmitters across the synaptic cleft of 15-20 nm in width.

- There are other cellular processes, which require transport of molecules over distances in mesoscale (say, 20 nm - 1 μm), in which these two mechanisms are not effective. An example is the lateral motion of transmembrane proteins in the plasma membrane.

We now demonstrate that a non-uniform concentration field $n(\boldsymbol{x})$ of anchored proteins can generate a spatially varying and temporally stable free-energy landscape $U(\boldsymbol{x})$ to guide the motion of other (non-motor) mobile proteins in the region.

The free-energy of a mobile protein is increased by $-k_BT \ln[1- n(x)] \approx n(x)\, k_BT$ (for small n) due to the reduced available space. This entropy-driven potential field, $U(x) \approx n(x)\, k_BT$, will push the mobile proteins to move from a high concentration region of anchored proteins to a low concentration region.

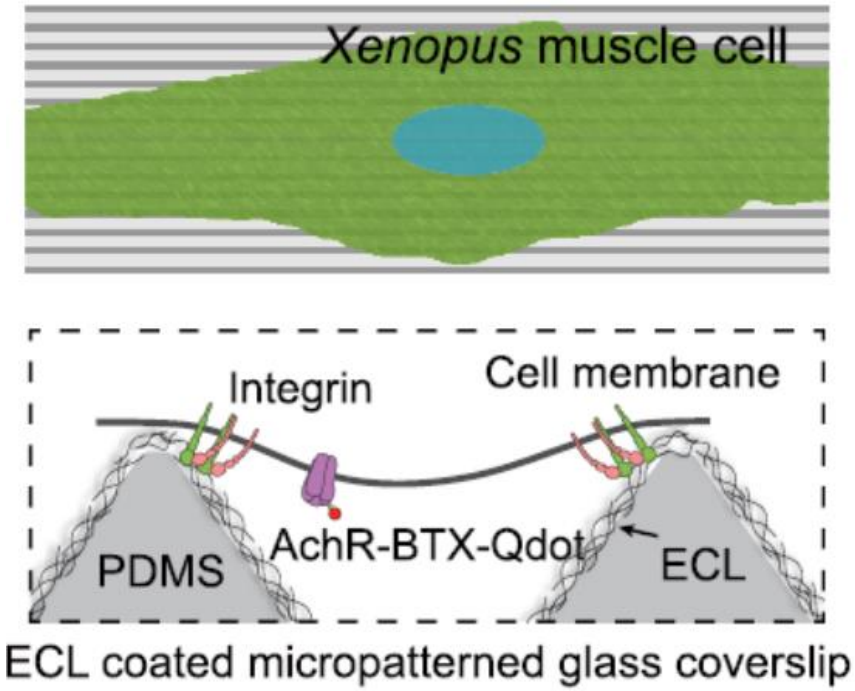

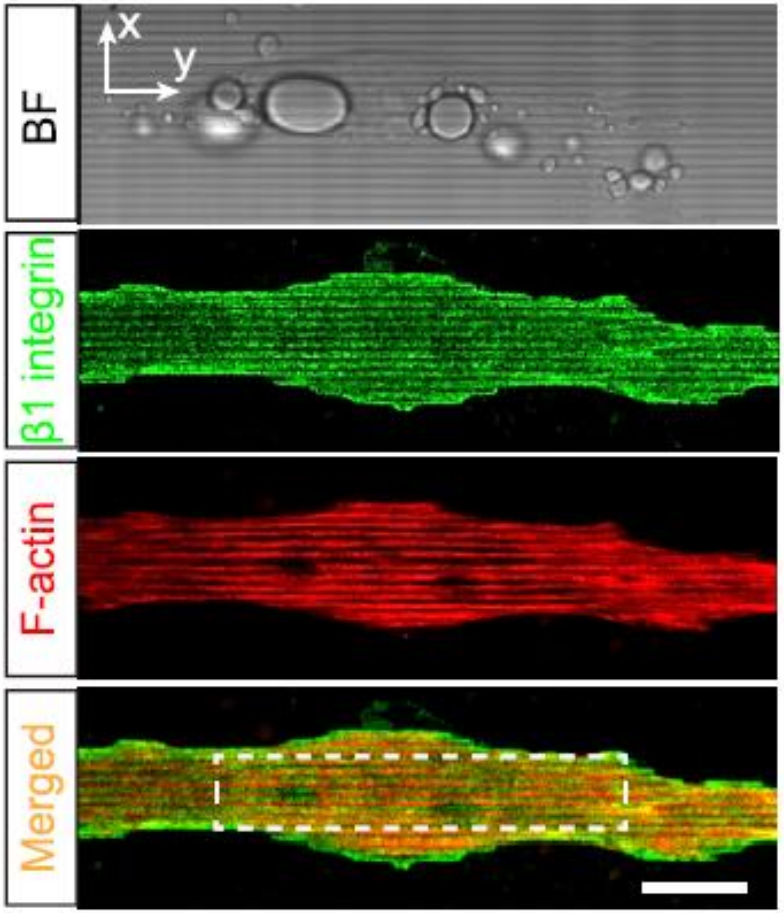

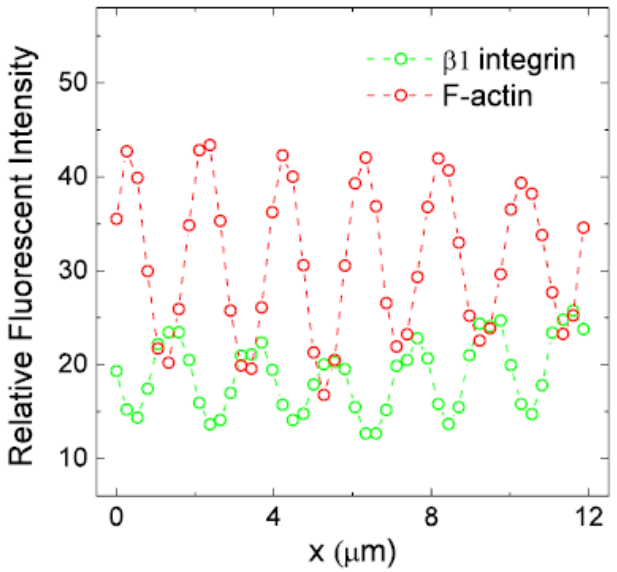

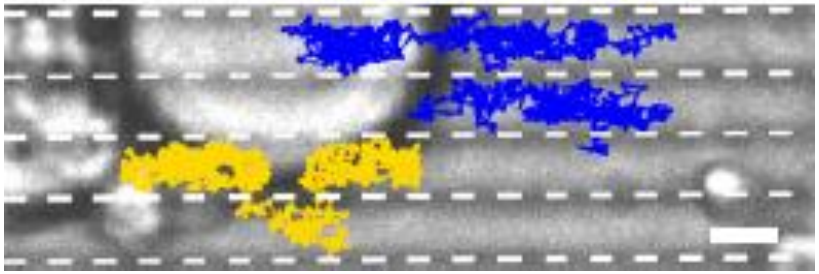

- Microgroove-patterned substrate induces a periodic array of 1D potential traps for mobile AChRs.
- Obtain a large volume of AChR trajectories from 385 live cells over a wide range of sampling rates (≤80 Hz) and long durations (≤300 s).

Shen, *et al*., Phys. Rev. Research. **3**, 043195 (2021)

Effective potential $U(x)$

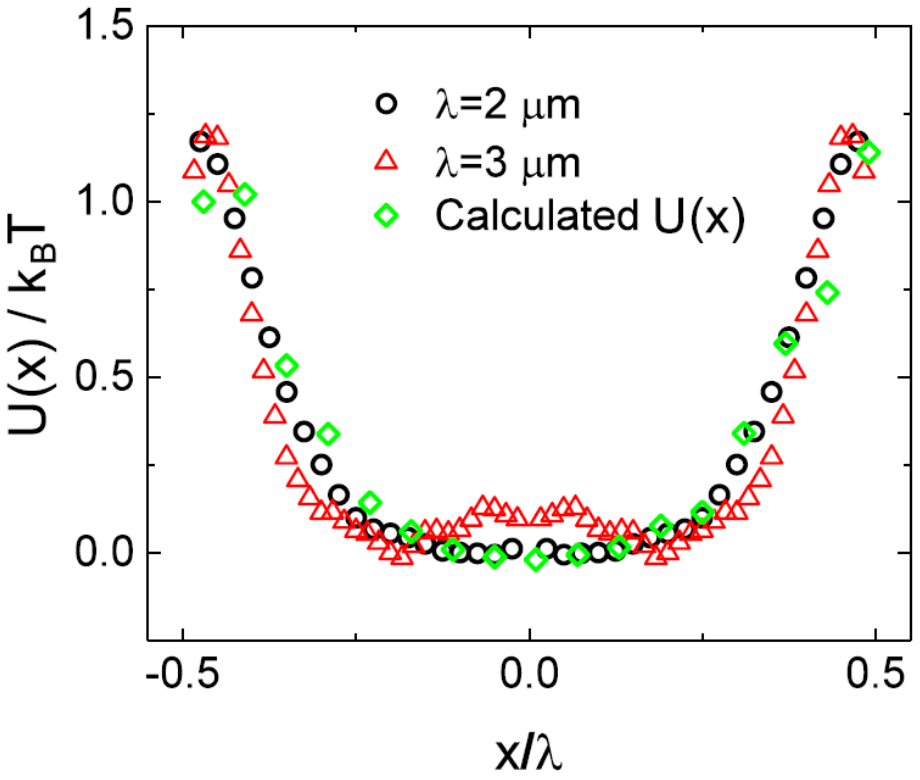

Fluorescent intensity profile $I(x)$

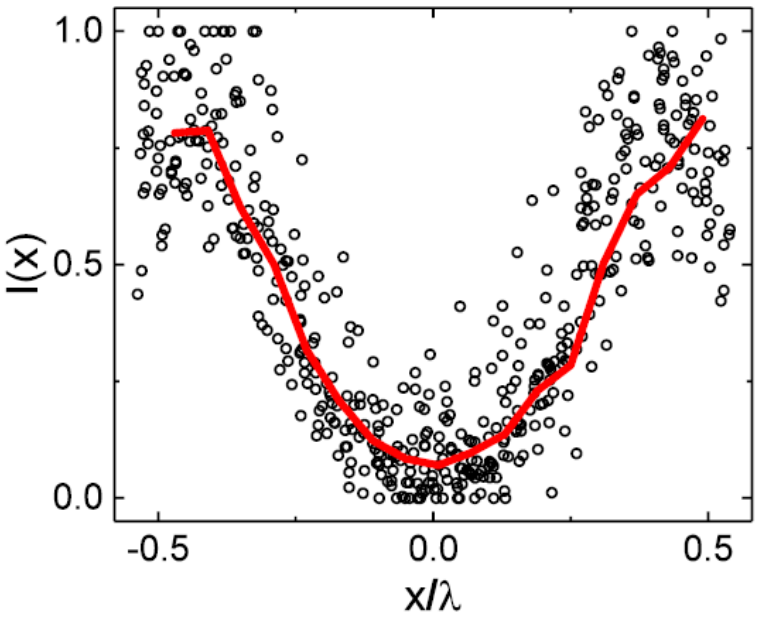

$n(x) = \beta I(x)$

From the equilibrium population PDF $H(x)$, we find the effective potential $U(x) = -k_B T \ln H(x)$ (by Boltzmann distribution)

$$U(x) \simeq -k_B T \ln\{[1 - n(x)][1 + \alpha n(x)]\}$$

with the fitting parameters $\alpha = 0.55$ (attractive interaction) and $\beta = 0.95$

Statistical properties of the displacements $\Delta x(\tau)$ and $\Delta y(\tau)$ for mobile AChRs inside the potential $U(x)$

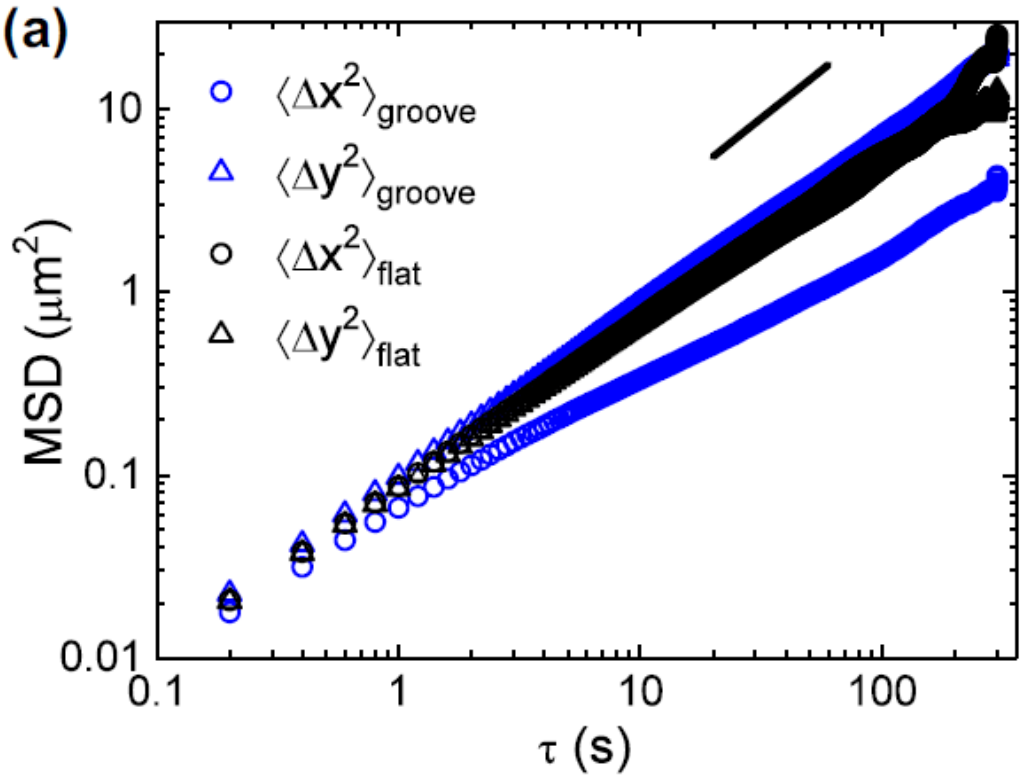

- MSD reveals a confined anisotropic diffusion across a single groove.
- $\langle \Delta x^2(\tau) \rangle$ exhibits a crossover behavior from short-time diffusion ($\tau < \tau_L \approx 1$ s) to longtime diffusion ($\tau > \tau_H \approx 50$ s).

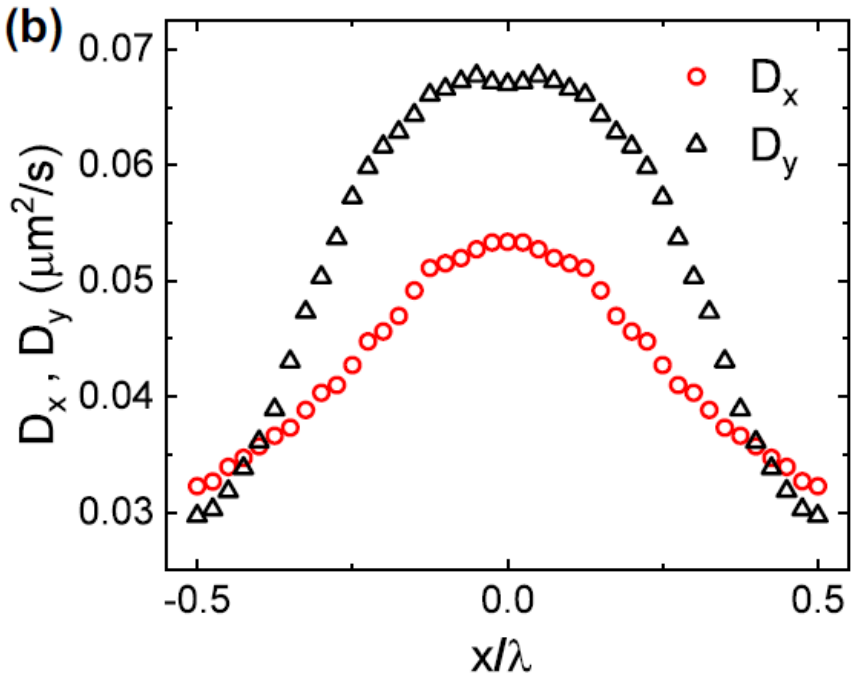

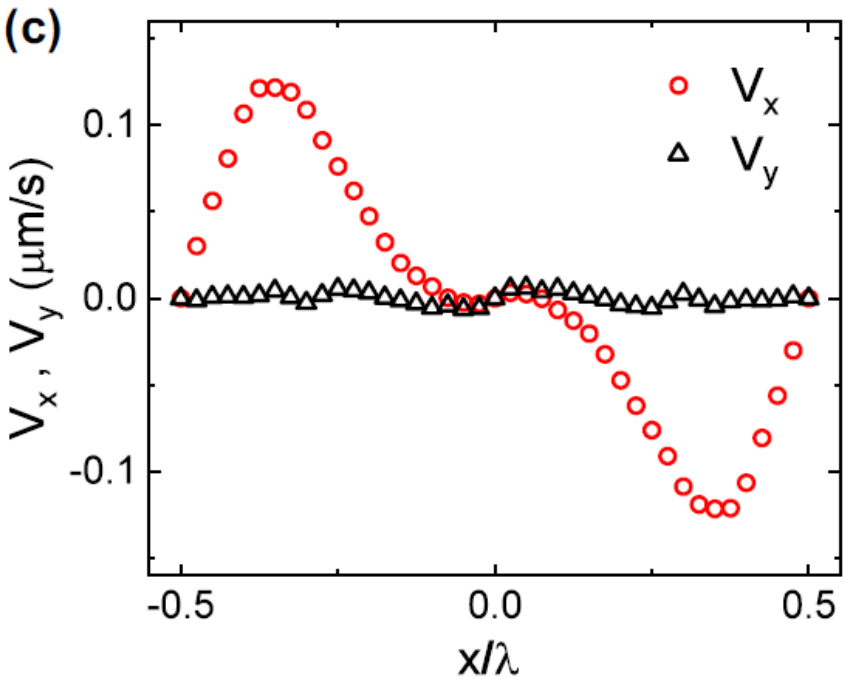

- local diffusion of AChRs reveals a strong x-dependence with its maximal value at the bottom of the microgroove and the value of $D_x(x)$ is reduced by more than 40% at the ridge of the microgroove.

- $U(x)$ produces a nonzero drift velocity V_x, which reaches its maximal value $(V_x)_m \approx 0.13$ μm/s in the ridge region, where the anchored integrins has the large concentration gradient. With this drift velocity, AChRs move 10 times faster than diffusion over a distance of 1 μm (for only ~8 s).

Effects of the Matrigel treatment

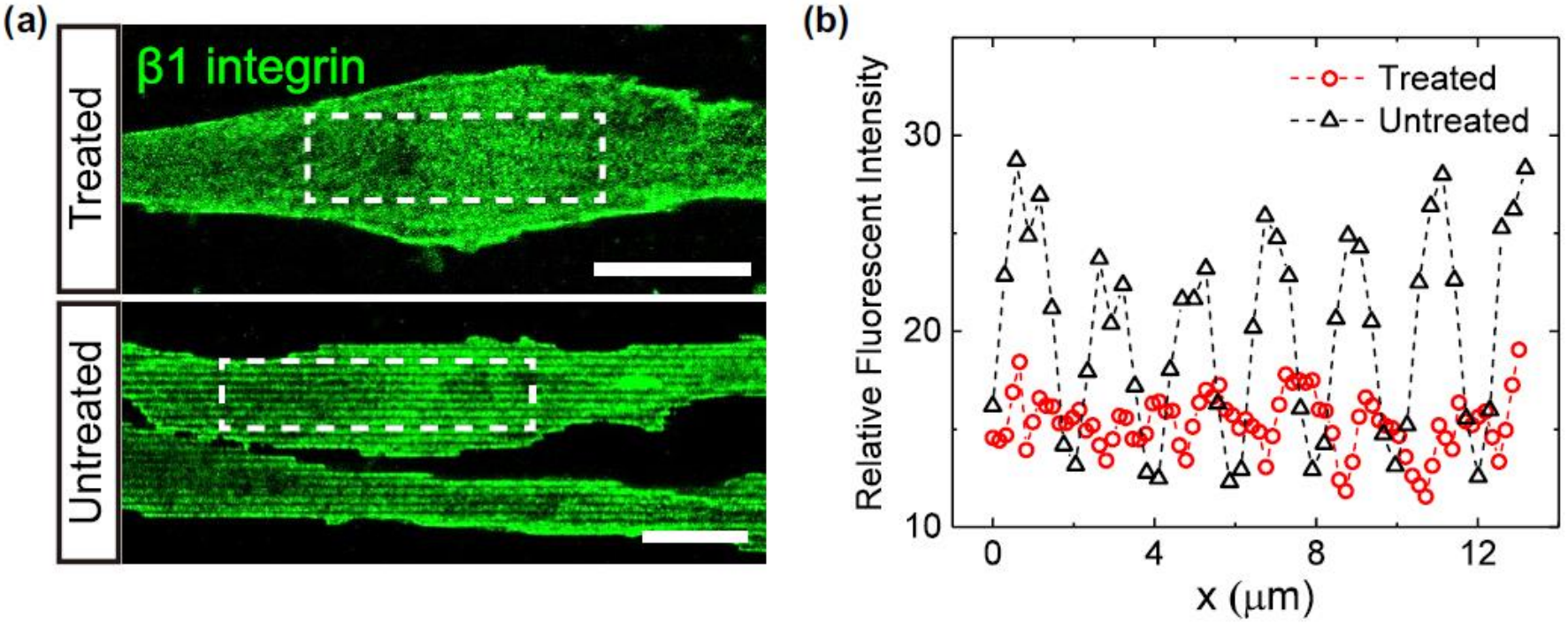

The substrate-induced distribution of anchored integrins can be altered by adding soluble extracellular matrix (ECM) proteins (Matrigel) in the culture medium, which adsorb on the outer side of the suspended cell membrane, allowing integrins to anchor in the suspended membrane.

Effects of the Matrigel treatment

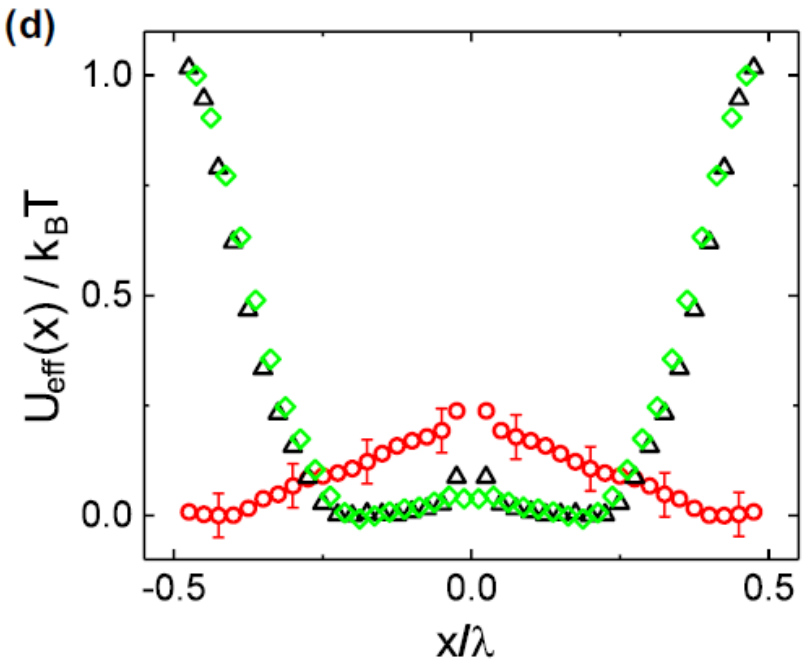

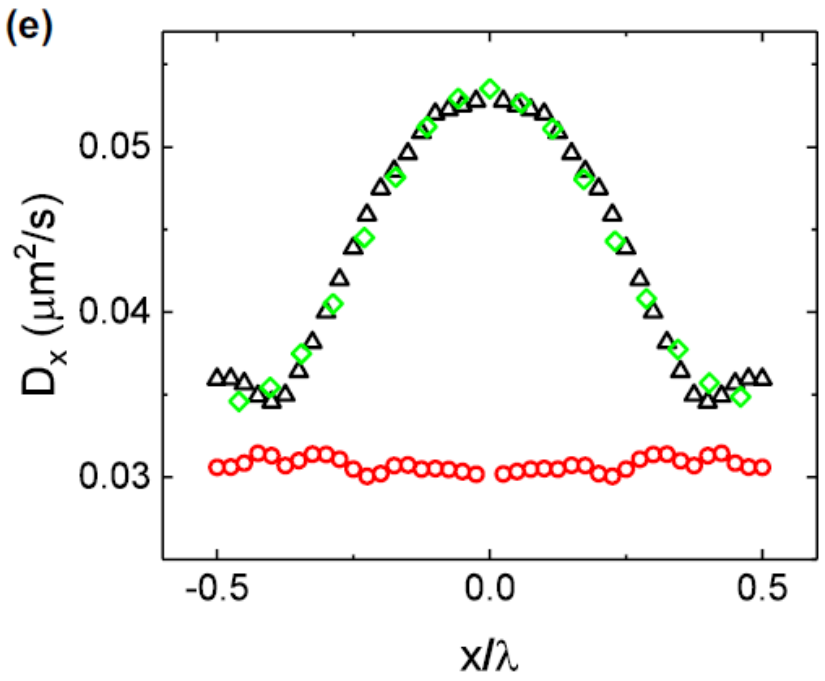

Theoretical predictions:

$$D_x(x) \simeq D_0 \frac{1 - n(x)}{1 + \alpha n(x)}$$

$$\frac{D_x(x) - D_{\min}}{D_{\max} - D_{\min}} \simeq \frac{1 - n(x)}{1 + \alpha n(x)}$$

with $\beta = 0.95$, $\alpha = 0.55$, $D_{min} = 0.028$ μm²/s, $D_0 = D_{max} - D_{min} = 0.03$ μm²/s

Effects of the Matrigel treatment

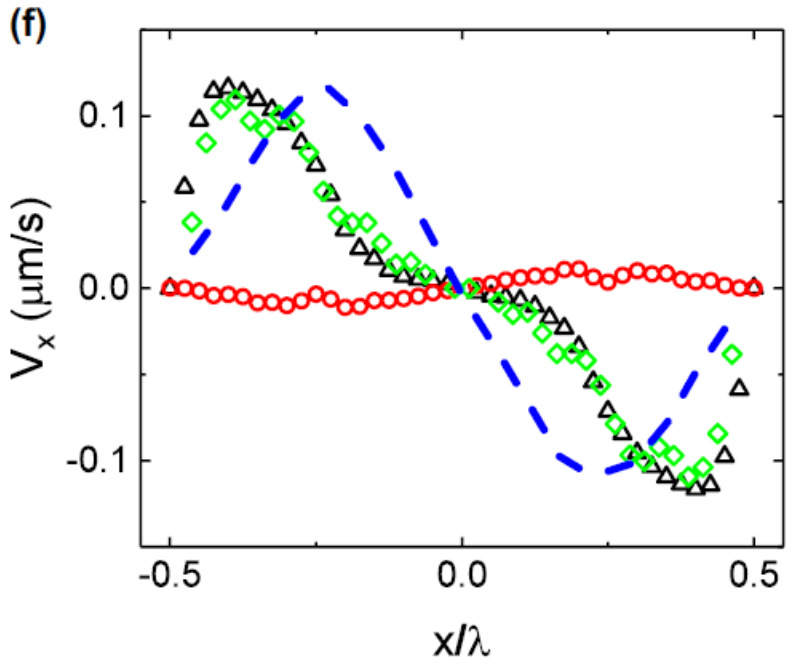

Theoretical predictions:

$$V_x(x) \simeq \frac{-D_x(x)}{k_B T}\frac{dU(x)}{dx} + \frac{dD_x(x)}{dx}$$
$$= -2D_0 \frac{dn(x)/dx}{1+\alpha n(x)},$$

with $\beta = 0.95$, $\alpha = 0.55$, and $D_0 = 0.03\ \mu m^2/s$

Microwell-patterned substrate induces a periodic array of 2D potential traps for mobile AChRs.

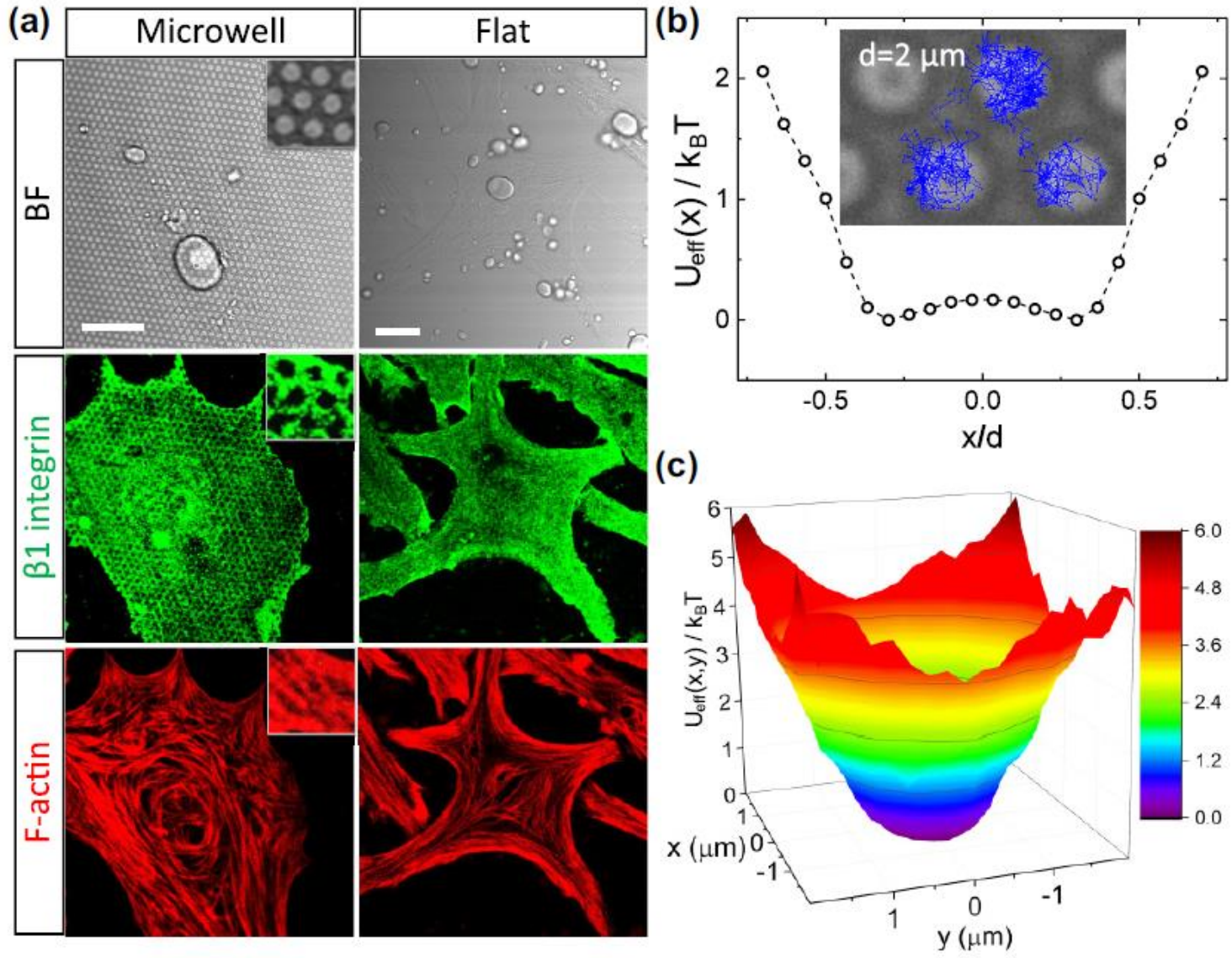

6. Summary

- Living cells are complex non-equilibrium systems, which involve both structural complexities, such as various filamentous networks and organelles made of different proteins, and dynamic complexities ranging from dynamic heterogeneity to molecular motors and ATP-driven polymerization/ depolymerization.

- Compared to the well-studied active components of living cells, such as molecular motors, our current understanding of nonmobile components in living cells, such as anchored proteins, is still primitive. We do not know why living cells want to spend energy (ATP) to lock certain proteins in place, which in turn put a brake on all other mobile proteins in the cell.

- In this work, we demonstrate that anchored proteins inside the cell can generate a spatially varying and temporally stable potential (free-energy) landscape for intracellular or membrane transport in mesoscale.

- The discovery of this stable energy landscape thus offers a novel transport mechanism that has important biological implications, ranging from directed molecular transport in mesoscale to enhanced protein trapping and protein-protein interactions over a long range.

- Our finding represents an important and biologically tunable mechanism for transport in living cells and for protein interactions mediated not by specific chemical signaling (such as post-translational modification or binding of small molecules), as is usually assumed, but by non-specific physical forces that yield remarkably simple universal laws.

- Our theoretical modeling, which is primarily based on equilibrium statistical mechanics, is found to be in good agreement with the experimental results. Why does the equilibrium theory work so well for protein diffusion on live cell membrane?

- Living cells involve both out-of-equilibrium processes, such as cargo transport and active contractions of the cortical skeleton that need non-equilibrium theory to explain, and near-equilibrium processes, such as protein folding, formation of macromolecular complexes and supramolecular structures including plasma membrane and protein phase separation that have been explained largely by the equilibrium thermodynamics and statistical mechanics.

- Understanding how a living cell can manage these two physically very different aspects coherently in the same material system is clearly of current interest in physics and in biology.

- The plasma membrane of a living cell offers a good experimental platform for the study of this near-equilibrium and out-of-equilibrium duality of the living cells. On one hand, the cell membrane itself does not contain molecular motors or involve ATP-dependent polymerization/depolymerizations directly. On the other hand, it couples to an “active thermal bath” of actin cortex through the anchored proteins, such as integrins. Cellular ATP is required to keep these anchored proteins in place against random diffusion.